ISC '21

1'st International Symposium on Characterization

www.jcharacterization.com

1'st INTERNATIONAL SYMPOSIUM ON CHARACTERIZATION ISC'21

PROCEEDINGS BOOK

08 - 09 October 2021

JOURNAL OF CHARACTERIZATION

Online Turkey

ISC'21
1'st International Symposium on Characterization

Designed by Soner Savaş

1st INTERNATIONAL SYMPOSIUM on CHARACTERIZATION

OCTOBER 8-9, 2021

PROCEEDINGS Book

EDITORS

Prof. Dr. Atilla Evcin

Prof. Dr. Ibrahim Gunes

Publication Date: 15.12.2021

Contents

Dear 1ˢᵗ International Symposium on Characterization attendees,

We had an amazing time in first week of October and hope you did too! We wanted to send a quick thank you for all of the great connections made, memories created, and laughs shared.

Thank you for all your excellent work!

It is fair to conclude that the conference was a great success! So many people have contributed in so many ways to turn this event into a smoothly running meeting with many very interesting presentations and posters and a very good atmosphere for discussion and networking.

I owe much gratitude to international scientific committees for giving structure to the program and for organizing the first of our symposium.

I thank all sponsors for their generosity and interest in the conference.

Soner Savaş was very helpful with original ideas, design of the logo, and knowledge. He designed the graphic style of the symposium. Ismail Yıldız assisted in the contacts with the social media. The students of the Faculty of Engineering are especially thanked for their enormous and high-quality support. They coordinated the zoom meetings during the symposium. Oğuzhan Evcin composed the program book and abstract book.

You as participants are thanked for all your great scientific input and for many fruitful discussions and scientific interaction.

"This was a great meeting" many of you have said to me. Thank you for being so positive!

Remember, if there are any abstract you'd like to look over again, it is listed in your abstract book in the webpage. We're also here for any questions you may have.

Thank you,

Prof. Dr. Atilla Evcin

Prof. Dr. Ibrahim Güneş

INVITED SPEAKERS

Invited Speakers		University	Presentation Tilte
Prof. Dr. Cenk AKTAŞ		**Christian-Albrechts-University, Institute of Materials Science, Kiel, Germany**	Single source precursor approach for functional nanomaterials
Prof. Dr. Yogendra Kumar MISHRA		University of Southern Denmark, Mads Clausen Institute, NanoSYD, Denmark	Tetrapods based smart materials for advanced technologies
Prof. Dr. Burç MISIRLIOĞLU		Sabancı Üniversitesi, Malzeme Bilimi ve Mühendisliği, Türkiye	Identifying defect contributions to structural phase transitions: Bulk properties vs. thin films
Assoc. Prof. Fabienne DUMOULIN		Acıbadem Üniversitesi, Tıp Mühendisliği Bölümü, Türkiye	Characterising the potential of phthalocyanines for photodynamic therapy

		NED University of Engineering and Technology, Department of Materials Engineering, Pakistan	Electrical and magnetic properties of strontium titanate based ceramics
Assoc. Prof. Fayaz HUSSAIN			

INVITED SPEAKERS

Yogendra Kumar Mishra is Professor MSO at Mads Clausen Institute, NanoSYD, University of Southern Denmark (SDU), Denmark. Prior joining to SDU, he worked as group leader at Functional Nanomaterials Chair, Kiel University, Germany. He did Habilitation in Materials Science from Kiel University in 2015 and Ph. D. in Physics in 2008 from Jawaharlal Nehru University (Inter University Accelerator Centre), New Delhi, India. In Kiel, he introduced a new flame-based process for metal oxide tetrapod nanostructuring and their 3D networks which showed many applications in engineering and biomedical fields. Additionally, tetrapods can be used as templates to create hybrid and new 3D materials. At NanoSYD, he is heading 'Smart Materials' group with the focus to develop new materials for green and sustainable technologies.

Publications > 220, Citations> 10000, H-index: 56

https://portal.findresearcher.sdu.dk/en/persons/Mishra

https://scholar.google.com/citations?user=TW4Bq_oAAAAJ&hl=en

Burc Misirlioglu was born in İstanbul. He received his B.Sc. and M.Sc. in Metallurgy (1998) and Materials Science (2001) from İstanbul Technical University. He obtained his Ph.D. degree from University of Connecticut in 2006. He was with Max Planck Institute of Microstructure Physics followed by a researcher position at MIT during 2007–2008. Since 2008, he has been a faculty member in the Faculty of Engineering and Natural Sciences of Sabanci University, İstanbul, Turkey.Professor with a demonstrated history of working in the higher education industry. Skilled in Mechanical Properties, Materials, Semiconductors, Interfaces, and Characterization. Strong education professional with a Ph.D. in Materials Science from University of Connecticut.

Our research is centered around understanding the effects of defects and microstructure on the physical properties of functional oxides. Using continuum level computational and experimental approaches, we try to reveal the mechanisms by which defects and interfaces impact the physical properties and at what magnitude this occurs. Such knowledge is the key to design and fabricate structures in various geometries for specific engineering applications. The applications governed by such phenomena encompass macro- and micro-scale capacitors for electric energy storage, non-volatile solid state memories, nanoscale devices and electrooptical thin films.

Associate Professor Dr. Fabienne Dumoulin first started university studying biology, graduated in biochemistry and then completed her PhD in organic chemistry in Lyon, France in 2002. After post doctoral studies in Pisa, Italy, she was a faculty member at Chemistry Department of Gebze Technical University from 2005 to 2019. She is now associate professor at Acıbadem Mehmet Ali Aydinler University in Istanbul,Turkey.

Her research focuses on the chemistry, properties and applications of phthalocyanines, mainly for photodynamic therapy. She has authored so far 82 research articles, three book chapters, and supervised many Master and PhD students. Fabienne has also been the recipient of several Young Scientist Awards: TUBA-GEBİP from the Turkish Academy of Sciences, BAGEP from the Bilim Akademisi and the Mustafa N Parlar Foundation of METU. She was elected officer of the executive committee of the European Society for Photobiology in 2015 and 2017, is an Associate Editor for *RSC Advances* and the *Journal of Porphyrins and Phthalocyanines*, and is a Member of the Royal Society of Chemistry.

Fayaz Hussain joined the department of Materials Engineering in 2007, first as a Lecturer, then after Assistant Professor in 2010 and promoted as an Associate Professor in 2020. Prior to this, he worked three years in metal industry. He is also editorial board member of journals of "Frontiers in Materials" and "Electroactive Materials". He has completed his PhD from the University of Sheffield, England, UK, in 2016-2017, worked on "KNN based lead-oxide free piezoelectric ceramics". This ABO3 system has been studied from the perspective of optimizing its performance for multilayer actuators; potentially for energy harvesting applications under the supervision of Professor Ian Reaney at the University of Sheffield. To fabricate the multilayers, a novel Wet-Multilayer-Method (WMM) was also developed to overcome the issues of delamination during firing of multilayers actuators. He has authored/co-authored publications in well reputed journals, around 30 papers including key articles on piezoelectric, capacitor and microwave dielectric ceramics in bulk and multilayers with 238-citations, h-index 8 and i10-index 6 of last five years. Current research interests: ynthesis of Piezoelectric Ceramics and their multilayers, Multiferroics, Thermoelectric Ceramics and Microwave dielectrics. Characterisation Methods: LCR, impedance spectroscopy, d33 meter for piezoelectric coefficient, Vibrating Sample Magnetometer for magnetic properties, XRD Analysis, SEM/ EDX, ferroelectric testing, etc.

Prof. Cenk Aktas earned his BSc and MSc in Materials Science and Engineering from Middle East Technical University-Turkey and Christian-Albrechts University-Germany, respectively. He joined Leibniz Institute for New Materials (Leibniz-INM) in 2004. After completing his PhD with distinction (summa cum laude) he was appointed as the Deputy Head of CVD Research Division. Between 2010-2015, Aktas acted as the Director of CVD/Biosurfaces Division at Leibniz-INM, which is situated in Saarbrücken/Germany. In addition to his academic duties (acting as senior instructor at Saarland University and Applied University of Kaiserslautern), he gained invaluable experiences at Leibniz-INM since it is a well-known scientific partner to national and international institutes and a provider of research and development for companies throughout the world. Aktas also acted as advisor and instructor in several professional training programs of various institutions including German Chemistry Society, Korean University of Technology, European Postgraduate School and etc. Currently he is carrying out research activities on synthesis of functional nanomaterials and their potential applications in diverse fields including energy, medicine, textile, surface, and composite technologies at the Institute of Materials Science, CAU-Kiel In addition, he acts as the PI at Cardiovascular Materials Laboratory at UdS-Homburg and is giving lectures in the Medical Faculty, UdS-Homburg. Aktas has been involved in various projects funded by EU, DFG, BMBF and similar public institutions.. Aktas published more than 70 research papers and 10 patents in different fields (on nanomaterials and nanotechnology). He has several prestigious awards including Prof. Werner Petersen Award, Prof. Horst Hardt Award, Prof. Baki Komsuoglu Award, International Nanomedicine Foundation Award and etc.

SCIENTIFIC COMMITTEE

Prof. Dr. Igor Gennadievich Sızov, East-Siberian State University of Technology, Russia

Prof. Dr. German Anibal Rodriguez Castro, Instituto Politecnico Nacional, Mexico

Prof. Dr. Michal Kulka, Poznan University of Technology, Poland

Prof. Dr. Mourad Keddam, University of Science and Technology Houari Boumediene, Algeria

Prof. Dr. Danute Vaičiukynienė-Palubinskaitė, Kaunas University of Technology, Lithuania

Prof. Dr. Beata Podkościelna Podkoscielna, Maria Curie-Skłodowska University, Poland

Prof. Dr. Rabia Almamlook, Western Michigan University, USA

Prof. Dr. Nodar Lekishvili, Ivane Javakhishvili Tbilisi State University, Georgia

Prof. Dr. Karima Akool AL-Salihi, Al Muthanna University, Iraq

Prof. Dr. Kaveh Ostad-Ali-Askarı, Isfahan University of Technology (IUT), Iran

Prof. Dr. Svetlana Lilkova-Markova, University of Architecture, Civil Engineering and Geodesy, Bulgaria

Assoc. Prof. Bassam Tayeh, Islamic University of Gaza, Palestine

Dr. Avinash Lakshmikanthan, Nitte Meenakshi Institute of Technology, India

Dr. Vijay Kumar S, Nitte Meenakshi Institute of Technology, India

Dr. Manjunath Patel G C, PES Institute of Technology and Management, India

Dr. Fatma Mourgan, Sohar University, Oman

Dr. İhsan Murat Kuşoğlu, Duisburg-Essen University, Germany

Dr. Eng. Massimo Rogante, Rogante Engineering Office, Italy

Prof. Dr. Erol Kam, Yıldız Teknik University, Turkey

Prof. Dr. Ender Sarıfakıoğlu, Çankırı Karatekin University, Turkey

Prof. Dr. Bahri Ersoy, Afyon Kocatepe University, Turkey

Prof. Dr. Tayfun Uygunoğlu, Afyon Kocatepe University, Turkey

Prof. Dr. Osman Gençel, Bartın University, Turkey

Prof. Dr. AdemÇiçek, Ankara Yıldırım Beyazıt University, Turkey

Prof. Dr. Galip İçduygu, Giresun University, Turkey

Prof. Dr. Betül Taşdelen, Tekirdağ Namık Kemal University, Turkey

ORGANIZING COMMITTEE

Prof. Dr. Atilla Evcin, Afyon Kocatepe University, Afyonkarahisar, Turkey

Prof. Dr. İbrahim Güneş, Giresun University, Giresun, Turkey

Doç. Dr. Atila Gürhan Çelik, Giresun University, Giresun, Turkey

Doç. Dr. Soner Savaş, Erciyes University, Kayseri, Turkey

Doç. Dr. Ayşe Kalemtaş, Bursa Teknik University, Bursa, Turkey

Doç. Dr. Harun Güney, Ibrahim Çeçen University, Ağrı, Turkey

Doç. Dr. Ali Günen, Iskenderun Tecnical University, Iskenderun, Turkey

Doç. Dr. Ziya Özgür Yazıcı, Afyon Kocatepe University, Turkey

Prof. Dr. Ilker Bekir Topçu, Osmangazi University, Eskişehir, Türkiye

Prof. Dr. Bahri Ersoy, Afyon Kocatepe University, Afyonkarahisar, Turkey

Dr. Yasemin Tabak, TUBITAK MAM, Gebze, Turkey

Dr Zeynep Taşlıçukur Öztürk, National Defence University, Istanbul

Prof. Dr. Mourad Keddam, University of Science and Technology Houari Boumediene, Algeria

Prof. Dr. Beata Podkościelna Podkoscielna, Maria Curie-Skłodowska University, Poland

Prof. Dr. Svetlana Lilkova-Markova, University of Architecture, Civil Engineering and Geodesy, Bulgaria

Dr. Vijay Kumar S, Nitte Meenakshi Institute of Technology, India

Prof. Dr. Michal Kulka, Poznan University of Technology, Poland

Prof. Dr. Kaveh Ostad-Ali-Askari, Isfahan University of Technology (IUT), Iran

Prof. Dr. Rabia Almamlook, Western Michigan University, USA

Prof. Dr. Nodar Lekishvili, Ivane Javakhishvili Tbilisi State University, Georgia

SECRETARIAT

Oğuzhan Evcin

Abdullah Alawadhi

Nuriye Kalkmaz

Ebru Özkara

CHARACTERISING THE POTENTIAL OF PHTHALOCYANINES FOR PHOTODYNAMIC THERAPY

Fabienne Dumoulin[1*]

[1] Acıbadem Üniversity, Medical Engineering Department, Turkey

The fascinating properties of phthalocyanines made them useful in a full range of applications, either for environmental, energy-related, and also biomedical applications. Their maximum absorption makes them particularly interesting as photosensitisers for photodynamic therapy because it matches the phototherapeutic window, allowing excitation at wavelengths that do not excite endogeneous chromophores and deeper tissue penetration of the light.

After an introduction on the general use of phthalocyanines in various applications, we'll focus on their characterization as photosensitisers for photodynamic therapy.

Keywords : Photodynamic therapy, Phthalocyanines, Photosensitisers

* Fabienne.Dumoulin@acibadem.edu.tr / dumoulin.fabienne@gmail.com

INVESTIGATION OF GREEN COMPRESSION STRENGTH AND GREEN SHEAR STRENGTH IN GREEN SAND MOULD USING ANT HILL SLIT AS A PARTIAL REPLACEMENT OF FOUNDRY SAND USING RESPONSE SURFACE METHODOLOGY

Prasad Chandran N [1], Manoj D. Naik [2], Manjunath Patel GC [3], Avinash Lakshmikanthan [4], Ganesh R. Chate [2]

[1] Department of Mechanical Engineering, Sahyadri College of Engineering and Management, Manglore 590006, Visvesvaraya Technological University, Belagavi 590018, India

[2] Department of Mechanical Engineering, KLS Gogte Institute of Technology, Belagavi 590006, Visvesvaraya Technological University, Belagavi 590018, India

[3] Department of Mechanical Engineering, PES Institute of Technology and Management, Shivamoga, Visvesvaraya Technological University, Belagavi 590018, India.

[4] Department of Mechanical Engineering, Nitte Meenakshi Institute of Technology,Bengaluru, Visvesvaraya Technological University, Belagavi 590018, India.

Abstract

In sand casting foundry, quality of sand mould is very important to get a high-quality casting. The present work is focussed on partial replacement of foundry sand by Ant hill clay (slit) and also to get good sand mould properties which in turn will give defect free castings. The, responses such as green compression strength (GCS), green shear strength (GSS), mould hardness number and permeability were studied. The factors considered for experimentation were Ant hill to Sand ratio (Ant hill quantity in terms of Percentage weight of sand), number of strokes, water quantity and coal dust. Experiments were carried out using central composite design of response surface methodology which is a part of Design of Experiments. Two replicates were done and also randomization and blocking is implemented during experimentation. The optimization is carried out to maximise GCS, Green Shear Stregth. The multi-objective optimization is done to get a same settings for both GCS and GSS.Thus obtained settings of factors were not there in experimental desig matrix, hence the confirmation tests wereconducted. The five confirmation test were carried out and the average Green Compression stregth was 1502gms/cm^2, the optimum level of GSS average valve of Green Shear Shtregth was 356gm/cm2 because of the conflection requirements of both GCS and GSS, multi objectives optimization is done by using discribable function approach and level for this average values 1373 gms/cm^2 and 335gms/cm^2.From optimized levels, 15% of sand can be replaced with ant hill clay without the need of bentonite.

Keywords: Sand Casting, Cental Composite Design, Ant Hill Slit, Green Compression Strength, Design of Experiments, Optimization.

BUCKLING ANALYSIS OF AXIALLY LOADED NANOBEAMS RESTING ON A ROTATIONAL ELASTIC FOUNDATION

Svetlana Lilkova-Markova [1]*, Dimitar Lolov [2]

[1] University of Architecture, Civil Engineering and Geodesy, Faculty of Hydraulic Engineering, Departmant of Technical Mechanics, Sofia, Bulgaria

[2] University of Architecture, Civil Engineering and Geodesy, Faculty of Hydraulic Engineering, Departmant of Technical mechanics, Sofia, Bulgaria

dlolov@yahoo.com

lilkovasvetlana@gmail.com

1. Introduction

Nanostructures are applied in various fields of industry – in nanoelectromechanical systems, biotechnology, aerospace, chemical sensors. The study of the mechanical behavior of nanobeams is not possible with the classical theory of continuous media. The nonlocal elasticity theory, the strain gradient elasticity theory, the modified couple stress theory and the surface elasticity theory are applied to nanomaterials [1]. The Eringen's theory of elasticity is applied in [2] to study the stability of a nanotube with different types of supports. The nanotube is divided into segments. In the analysis the exact solutions in each of the segments was used. Numerical examples have been solved. In [3] were examined cantilever nanobeams with a rectangular cross-section and the presence of cracks. The local theory of elasticity was used. An analytical solution and a parametric numerical study were performed to determine the buckling critical force. An analytical solution for bending, vibration and the buckling of a functionally graded nanobeams lying on a Winkler/Pasternak elastic foundation was presented in [4]. Two models of the nanobeam - a Timoshenko and an Euler-Bernoulli beam were considered. The nonlocal gradient theory and the principle of Hamilton were applied. The Eringen's nonlocal theory is applied to study the buckling behavior of a tapered nanobeam on a Winkler and rotational elastic foundation [5]. The differential equations are solved using the Chebyshev collocation method. The critical values of the compressive force on the beam are determined according to the parameters of the elastic base, geometrical characteristics of the nanobeam and boundary conditions.

An Euler-Bernoulli nanobeam lying on a Winkler elastic foundation and on different supports at both ends was studied in [6]. The small scale effect and the Eringen's nonlocal theory are taken into consideration. It was found that for clamped-clamped ends of the nanobeam and large values of the Winkler elastic foundation parameter, the effect of the small parameter is significant. A parametric study of the mechanical behavior of a nanobeam on an elastic foundation is presented in [7]. An analysis of the results for the vertical displacements, the critical force and the values of the natural frequency is presented.

The theoretical and atomistic simulations are presented in connection with the buckling of a Cu nanobeam subjected to uniaxial compression [8]. The critical strain of buckling, maximum defection and nominal failure strain are obtained. The stability of a multilayer nanopipe at different types of supports - stuttering - stuttering, stuttering - free end, stuttering - joint is studied in [9]. The nonlocal strain gradient theory is applied. The aim of the present study is to

determine the critical force for a simply supported nanobeam lying on a rotating elastic foundation.

1. Problem formulation

The present paper considers an Euler-Bernoulli nanobeam of length l, resting on a rotational elastic foundation and under an external axial compressive force F. The beam, shown in Fig.1, is hinged at its both ends.
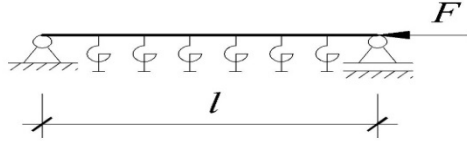
Fig. 1 *Static scheme of the investigated nanobeam*

The governing equation for the buckled slender beam, lying on a rotational foundation has the form:

$$EI\frac{d^4w}{dx^4} + (F - k_G)\frac{d^2w}{dx^2} = 0 \tag{1}$$

where EI is the rigidity of the beam, W is the lateral displacement of its cross-section as a result of the buckling and k_G is the rigidity of the rotational foundation.

The bending moment M of the nanobeam is represented by the function W of the lateral displacement of the axis

$$M = -EI\frac{d^2w}{dx^2} \tag{2}$$

Inserting equation (2) in equation (1), yields:

$$\frac{d^2M}{dx^2} = F\frac{d^2w}{dx^2} - k_G\frac{d^2w}{dx^2} \tag{3}$$

In this paper the nonlocal elasticity theory is employed for the stability analysis of the nanobeam. According to it the following holds:

$$M - (e_0 a)^2 \frac{d^2M}{dx^2} = -EI\frac{d^2w'}{dx^2} \tag{4}$$

where e_0 is experimentally determined material constant. a is also a constant, which denotes the characteristic internal length (lattice parameter and granular distance) of the material of the nanobeam.

$$M = (e_0 a)^2 \left(F \frac{d^2 w}{dx^2} - k_G \frac{d^2 w}{dx^2} \right) - EI \frac{d^2 w}{dx^2} \tag{5}$$

$$(e_0 a)^2 \left(F \frac{d^4 w}{dx^4} - k_G \frac{d^4 w}{dx^4} \right) - EI \frac{d^4 w}{dx^4} = F \frac{d^2 w}{dx^2} - k_G \frac{d^2 w}{dx^2} \tag{6}$$

$$EI \frac{d^4 w}{dx^4} - (e_0 a)^2 (F - k_G) \frac{d^4 w}{dx^4} + (F - k_G) \frac{d^2 w}{dx^2} = 0 \tag{7}$$

The differential equation for transverse displacements acquires the form:

$$\left[EI - (e_0 a)^2 (F - k_G) \right] \frac{d^4 w}{dx^4} + (F - k_G) \frac{d^2 w}{dx^2} = 0; \tag{8}$$

$$\frac{d^4 w}{dx^4} + \frac{(F - k_G)}{EI - (e_0 a)^2 (F - k_G)} \frac{d^2 w}{dx^2} = 0. \tag{9}$$

To simplify the equation, a new parameter is introduced:

$$k^2 = \frac{(F - k_G)}{EI - (e_0 a)^2 (F - k_G)} \tag{10}$$

Thus the following equation is obtained:

$$\frac{d^4 w}{dx^4} + k^2 \frac{d^2 w}{dx^2} = 0. \tag{11}$$

The solution of (11) has the form:

$$w(x) = C_1 \cos kx + C_2 \sin kx + C_3 x + C_4 \tag{12}$$

The boundary conditions for the nanobeam in Fig. 1 are:

$$\left| \begin{array}{l} w(0) = 0 \\ w''(0) = 0 \\ w(l) = 0 \\ w''(l) = 0 \end{array} \right.$$

(13)

Equation (13) represents a system of four homogeneous linear equations for the unknown integration constants $C_1 ;...; C_4$. In order to have a non-zero solution for the function of the lateral displacement w of the beam, the determinant of the coefficients in front of integration constants must be equal to zero. As a result the following equation is obtained:

$$\sin kl = 0$$

(14)

The solution of this equation is:

$$kl = n\pi; \quad n = 1, 2,...$$

(15)

For the function of the lateral displacement is obtained the following:

$$w(x) = C_2 \sin kx$$

(16)

From equations (10) and (15) could be obtained the critical force. The minimal critical force for the nanobeam is obtained when $n = 1$:

$$F_{cr} = k_G + \frac{\pi^2 EI}{l^2 + \pi^2 (e_0 l)^2}$$

(17)

3. Results and Duscussion

Numerical studies have been carried out for the nanobeam in Fig. 1

The geometric and the material characteristics of the beam are: Young's modulus $E = 200 GPa$, the length of the beam $l = 400 \; nm$. The cross section of the beam is circular with radius R. The nonlocal parameter $e_0 a = 1,5 \; nm$.

For a nanobeam with a radius of the cross-section $R = 5nm$ is obtained the critical force for different values of the rigidity of the rotational foundation. The results are shown in Fig.2.

It is obvious that the rotational foundation has a stabilizing effect over the beam - with increasing the rigidity of the foundation the critical force increases.
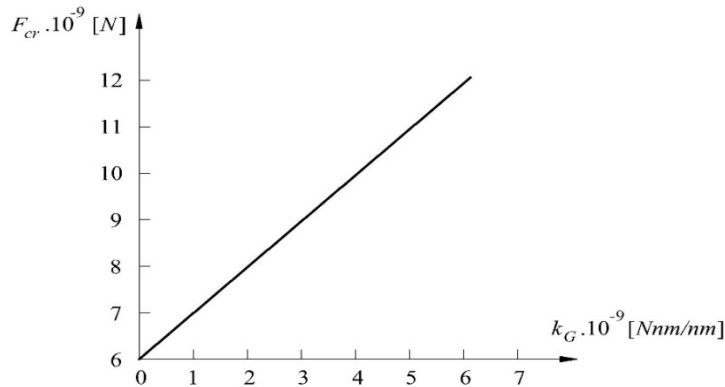
Fig. 2 *Critical force versus the rigidity of the rotational elastic foundation*

Fig. 3 shows the numerical results reflecting the relationship between the critical force and radius of the circular cross-section of the nanobeam for different rigidity of the rotational elastic foundation.
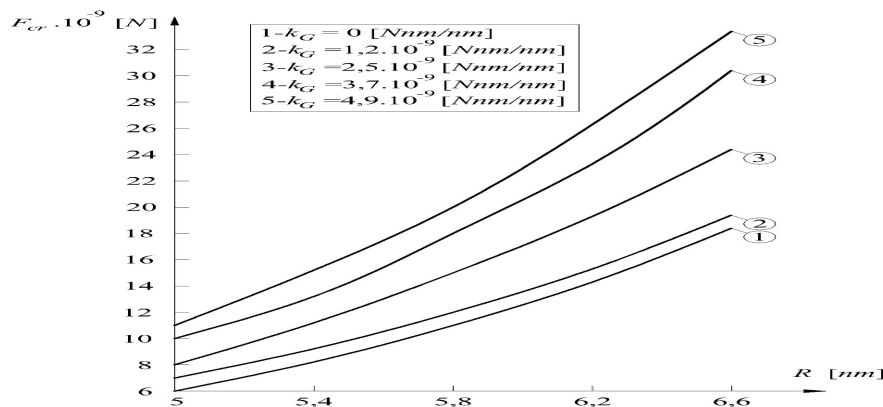
Fig. 3 *Critical force versus the radius of the cross-section*

4. Conclusion
The results from numerical investigation show that for all considered beams the critical force of the nanobeam increases when the rigidity of the rotational foundation is increased. Thus the rotational foundation has a stabilizing effect on the beam.

5. References
[1] A. C. Eringen, Nonlocal Continuum Field Theories. New York: Springer-Verlag, 2002.

[2] W.Glabisz, K. Jarczewska, and R. Hołubowski, "Stability of nanobeams under nonconservative surface loading", Acta Mechanica, vol. 231, pp. 3703 – 3714,   2020.

[3] H. Arif, and J. Lellep, "Buckling analysis of cantilever nanobeams with defects" , Applied Nanoscience, 2021.

[4] D. Hieu, D. Chan, and H. Sedighi, "Nonlinear bending, buckling and vibration of functionality graded nonlocal strain gradient nanobeams resting on an elastic foundation", Journal of Mechanics of Materials and Structures, vol. 16, no. 3, pp. 327 – 346, 2021.

[5] M. S. Sari, W G. Al-Kouz and A. Atieh, "Buckling Analysis of Axially Functionally Graded Tapered Nanobeams Resting on Elastic Foundations, Based on Nonlocal Elasticity Theory".Journal of Mechanical Engineering, vol. 64, pp. 1-11, 2018.

[6] C. Demir, K. Mercan, H. M. Numanoglu, and O. Civalek, "Bending Response of Nanobeams Resting on Elastic Foundation", Journal of Applied and Computational Mechanics, vol. 4, no. 2, pp. 105-114, 2018.

[7] S. Enayat, M. Hashemian, D. Toghraie, and E. Jaberzadeh, "A comprehensive study for mechanical behaviour of functionally graded porous nanobeams resting on elastic foundation", Journal of the Brazilian Society of Mechanical Sciences and Engineering, vol. 42, Article number 420, pp. 1-24, 2020.

[8] J. Guo, Y. Hu, Z. Jiang, X. Liu, and Y. Cai, "A Simplified Model for Buckling and

   Post-Buckling Analysis of Cu Nanobeam Under Compression", Computer Modelling in Engineering & Sciencies, vol. 125, no. 2, pp. 611 – 623, 2020.

[9] M. Alazwari, A. Daikh, M. Houari, A. Tounsi, and M. Eltaher, "On static buckling of multilayered carbon nanotubes reinforced composite nanobeams supported on non-linear elastic foundations" , Steel and Composite Structures, vol. 40, no. 3, pp. 389 - 404, 2021.

TENSILE CHARACTERIZATION OF GLASS FIBER REINFORCED COMPOSITE MATERIALS WITH STRAIN GAUGE AND VIRTUAL EXTENSOMETER

Muhsin Alçı[1*], Recep Güneş[2]

[1] Niğde Ömer Halisdemir Üniversitesi Makine Mühendisliği Bölümü, Niğde, Türkiye

[2] Erciyes Üniversitesi Makine Mühendisliği Bölümü, Kayseri, Türkiye

Abstract

Fiber-reinforced composite (FRC) materials have become the indispensable basic materials of many industries due to their low weight and high strength today. As a result, intensive studies are carried out on the characterization of these materials and the development of material models. FRC materials are subjected to many characterization tests for different material models developed due to their anisotropic structures. The most basic of these are tensile tests. In order to determine the deformation in tensile tests, strain gauges specially produced for FRC materials are generally used. The use of strain gauges can be quite laborious and expensive in characterization studies. Although strain gauges are essential for some application areas, the measurement of strain with the Digital Image Correlation (DIC) method is becoming widespread for tests that can be imaged with the help of a camera today. In the DIC method, measurements can be made on uneven surfaces by taking images with more than one camera at the same time (stereo cameras) by calibrating the cameras. However, since a flat surface can be obtained on the composite in the tensile test, accurate results can be obtained by positioning a single camera directly opposite the measurement surface. In this study; Tensile tests of glass fiber reinforced composites produced by vacuum assisted resin infusion method was carried out according to ASTM D3039 tensile test standard, both with the help of strain gauges and with the help of virtual extensometer using DIC method with a single camera. The results show that a virtual extensometer can be used instead of a strain gauge in tensile tests of fiber-reinforced composites.

Keywords : Fiber Reinforced Composites, Tensile Characterization, Strain Gauges, Virtual Extensometers

* Corresponding Author e-mail : muhsinalci@erciyes.edu.tr

EFFECT OF CURING METHODS ON THE MECHANICAL STRENGTH AND DURABILITY OF PREFABRICATED CONCRETES INTENDED FOR ALGER MARITIME QUAY

Ben AmmarBen Khadda [1]

[1] Mohamed Khider University, Civil and Hydraulic Engineering Department, Biskra, Algeria

author e-mail: b.benammar@univ-biskra.dz

1. Introduction

The needs of the modern world require producing more, faster and cheaper, it's the prefabricated concrete. In order to accelerate the setting and hardening concrete treatments prominently among the different possible methods. Atmospheric steam curing is a heat treatment which has been used for many years to accelerate the strength development of precast concrete products [1]. The curing temperature will be a compromise between rate of strength gain and ultimate strength, because of the higher, the curing temperature, the lower and the ultimate strength [2]. [3] Concluded that in the delay in the commencement of steam curing operation by a period equal to the initial setting time of cement, higher strengths were obtained when the delayperiod was equal to the setting time. To fix ideas, we may admit that in the absence of any external load, the minimum strength to compressive should be located around 50 to 60% of the required strength (at 28 days under natural conditions) is 10 MPa [4]. In order to evaluate the carbonation potential of concrete in the laboratory, accelerated tests are carried out which involve submitting samples at CO_2 concentrations well above the "natural" concentration of the air, generally after a thermal pretreatment for packaging water. The required objective is to evaluate through experiments the influence of atmospheric steam curing on the mechanical strength of concrete and In the light of what has been mentioned above, the characterization of the open porosity of the zone of the concrete of coating of these concretes put into carbonation **[5]**.

2. Experimental program

2.1 Materials

Two cements from the clinker same are used: CEM I 42.5 and CEM II/B 42.5 (Biskra - Algeria). Fineness = 3300 cm2/g, apparent density = 1215 kg/m3 and specific density = 3150 kg/m3.
The water is drinking water and having a temperature of 20 ± 1°C. Its quality conforms to the requirements of standard NFP 18-404.
The sand used is from the region of Biskra. Apparent density = 1630 kg/m3. Specific density = 2650 kg/m3, Fineness modulus = 2.82
We used crushed stone fraction 3/8, 8/15 and 15/25 mm of the region. Apparent density = 1340 kg/m3, Specific density = 2610 kg/m3.

2.2 Study of the temperature in the steam curing chamber and at ambient air

Our study is first to raise the temperatures in the open air using a thermometer and within the confines of conservation by other thermometers hourly and daily same time of 07 h to 21 h for 12 months of the year, the average of these monthly records are illustrated in fig. 1.
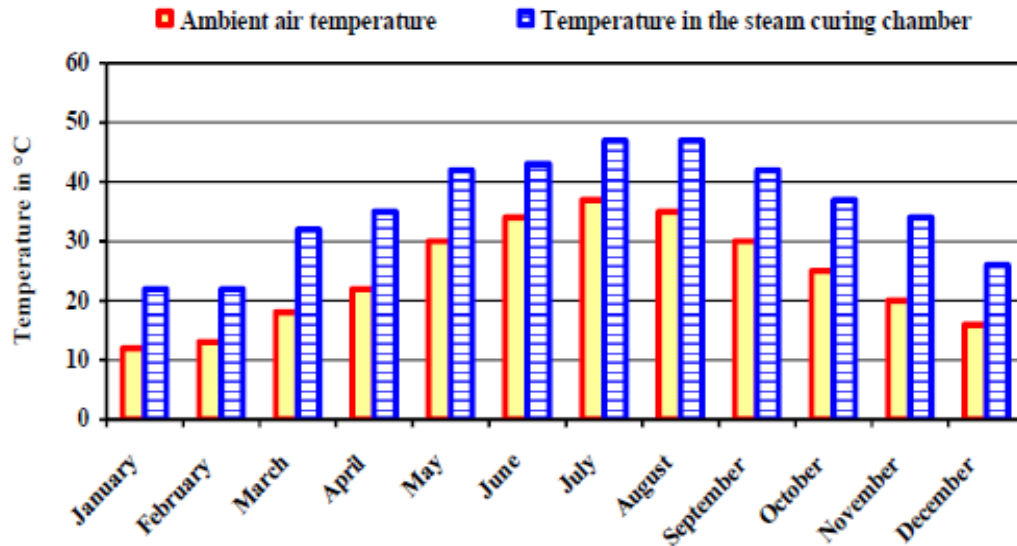
Figure 1: Monthly exchange in outdoor temperatures and the steam curing chamber

2.3 Formulation of concrete

Optimizing the formulation of concrete based on several criteria that are often a compromise between them: consistency, strength, durability and economy. The method of formulation is B. Scramtaiv (cone slump of 7 cm). In all tests the w/c = 0.4, A = 0.6, Dmax = 25 mm and S/CS = 0.33, (Table 1).

Table 1: Composition of concrete (Kg/m3)

Cement	Sand	Crushed stone (7/15)	Crushed stone (15/25)	Water
512	407	432	802	205

From the graphs of the temperature variation with time of 12 months, we can say that for six months from April to September, the average temperature (K1 = 1.70), and October to March, the average temperature is: (K2 = 1.40). K: the average temperature (K = 1.55). Based on the findings deduced from the variation curves of temperature versus time inside the chamber, we select the six months which corresponds to the seasons: spring and summer (Table 2) and autumn – winter (Table 3).

Table 2: maximum temperatures in the room (spring-summer)

Month	Apr	May	Jun	Jul	Aug	Sept
Cycles	3×8×3	3×8×3	3×8×3	3×9×3	3×9×3	3×8×3
Max. T°	38	43	44	46	48	43

We opt for cycle 1: (3×8×3) (45 °c).

Table 3: maximum temperatures in the room (autumn - winter)

Month	Oct	Nov	Dec	Jan	Feb	Mar
Cycles	3×8×3	3×7×3	3×7×3	3×7×3	3×7×3	3×8×3
Max. T°	34	32	30	28	23	34

We opt for cycle2: (3×7×3) (29°c).

2.4 Preparation of specimens

The strength is expressed by the power of concrete to resist destruction under the action of stresses due to different compressive strength. Specimens of cubic (100×100×100 mm) to determine the compressive strength.

The concretes studied: a control concrete stored in water at an ambient temperature of $20 \pm 1°c$, concrete cured outdoors without irrigation, and concretes subjected to two cycles of steam curing. After mixing the concrete, demolding, the specimens are introduced into the steam curing chamber by solar energy with the rise of the temperature in the chamber, the thermometer was placed outside of the chamber can adjust the temperature level selected at 45°c in the chamber for the warm period of the year. (6 months from October to March) and 29°c for the cold period (6 months from April to September), for durations of steam curing 1, 2, 3 and 7 days hardening in open air without spraying of 3 and 7 days.

2.5 Accelerated laboratory carbonation test

Carbonation tests were conducted using two different protocols to compare their respective results and analyze the relevance of the accelerated test.

Then the samples of concrete are removed from the enclosure and weighed. From the splitting of the specimens, the depth of carbonation is measured on fresh fractures using a color indicator of pH.

Figure 2: (a) Accelerated carbonation chamber; (a) Specimens in the carbonation chamber under accelerated conditions

2.5.1 Detection of the depth of carbonation by phenolphthalein

To evaluate the depth of carbonation, we mainly used the phenolphthalein test AFGC-AFREM [6], (figure 3).
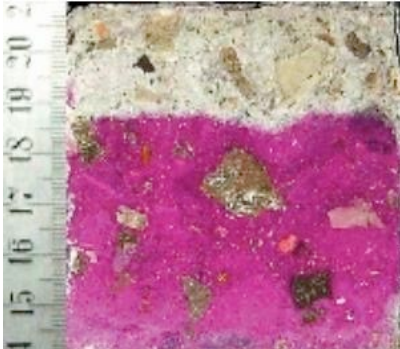
Figure 3: Phenolphthalein test and measurement of the carbonation front

After a few minutes, the depth of carbonation is measured, for each face, according to the procedure of AFPC-AFREM [7]. We have grouped together all the results of the phenolphthalein tests and the measurement of the carbonation fronts of the different concretes at different times in fig 4.

Figure 4: Demonstration of the carbonation fronts visualized following the spraying with phenolphthalein.

3. RESULTS AND DISCUSSIONS

3.1 Consistency
The slump test to Abrams cone NF P 18-451 is currently in use worldwide. Depending slump obtained, class consistency of different concrete is plastic (slump varies from 6 to 8 cm).

3.2 Compressive strength
The strengths are estimated at 1, 2, 3 and 7 days of steam curing, 28 days in wet and dry. The results of compressive strength of concrete in water, the open air and concretes having undergone a steam curing (figure 5: a, b, c and d).
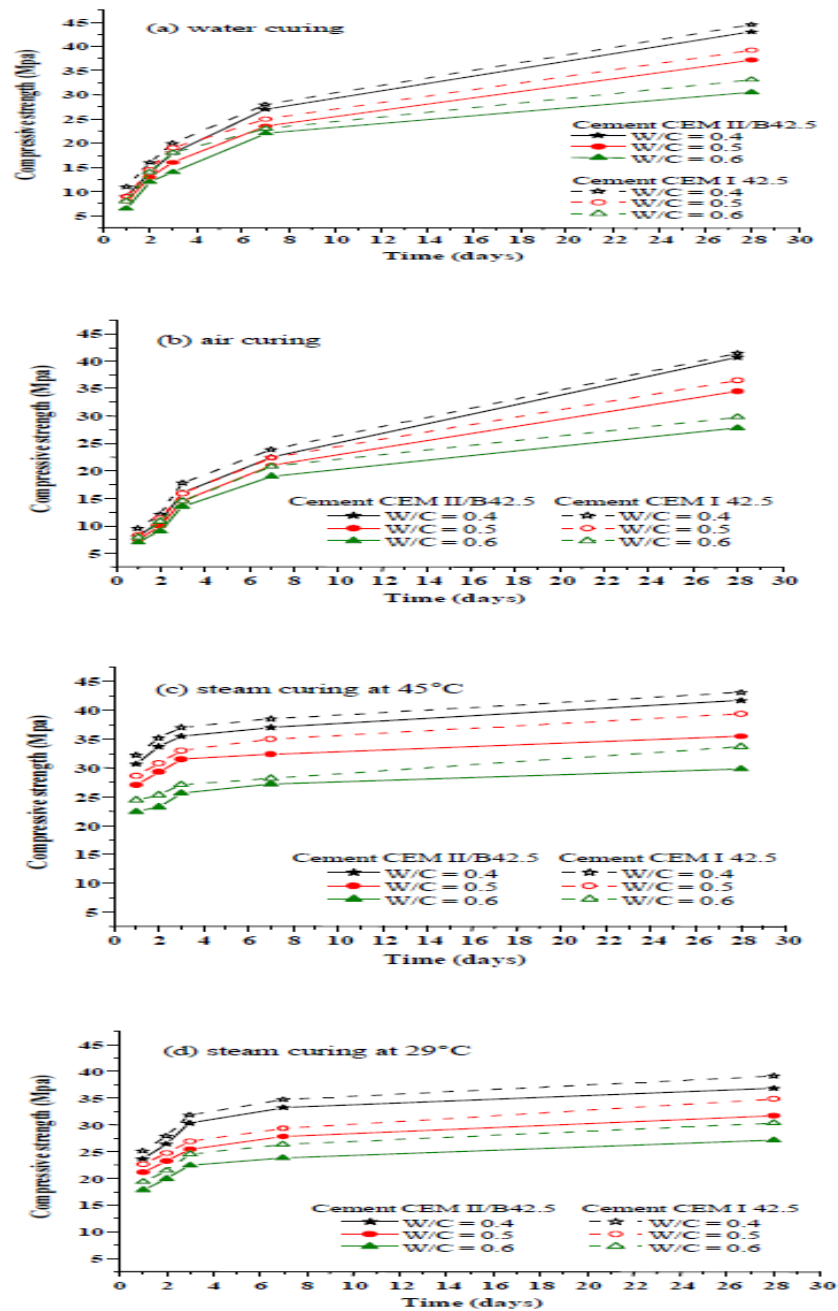
Figure 5 : Effects of curing methods, cement type and w/c ratio on the compressive strength

3.3 Extension of hardening of concrete in the open air

1) One day of steam curing at 45°c and hardening of 3 and 7 days

The strengths estimated from (1d steam curing and air 3 days) and (1 day steam curing and air 7 days) for steam curing at 45°c are shown in table 4.

Table 4. Compressive strength of concrete (1 day steam curıng at 45°c + aır 3 and 7 days)

Strength (MPa)	1 d steam curing + air 3 d	(%) harden	1 d steam curing +air 7 d	(%) harden
Compressive	40	99	43	105

2) One day of steam curing at 29°c and hardening of 3 and 7 days
The strengths estimated after (1 day of steam curing and air of 3 days) and (1 day of steam curing and air 7 days) for steam curing at 29°c are shown in Table 5.

Table 5. Compressive strength of concrete (1 day of steam curıng at 29°c + aır 3 and 7 days)

Strength (MPa)	1 d steam curing + air 3 d	(%) harden	1 d steam curing + air 7 d	(%) harden
Compressive	39.30	96.50	41	100

3 RESULTS AND INTERPRETATIONS

3.1 Influence of the w/c ratio and cement type on the accelerated carbonation depth

Figures 6 (a) and 6 (b) show the results of varying the carbonation depth at the age of 28 days of the various concretes, as a function of the w/c ratio. That is an increasing function of the w/c ratio. In other words, the w/c ratio increases with the depth of carbonation.

This depth is maximal for uncured concrete with a water/cement ratio of 0.6 which has a remarkable effect on the carbonation kinetics by reducing about twice the carbonation depths reached in the case of water conservation and this for the 02 types of cements.
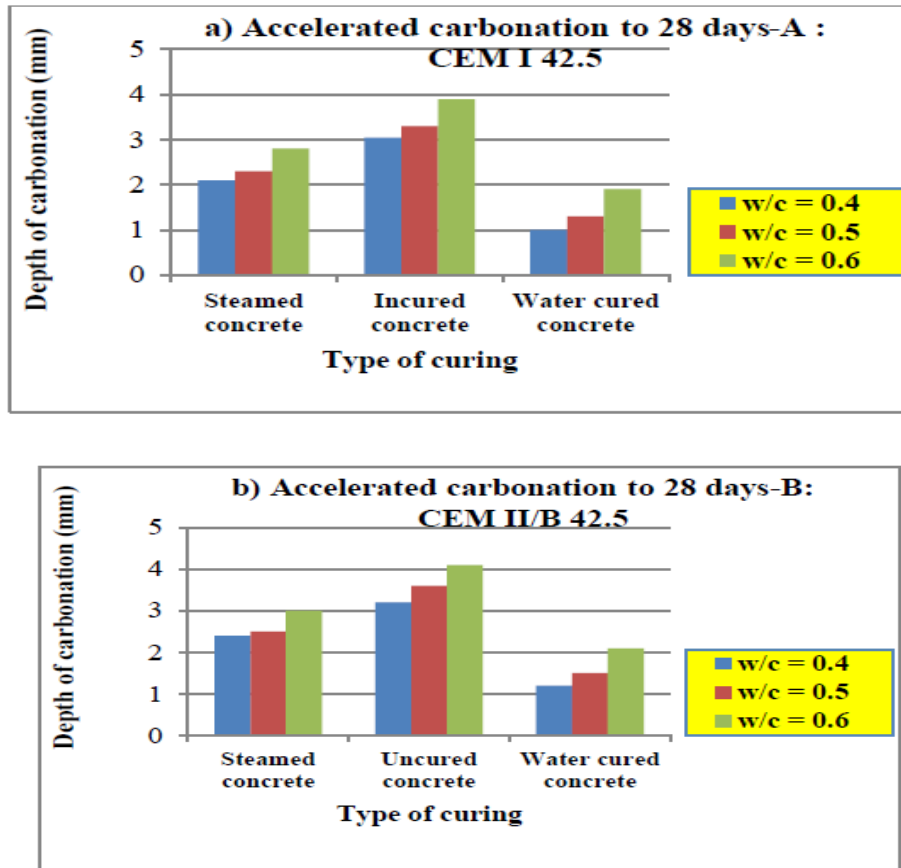
Figures 6 (a, b): Evolution of accelerated carbonation depth

4. Conclusion

- The technique of steam curing is an effective technique for Portlands cements for accelerated hardening of concrete.
- The demolding is assured after all steam curing at 45 or 29°c, since we met exceeds the minimum strength to compressive which is approximately 10 MPa after one day of steam curing, which ensures high productivity molds.
- We reached the 28 days strength after one day and 3 days of hardening in open air, for 02 types of steam curing, which has a gain of time and shorter manufacturing lead times.
- This hardening technique which is rich in solar energy and the use of this renewable energy in the heat treatment of concrete parts in areas with high radiation concentration and long periods, which reduces the cost of concrete parts, resulting in a remarkable economy for production companies.
- Carbonation of concrete is one of the causes of degradation of reinforced concrete structures insofar as it leads to the passivation of armatures for reinforced concretes and their oxidation.

References
[1] Maltais Y, Marchand J. (1997). Influence of curing temperature on cement hydration and mechanical strength development of fly ash mortars. Cement and Concrete Research 1997;27(7):1009-1020.
[2] Mindess S, Young J.F. Concrete. Prentice-Hall, Inc., Englewood Cliffs, NJ. 1981.

[3] Erdem T.K, Turanli L, Erdogan T.Y. (2003). Setting time: An important criterion to determine the length of the delay period before steam curing of concrete. Cement and Concrete Research 2003;33(5):741-745.

[4] ACI 517.2R-87 revised. (1992). Accelerated curing of concrete at atmospheric pressure-state of the art. American Concrete Institute, Farmington Hills Michigan. 1992. 17p.

[5] Haque, M.N. and AI-Khaiat, H... "Carbonation of Concrete Structures in Hot Dry Coastal Regimes". Cement and Concrete Composites, 19 (1997) 123-129.

[6] AFGC AFREM « Méthodes recommandées pour la mesure des grandeurs associées à la durabilité » Compte rendu des journées techniques AFGC-AFREM, Durabilité des bétons, 1997.

[7] AFPC-AFREM, Essai de carbonatation accélérée, Mesure de l'épaisseur de béton carbonaté, Mode opératoire recommandé par l'AFREM. Compte rendu des journées techniques AFPC-AFREM « Durabilité des bétons », 11 et 12 Décembre 1997, Toulouse, pp:153158.

NEUTRON BEAM ANALYSIS OF AGING AND CREEP PROCESSES IN MATERIALS AND PARTS FROM DECOMMISSIONING OF NUCLEAR FACILITIES

Massimo Rogante [1*]

[1] Studio D'ingegneria Rogante, Contrada San Michele, n. 61 62012 Civitanova Marche (MC) Italy

www.roganteengineering.it

1. Introduction

Ageing and creep resistance, similar to other mechanical properties, depends to a great extent from the nano- and micro-structure formed in the metals. A non-uniform degradation can accelerate the advance of cracks favouring the critical reduction of the lifetime of a component and therefore of the system [1]. Radioactive radiation and high operational temperature may produce significant changes in the nano- and micro-structure of metallic components of NFs - e.g., irradiated materials of the reactor vessel, plates, piping, pumps of the primary circuit, inside components of pumps, pressurizer, vapour generator and welds - and also of non-metallic parts such as those made of concrete for shielding, moreover varying their macroscopic characteristics. A consequence of these changes is the weakening of the mechanical properties that are crucial for safety and lifetime of NFs. Lifetime extension, in particular, is a major economical interest, as the operational cost of a NF, especially of a Nuclear Power Plant (NPP), is not significant as compared to the investment cost. To elongate lifetime, it is essential to get accurate information about structural alterations of the most important construction components.

The usual methods to assess macroscopic properties (primarily, those mechanical) allow measuring the net sum effect of the microscopic variations. The damage produced by the irradiation can be studied on model materials or on specimens belonging to real construction elements. Nuclear safety conditions also include monitoring of the materials' state (i.e., mechanical characteristics) using the tests with control samples of the same materials working in the identical regime - even taking larger forth-coming fluence - to provide an early observation of dangerous trends in the changes of materials' properties. Tests are carried out, furthermore, in which materials or parts sensitive to damage from radiation and whose functional safety characteristics may be undesirably affected by exposure to radiation during exercise, are irradiated to simulate such exposure. Radiation aging, in this case, is performed on the sample under normal and abnormal operating conditions, and it is comparable to what the component is undergoing during employment as regards both the type of radiation and the exposure dose. The said test is carried out also varying key parameters such as types of radiation (that can be applied separately) and exposure rate, always ensuring the absence of effects other than those faced in the operating conditions. In addition to the effects of radioactive radiation, those of temperature should be taken into account, which are part of the main factors that determine ageing and creep processes. New machine learning platforms, moreover, have been recently set up to detect and quantify radiation-induced defects of parts and testing materials in nuclear reactors [2].

The measurements on model materials, anyhow, need to be linked with complementary measurements on real structural materials, as the irradiation damage strictly depends on various

factors such as the used technologies and the concentration of alloys' components.

In addition to the measurements on model materials, traditional investigation methods involved by the existing norms for the NPP sector include mechanical tests - that allow measuring only the alterations of macroscopic properties -, X-rays and mechanized ultrasonic investigations concerning pre-service inspection and phased array ultrasonic testing. The obtainable information, however, is not exhaustive and requires to be completed. In this context, NBT present significant advantages in comparison with the classic methods of materials' analysis and fractography, contributing to solve essential problems linked with the methodological limitations of these methods [3, 4].

A unique chance to perform advanced analyses of really aged materials and components is represented by NF decommissioning (e.g., old NPPs with gas-cooled, graphite-moderated or boiling water reactors), which is usually defined as the cessation of operations and the withdrawal of the NF from service [5]. Decommissioning is also a singular opportunity to exploit innovative diagnostics and carry out actions with the perspective of future installation of new components, with the aim to increase security and consistency.

Despite the risks during this final stage of the NF life cycle are lower than those existing during the plant's operating life, also considering that the process and the auxiliary systems are no longer subjected to the mechanical and thermal stress due to pressure and exercise conditions, researches of accumulated defects in decommissioned materials and parts as dependent on duration and intensity of the irradiation (fluence) are very relevant. Neutron structural studies of the ageing of materials which were submitted to irradiation and other factors (mechanical loading, high temperatures, chemical attacks), in this case, can give a fundamental support. It should be stressed that these nano- and micro-scale defects (vacancies, dislocations, pores and cracks) are resulting from operative conditions (irradiation, mechanical and thermal stress): knowledge of nature and features of these damages, thus, enables understanding the trends of materials fracture and evaluating a latent picture of preliminary degradation processes leading to any fast crash of material.

It is well known that: a lot of the nuclear safety conditions that require careful checks of the preservation state and structural checks of the systems components, in the case of decommissioning, do not exist; the systems that are classified relevant for safety, during the decommissioning phase are very reduced in number and extension and they tend to decrease during this process. Nuclear safety conditions, anyhow, include the monitoring of the state (mechanical characteristics) of materials using the tests with control samples made of the same materials and working in the same regime - even taking larger forth-coming fluence - to provide the early observation of dangerous trends in the changes of materials' properties. A main aim of the investigation by NBT is a subtle analysis of structure of these samples used for monitoring, to find the same structural features like in broken (or very aged) decommissioned materials, which got very high doses of radiation or undergone other actions damaging their structure. The damages that neutron irradiation can have allowed, e.g., to the vessel's structures, are of high interest also when the vessel during the decommissioning is without fuel and it is practically submitted to the only load of its own weight: the study of effects on structure in decommissioned reactor vessels, indeed, can discover in detail the structural transformations of the involved material during a very long period of its exploitation, supplying excellent data to restore the kinetics of structural degradation and elaborating the criteria of durability of the existing reactor equipment. Moreover, it can be taken into account also the fact that the rather limited amount of economical budget sometimes does not allow beginning immediate dismantle of the equipment of the shut down nuclear units without accumulation of sufficient financial

resources, that, alongside with the time needed to build storage and disposals, results in choice of variant with long safe storage of units under surveillance [6].

Although phenomena such as thermal shock under pressure, which are a main concern for the reactors in operation due to the embrittlement of the vessel's materials, may have a reduced importance in the case of decommissioning, a comparative study of structural changes in the original (fresh-prepared) materials and in the fragments of decommissioned materials is very important. Both kind of materials, with this purpose, should be mechanically and/or thermally loaded, to observe the development of embrittlement as induced by structural defects (e.g., nano-phase inclusions, which are clear visible in neutron scattering).

Also if safety authorities have not yet raised the issue of the integrity of the systems in terms that should require NBT, the application of such methods for deep subtle structural analysis of reactor materials is in progress worldwide and the certification of cold neutrons scattering methods, as briefly described in Chapter 2, can be issued as a result of both numerous experiments performed and highly developed data treatment methods. In this perspective, several positive recommendations from the International Atomic Energy Agency (IAEA) exist to employ NBT for reactor materials control.

A main technological and scientific aim in the nuclear sector, finally, is to create a scientific background for the elaboration of widely used effective methods of diagnostics of reactor materials to extend the duration of their safe exploitation.

2. Neutron beam techniques

2.1. Neutrons

Neutrons are elementary particles practically devoid of electric charges, constituting - together with protons - the atomic nucleus. The characteristic of not interacting electrically with electrons and nuclei in matter has the great advantage of being able to penetrate the same matter in depth. In fact, while X-rays offer excellent resolution but are easily absorbed by materials (being able to penetrate only surface layers), neutrons, possessing a linear absorption coefficient about 1000 times weaker than the first, penetrate matter up to several centimetres (about 2-3 cm for steels, about 5-6 cm for aluminium and its alloys).

Neutrons are produced by continuous sources (nuclear reactors) or by pulsed sources (accelerators). In continuous sources, neutrons are produced by the fission reaction of heavy nuclei such as ^{235}U or ^{239}Pu, and are initially characterized by a very high energy; neutrons are subsequently slowed down to thermal energies by means of moderators, then they are subjected to collisions that further slow them down to bring them into thermal equilibrium with the surrounding medium. This thermal equilibrium allows using the energy equipartition theorem as follows:

1/2 mv^2 = 3/2 kT (1)

and also:

λ^2 = h^2/3mkT (2)

where k is Boltzmann's constant, m, v, λ are respectively the mass, velocity and wavelength of the neutron, T is the temperature.

The consequent distribution of neutrons as a function of velocities belongs to the Maxwellian type, and it is such that λ is between 1.55 and 1.33 Å for T in the range 0÷100 °C.

Special guide channels have the task of transferring the neutrons produced from inside the core to the different instruments (e.g., diffractometers and spectrometers).

2.2. Small angle neutron scattering

Small angle neutron scattering **(**SANS) allows an accurate and complete characterisation at the nano- and micro-scale, providing statistically precise information of 10÷1000 Å sized inhomogeneities, averaged over a macroscopic volume. Neutrons' scattering on the sample is comparable to that of the photons, as described by the neutrons' wave optics. In addition, neutrons interact with the magnetic moments of the atoms and allow exploring magnetic inhomogeneities (e.g., different phases), precipitates or voids in the studied parts. Determination of nano- and micro-structure, actually, is an important step in characterising mechanical properties. The following parameters relative to the scattering objects (defects), in particular, can be monitored in materials submitted to irradiation or thermo-mechanical treatments (e.g., creep, fatigue and ageing): size, shape, concentration, volume fraction, area of interface and chemical compound. Fundamental information on chemical or magnetic inhomogeneities such as matrix heterogeneities (gas bubbles, pores and precipitates) can be achieved, considering also the eventual local deviations in composition and technology, supplying information on ageing and degradation levels of the considered materials and parts. The specimen can be studied or measured any number of times after either further usage or treatment. The theoretical bases of the SANS technique can be found in [3, 4, 7-10].

2.3. Neutron diffraction

Knowledge of directional and spatial residual stresses (RS) distribution is necessary to understand material's behaviour, being a decisive factor for safety, quality and service life assessment. Stress concentration should be avoided to increase fatigue life and keep away from material's ageing related phenomena. Neutron diffraction (ND) represents an excellent and complete method for non-destructive and non-invasive strain/stress measurement, able to provide data also including the effects of undesirable thermal variations, which are problematic to be studied only theoretically. In a ND measurement, the interplanar distance, the lattice strain and the stress values can be determined, also with reference to the main axes of the investigated object. Additional information can be attained linked with the number of dislocations and hence with the plastic strain of the investigated material. Any alteration in the FWHM from the reference distribution (on an unstressed sample) may be correlated to the increase of plastic deformation, so the plastic zone may be assessed as the area where the FWHM is over that for the unstressed material. The results, besides the evaluation of the tensile or compressive condition, consent studying the efficiency of post-welding relaxation treatments or the effect of further heat treatment (HT), the RS relaxation fraction at the work temperatures and after a long time, and the RS concentration related to notches and cracks. The theoretical bases of the ND technique can be found in[3, 4, 11-13].

2.4. Prompt gamma activation analysis

Prompt gamma activation analysis (PGAA) is based on the detection of characteristic prompt gamma photons originating in (n,γ) nuclear reactions. Every atomic nucleus, apart from ^{4}He, may undergo a (n,γ) reaction with diverse probabilities and the energies of the emitted γ-photons are characteristic for every given isotope. The gamma peaks intensities are proportional to the amount of a given isotope and this phenomenon allows using a quantitative elemental (isotopic) analysis method known as PGAA or PGNAA (prompt gamma neutron activation analysis). The prompt gamma spectra are recorded using a high purity Germanium detector surrounded with Bismuth Germanate scintillators dedicated to perform the Compton–suppressed measurement mode. The signals coming from the detectors are treated adopting a multichannel analyser and the spectra are evaluated by using a Hypermet-PC; the element identification is based on a prompt gamma library. PGAA consents a quantitative analysis (mass ratios or equally weight-percentage ratios of elements) and a comparison between the investigated samples, carried out by using a principal component analysis, which evidences similarities and differences. The detection limits depend on composition of the investigated specimen and they can be enhanced by increasing the acquisition time. PGAA, due to the high penetrability of neutrons, is able to provide an average composition of the inside material, i.e. of the component in its whole. This technique can be employed, e.g., to examine whole specimens or their fragments. The theoretical bases of the PGAA technique can be found in[3, 14, 15].

2.5. Neutron radiography

Neutron radiography (NR)allows penetrating a sample through a neutron beam, which is attenuated (according to the basic law of radiation attenuation) by the investigated material - also by some light materials such as hydrogen, and lithium - and detected by an imaging device. The obtained information is related to the material and the structure inside the specimen. NR consents, e.g., visualising and measuring material's distribution within macroscopic volumes of cement's samples, as well as defining water's movement through the investigated cements. NR images of concrete structures are also helpful to validate conventional measurements. The theoretical bases of the NR technique can be found in various references, e.g. in [3, 16-18].

3. Examples of applications

Welding is a major source of RS, frequently generating, especially in the heat affected zone (HAZ), large tensile stresses reaching values roughly equivalent to the material's yield strength, balanced by minor compressive RS wherever else in the studied part. Contraction of molten weld metal all through solidification is opposed by adjacent colder metal, thus generating RS. The major problems associated with welding involve the formation of heterogeneities too, typically inducing a lower chemical stability as well as a higher concentration of mechanical defects. The duration of parts submitted to very high temperature, cyclic loadings and/or erosion, therefore, is decreased since creep, fatigue and wear damages in welded zones result enlarged. Intercrystalline and intergranular stress corrosion cracking (SCC), in addition, can appear in narrow welded zones (e.g., in pipes and vessels), due to both RS generated during the production process and possible occurrence of aggressive elements [19].

The global state of the art of welding project processes linked with nuclear/traditional industrial applications consists practically in numerical models reproducing welding procedures and in primary interests in investigating welds to enhance their qualities. New welding project

methods were studied based on both FEM calibrated against conventional experimental results and real key parameters' values obtained through nano- and micro-structural investigations - performed also by NBT - of different welded joints, considering different metallic materials and welding processes [20].

Numerous analyses of welds have been carried out, till now, showing the advantages of exploiting NBT to achieve essential data not available by using other means. SANS and ND allow analysing, e.g., massive and bi-metallic welds, friction welded parts, repair welds and TIG welds, also investigating the effects of radiation on RS and defects' formation. NBT make possible also:

- to study the factors that control the fatigue behaviour of welded components
- to improve analytical methods to assess the total fatigue life of welds submitted to surface treatments and/or exposed to variable-amplitude loading, to find potential means to increase fatigue strength
- to apply probabilistic methods to assess potential nucleation of nano- and micro-cracks within a joint due to fatigue damage processes.
- Knowledge of the inner and sub-surface RS distribution determined by ND in massive samples allows revealing the cause-effect unknown connections between the existing state of a given metallic part and the possible future types of failure under operating conditions. It is possible, consequently, to forecast also the material resistance to crack propagation under operating conditions. To build a suitable failure predictive model e.g., requires the involvement of valid methods for specimen's collection, cataloguing and data analysis [21-23]. An example of RS determination by ND in pipes is shown in Fig. 1, which reports hoop RS (5 mm depth) assessed by ND in a 2.25 Cr1Mo ferritic arc welded pipe before and after relaxation HT [24].
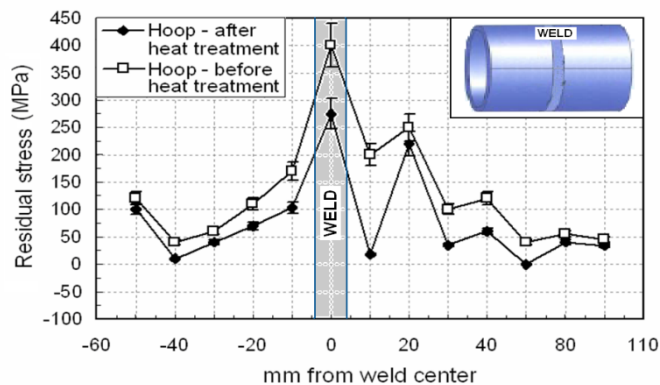
Fig. 1. Hoop residual stresses (5 mm depth) determined by neutron diffraction in a 2.25 Cr1Mo ferritic arc welded pipe before and after HT, with representative geometry of diffraction [24].

Neutron-based investigations of welded joints related to NPPs can be carried out with reference to dismantled parts and new welded joints made of the same constitutive materials. In welded joints of austenitic steel pipes of NPPs, delayed reheat cracking can occur in the HAZ, needing repair if major cracking arises. Such repair welds influence the RS distribution, which is important to know, to evaluate the effectiveness of the repair and to forecast the kinetics subsequent creep damage, and ND can supply crucial information. The greater risk of joints' fracture is due to the non-uniform mechanical stresses and to other factors producing ageing such as fatigue and thermal-related RS produced by HT. Notions of metal fracture and welded joints are currently basically founded on the use of optical and electron microscopy - especially, scanning electron microscopy (SEM) - to examine surface structures and defects in thin slices

[25, 26]. Fracture surface areas and fractal properties of profiles and surfaces were examined as a part of various fracture studies. The concept of fractals was developed underlining the different natural self-similar structures [27]: the two most significant classes of fractal structures are volume fractals (i.e., aggregated clusters of small particles) and surface fractals (i.e., systems with irregular interfaces and grain boundaries). SANS allows verifying the fractal nature of structures and assess the fractal dimensions [28] and can provide key information in investigating turbo-machinery parts and samples of constitutive materials (e.g., Inconel 738, Udimet 520 and Udimet 720), characterizing precipitates in a non-destructive and non-invasive way [29-31], also dependently on temperature, hours of serviceand ageing time: thereby evaluating parameters largely responsible for the functional properties of these parts.Fig. 2 reports the volume distributions of precipitates vs. size, for positions 1 and 9 of two turbine blades made of Inconel 738, one in the as-fabricated state and the other one after 25,000 hours of service, investigated by SANS by adopting a neutron beam cross-section of 3×15 mm^2 [21].
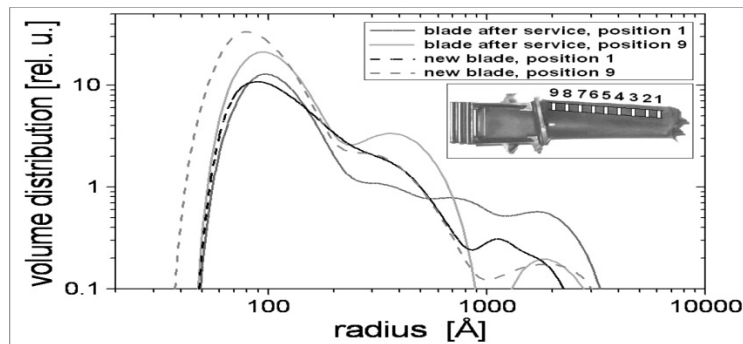

Fig. 2. Volume distributions of precipitates vs. size, for two turbine blades made of Inconel 738, one in the as-fabricated state and the other one after 25,000 hours of service, investigated by SANS [21].

Three populations of precipitates differing by characteristic size are revealed, showing the larger differences along the scan in the blade after service.

To trace nano- and micro-structure alterations disjointedly in materials belonging to reactors of working NPPs (hence, submitted to elevated neutron radiation and severe thermal conditions), structure and precipitate morphology of vessel steel materials were investigated by SANS. Samples cut from 15Kh3MFA steel cracked specimens belonging to standard VVER-440 reactor materials were analysed, after an ageing HT at 295°C for 360 days. An anisotropic precipitate structure formed at the nanoscale level was discovered, due to macroscopic texture, together with the inhomogeneity of the vessel raw material [32].

An AISI 316L steel specimen was submitted to cyclic surface heating and simultaneously cooled by low pressure water flowing through channels across the specimen, simulating thermo–mechanical RS linked with the pulse nature of thermonuclear fusion reactor, in order to assess these RS by ND as a function of depth along a line from surface to central hole axis [33].

Base and welded metal of a 100 mm thickness sample cut out from a 08H18N10T austenite stainless steel plate, wire welded in electric arc and submitted to HT, cooling down in water from the initial temperature of 1050°C, were probed by SANS. The cross sections showed three fractions of point like defects, having a larger amount (by factor 5) in the base metal as compared to the welded one [20].

A feasibility study was performed for a SANS investigation of P91 martensitic steel (9Cr1MoVNb) specimens obtained by cutting 24" pipes, having a thickness of 14 mm and

submitted to 3000÷8000 hours accelerated creep tests consisting in 7,000 start cycles after 100,000 hours with a max. gradient<10°C/min, contained longitudinal welds in straight parts and double axial welds in the connections. The test temperature ranged from ~545°C to ~625°C, while the test pressure was ~50bar. The HT caused the growth of some precipitates, of which SANS allows obtaining information on characteristics (i.e., number and size distribution) by knowing their chemical nature (e.g., Cr_6C_{23} carbides). SANS investigation was considered for samples (including welds) before and after the test, to study nano- and micro-structural changes (e.g., nano-defects and voids). The main aims of this creep tests were:

- to determine, before reaching the 30,000 operative hours, the accelerated data that facilitate the prediction of the stress/strain level at 100,000 hours
- to contribute to the elaboration of constitutive equations (representing the strain as a function of temperature and stresses, also taking into account the voids' changes after HT) able to perform interpretative analyses of effects such as temperature, strain and RS, as a correct step to study the relations with primary/secondary phases of the creep [28].

Austenitic stainless steel with the GOST mark 08X18H10T is adopted, e.g., to built reactor internals, collectors of parogenerators and loop pipelines of the primary circuit. Maintenance and repair of primary circuit components involve high nickel weld filler. RS determination by ND was carried out on NPP construction parts made of austenitic stainless steel coated with high-nickel alloy, in order to prove the mechanical analysis and to verify RS determination on welded material by numerical computer welding simulation. Measurements were performed on 25 and 15 mm thick samples, obtaining normal and transverse RS components [34].

NBT can contribute also to the study of other materials and parts linked with decommissioning of NFs including nuclear waste treatment. Study of dense cements, ceramics and related materials (e.g., cement stones) is significant to create novel advanced components for nuclear–safety related structures, with high functional properties (such as ageing resistance, cracks' formation, hardness, durability, stability of mechanical modules and ecological criteria).These high-performancematerials can be considered as constitutive of corrosion resistive coatings for nuclear waste containers.Knowledge of their thermo-physical properties in broad temperature and moisture ranges is important for realistic modelling of potential accidents in NPPs [35]. Conventional investigations of cements, including those for nuclear industry, use standard methodologies to get information on aspects primarily related to micro-structure, fatigue behaviour and computational mechanics. These investigations rely essentially on standard tests, theoretical studies and simulation-based analyses. Porosity, e.g., is a main parameter for cement, affecting mechanical and heat-insulation features. This parameter is generally assessed through gravimetric techniques, gas and liquid porosimetry (e.g., mercury intrusion porosimetry) and acoustic methods [36]. A campaign of various SANS investigations was carried out by the Rogante Engineering Office on polymer cement concretes made of Portland cement with added nano Al_2O_3 (γ type) mixed with PAV 22 polymer, produced by the Institute of Material Sciences and Metallurgy of the Ural Federal University, Yekaterinburg, Russian Federation. Results concern significant data on basic parameters connected with degradation, fracture and other phenomena: they are related in particular to the size distribution of nano-sized pores, which can help to comprehend the structural basis for the physico-chemical properties and thus to improve quality and durability of the considered materials, allowing a more reliable lifetime assessments. These results can contribute to optimise the material's consistency, the design of operating conditions of structural elements and the design of the procedures that support ecological criteria and enhance quality and safety levels [37-40].

Various other neutron studies have been carried out concerning radiation damages in aged materials of NFs, e.g. [41-44]. The nanostructure of SAV-1aluminum alloy, as constructional

material of a WWR-M reactor core (e.g., reactor vessel, support grid) was examined by SANS for an original sample and a sample-witness with accumulated the high dose $2.25 \cdot 10^{21}$ n/cm^2 of fast neutrons in reactor zone. As a result, the presence was detected of nano-phase inclusions (Mg2Si and Si) having gyration radii $R_G \sim 3\text{-}40$ nm. The irradiation produced a reduction of the volume fraction of large entities as well as the increase of content of smaller particles (size ~ 8; 20 nm), as a fragmentation of large entities under irradiation since the total area of particles surface did not change [44].

The final stage of the NF life cycle can involve both mechanical and hot cutting processes such as plasma torch and oxyacetylene arc metal.Analyses performed on pipes and plates exposed to the reactor coolant steam - by use contaminated components below the free release level of $1 \cdot 10^4$ Bq/m^2, not yet considering radioactivity - allowed accurate estimations of the chemical and physical characteristics of the emissions produced during hot cutting tests, as well as technical parameters such as cutting time and cutting rate vs. pipe diameter or plate thickness. The results focused on a comparison of the effects of plasma and oxyacetylene cutting processes and the chemical composition of the dusts collected by filtering the gaseous emissions [45-49]. For instance, Fluoropore^{TM}membrane filters (hydrophobic polytetrafluoroethylene membrane bonded to a high density polyethylene support) having a thickness of 150 μm a pore size of 1 μm and a 85% porosity, used to capture the gaseous emissions, were investigated by SANS. The inhomogeneities forms distribution was evaluated in the range $10^0 \div 10^4$ Å, achieving information complementary to those obtained by transmission electron microscopy (TEM): while SANS supplied data on nano- and micro-structural characteristics, averaged on a volume in the range between 1 mm^3 and 1 cm^3, TEM referred to very limited surfaces. Fig. 3 concerns SANS graphs of two different used Fluoropore^{TM}membrane filters (in the picture, shown as fixed in the respective sample holders).
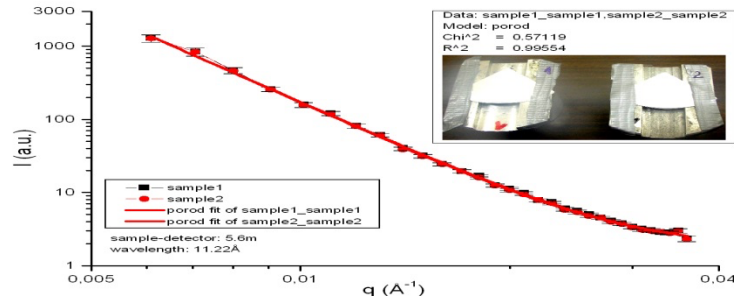
Fig. 3. SANS graphs of two different Fluoropore^{TM}membrane filters used to capture the dusts of gaseous emission produced during plasma torch and oxyacetylene cuts of pipes and plates of a NPP during decommissioning.

Such graphs, despite a good scattering - with a Porod exponent close to 4 that means that the scattering objects have sharp surfaces -, show very low differences between the two investigated filters.

Conclusion

Safety of NFs and the need to eliminate any possible technological risk makes the most real a development of methods to forecast exploitation resources of nuclear installations.

The NF decommissioning activity is a real opportunity to carry out important comparative studies in depth of nano- and micro-structural features and difectoscopy of aged parts exploited

for very long periods (in practice > 20-30 years) and fresh prepared samples, in order to found relationships between defects' characteristics and macroscopic functional properties of materials.

This is a key factor especially to progress new NFs components and their constitutive materials, contributing in the assessment of their suitability, since the more deep understanding of their behaviour.

Neutron techniques represent a valuable advance, helping to better study ageing and creep processes and to develop the knowledge of various safety-related properties and other important features of the involved materials.

References

[1] M. Rogante, V. T. Lebedev, Nanostructure characterisation by SANS for investigation on ageing, Proc. 31st ESReDA (European Safety, Reliability & Data Association) Seminar Hosted by Vuje VTS, Smolenice Castle, Slovakia, 07-08/11/2006, L. Petterson, G.M. Cojazzi, Eds., JRC European Commission, Vuje (2007), EUR 22887 EN, pp. 67-78.

[2] J. Kite-Powell, Researchers Use Augmented Reality To See Radiation Defects In Nuclear Reactors, Forbes, Oct. 11, 2021. Web page https://www.forbes.com/sites/jenniferhicks/2021/10/11/researchers-use-augmented-reality-to-see-radiation-defects-in-nuclear-reactors/?sh=565594de2c89 (accessed on Oct. 12, 2021)

[3] M. Rogante, Applicazioni Industriali delle Tecniche Neutroniche, Proc. 1st. Italian Workshop for Industry "Industrial Applications of Neutron Techniques", Rogante Engineering (Ed.), Civitanova Marche, Italy, 12-14 June 2008, Rogante Engineering, Ed. (2008), pp. 40-120.

[4] M. Rogante, L. Rosta, Nanoscale characterisation by SANS and residual stresses determination by neutron diffraction related to materials and components of technological interest, Proc. SPIE 5824, Opto-Ireland 2005: Nanotechnology and Nanophotonics, W.J. Blau, D. Kennedy, J. Colreavy (Eds.), Bellingham, WA (2005), pp. 294-305.

[5] M. Rogante, F.G. Cesari, M. Giorgi, Decommissioning of Nuclear Facilities: general considerations and suggestions not regarding activated parts, Proc. 10th International Conference "Mechanical Technologies and Structural Materials" MTSM 2021, Split, Croatia, 23-24/09/2021, S. Jozić, B. Lela, N. Gjeldum, Eds., Croatian Society for Mechanical Technologies, Split, Croatia (2021), ISSN 1847-7917, pp. 133-137. http://www.strojarska-tehnologija.hr/img/pdf/Conference_Proceedings_MTSM_2021.pdf#page=141

[6] S. Nemytov, V. Zimin, NPP Decommissioning: the concept; state of activities, International Meeting "Nuclear Power in Eastern Europe: Safety, European Integration, Free Electricity Market" and The 10th Anniversary of Bulgarian Nuclear Society, Varna, Bulgaria, 18-20 Jun. 2001 (2001), p. 9. https://inis.iaea.org/search/search.aspx?orig_q=reportnumber:%22INIS-BG--0350%22

[7] O. Glatter, O. Kratky, Small Angle X-ray Scattering, Academic Press, London, UK (1982), p. 515.

[8] C. Williams, R.P. May, A. Guinier, Small-Angle Scattering of X-rays and Neutrons, Characterisation of Materials, Lifshin E., ed., "Materials Science and Technology", vol. 2B, VCH Verlagsgesellschaft, Weinheim (1994), pp. 611-656.

[9] H.M. Rietveld, Line profiles of neutron powder-diffraction peaks for structure refinement, Acta Crystallographica, 22 (1967), pp.151-152.

[10] H.M. Rietveld, Profile refinement method for nuclear and magnetic structures, Journal of Applied Crystallography, 2 (1969), pp. 65-71.

[11] I.C. Noyan, J.B. Cohen, Residual Stress - Measurement by Diffraction and Interpretation, B. Ilschner, N. J. Grant, Eds., Springer-Verlag, New York, USA (1987), p. 276.

[12] M. Rogante, Caratterizzazione, mediante scattering neutronico, di materiali e componenti per l'impiantistica nucleare ed industriale, PhD thesis, University of Bologna, Italy (1999), p. 223.

[13] M. Rogante, Inside welds: advanced characterization of residual stresses by neutron diffraction - Метал швів: удосконалення методу оцінки остаточних напружень за допомогою нейтронної дифракції, Automatic Welding - Автоматическая сварка, Vol. 11 (2020), pp. 20-26; The Paton Welding Journal, Vol. 11 (2020), pp. 18-24. https://patonpublishinghouse.com/eng/journals/as/2020/11/04

[14] *Zs. Révay, T. Belgya, Zs. Kasztovszky, J.L. Weil, G.L. Molnár, Cold neutron PGAA facility at Budapest, Nuclear Instruments and Methods in Physics Research Section B: Beam Interactions with Materials and Atoms, Vol. 213 (2004), pp. 385-388.* https://doi.org/10.1016/S0168-583X(03)01653-7

[15] Zs. Révay, G.L. Molnár, T. Belgya, Zs. Kasztovszky, R.B. Firestone, A new gamma-ray spectrum catalog and library for PGAA, Journal of Radioanalytical and Nuclear Chemistry, Vol. 248 (2001), pp. 395-399. https://doi.org/10.1023/A:1010684210532

[16] M. Balaskó, M. Rogante, La radiografia neutronica al servizio dell'industria, Progettare, 273 (2003), pp. 35-39.

[17] M. Balaskó, E. Sváb, Neutron Radiography in Research and Development, Nukleonica 39 (1994) 1/2, pp. 3-22.

[18] H. Berger, Neutron Radiography. Methods, Capabilities, and Applications, Elsevier, New York (1965), p. 146.

[19] M. Rogante, P. Battistella, F. Cesari, Hydrogen interaction and stress-corrosion in hydrocarbon storage vessels and pipelines weldings, International Journal of Hydrogen Energy, 31/5 (2006), pp. 597-601. https://doi.org/10.1016/j.ijhydene.2005.05.011

[20] M. Rogante, V. T. Lebedev, S. Kralj, L. Rosta, Gy.Tőrők, Neutron techniques for welding project methods development in nuclear/traditional industrial application, Multidiscipline Modeling in Materials and Structures, Vol. 2, Number 4, (2006), pp. 419-433. https://doi.org/10.1163/157361106778554824

[21] M. Rogante, Materials and Components From NPP Decommissioning: Opportunities of Investigation by Neutron techniques, Energy-Environment-Economics, R. Benelmir, (Ed.), Nova Science Publishers, Hauppauge, New York (2014), ISBN: 978-1-62948-862-2, pp. 109-124.

[22] M. Rogante, Materials and Components From NPP Decommissioning: Opportunities of Investigation by Neutron techniques, International Journal of Energy, Environment and Economics, Vol. 20, Issue 2 (2012), pp. 107-122. http://www.novapublishers.org/catalog/product_info.php?products_id=31262

[23] M. Rogante, Considerations on the investigation of materials and components obtained from NPP Decommissioning. Chapter 5 of: Nuclear Power Plants, G. Petridis, D. Nicolau (Eds.), Series Nuclear Materials and Disaster Research, Physics Research and Technology, Nova Science Publishers, Hauppauge, NY (2011), pp. 119-138. http://www.novapublishers.org/catalog/product_info.php?products_id=32530

[24] P. Genta, M. Rogante, Failure predictive models for pipelines through Neutron Diffraction-based stress assessment tools, The Open Petroleum Engineering Journal, Vol. 2 (2009), pp. 12-16. https://doi.org/ http://dx.doi.org/10.2174/1874834101002010012

[25] K. Wright, B. Karlsson, Topographic quantification of non-planar localized surfaces, Journal of Microscopy, Vol. 130 Issue 1 (*1983*), *pp. 37–51*. https://doi.org/10.1111/j.1365-2818.1983.tb04196.x

[26] H.E. Exner, M. Fripan, Quantitative assessment of three-dimensional roughness, anisotropy and angular distributions of fracture surfaces by stereometry, Journal of Microscopy, Vol. 138 Issue 2 (*1985*), *pp.* 161-178. https://doi.org/10.1111/j.1365-2818.1985.tb02610.x

[27] B.B. Mandelbrot, The fractal geometry of nature, H. Freeman and Co., San Francisco, USA (1982), p. 460.

[28] M. Rogante, F.G. Cesari, V.T. Lebedev, Defectoscopy and perspectives related to metallic materials adoptable in hydrogen storage pressure tanks production, Proceedings of the NATO Advanced Research Workshop on Hydrogen Materials Science and Chemistry of Carbon Nanomaterials (ICHMS'2005), Sevastopol, Crimea, Ukraine, 05-11/09/2005, T.N. Veziroglu, S.Y. Zaginaichenko, D.V. Schur, B. Baranowski, A.P. Shpak, V.V. Skorokhod and A. Kale, Eds., NATO Security through Science Series, Vol. XLI (2007), pp. 135-144. https://doi.org/10.1007/978-1-4020-5514-0_16

[29] M. Rogante, J. Šaroun, P. Strunz, G. F. Ceschini, V. Ryukhtin, P. Lukáš, V. Marinčák, Nanoscale investigation by SANS of Inconel 738 turbine blades after high-temperature operation, Kovové Materiály - Metallic Materials, Vol. 43, Issue 5 (2005), pp. 371-381. http://www.kovmat.sav.sk/abstract.php?rr=43&cc=5&ss=371

[30] M. Rogante, V.T. Lebedev, Small angle neutron scattering comparative investigation of Inconel 738 samples submitted to different ageing treatments, Materials & Design, Vol. 29, Issue 5 (2008), pp. 1060-1065. https://doi.org/10.1016/j.matdes.2007.04.008

[31] M. Rogante, V. Lebedev, Small angle neutron scattering comparative investigation of Udimet 520 and Udimet 720 samples submitted to different ageing treatments, Journal of Alloys and Compounds, Vol. 513 (2012), pp. 510-517. https://doi.org/10.1016/j.jallcom.2011.10.106

[32] E. Rétfalvi, Gy. Török, L. Rosta, Anisotropic small angle neutron scattering analysis of thermally aged reactor-vessel materials, Applied Physics A, Vol. 74 (2002), pp. s1415-s1417. https://doi.org/10.1007/s003390201743

[33] G. Albertini, G. Bruno, F. Fiori, M. Rogante, F. Rustichelli, Studies of residual stresses, microstructural evolution and texture in steels and alloys by neutron techniques, Proc. ECSC Workshop "Modelling of steel microstructural evolution during thermomechanical treatment", Brussels, Belgium, (1997) pp. 185-195; ISBN 92-827-9891-7; CG-NA-17585-EN-C.
[34] R. Hinca, G. Bokuchava, Neutron diffraction measurements of residual stresses in NPP construction materials, Proc. Int. Youth Nuclear Congress 2000, April 9-14, 2000, Bratislava, Slovakia, p. 4.
https://inis.iaea.org/collection/NCLCollectionStore/_Public/33/011/33011213.pdf
[35] F. Vodák, R. Černý, J. Drchalová, Š. Hošková, O. Kapičková, O. Michalko, P. Semerák, J. Toman, Thermophysical properties of concrete for nuclear-safety related structures, Cement and Concrete Research, Vol. 27, Issue 3 (1997), pp. 415-426**.** https://doi.org/10.1016/S0008-8846(97)00033-1
[36] M. Rogante, A. Selezneva, Cements for nuclear industry: a feasibility study of neutron-based investigations, Proc. 2nd Int. Conf. "Mechanical Technologies and Structural Materials" MTMS 2011, Split, Croatia, 29-30/09/2011, D. Živković, Ed., Croatian Society for Mechanical Technologies, Split, Croatia (2011), ISSN 1847-7917, pp. 39-45. http://www.strojarska-tehnologija.hr/img/pdf/ZBORNIK_RADOVA_MTSM_2011.pdf#page=45

[37] M. Rogante, V.T. Lebedev, Advanced characterization of Polymer Cement Concretes by Small Angle Neutron Scattering, Proc. 9th International Conference "Mechanical Technologies and Structural Materials" MTSM 2019, Split, Croatia, 26-27/09/2019, S. Jozić, B. Lela, Eds., Croatian Society for Mechanical Technologies, Split, Croatia (2019), ISSN 1847-7917, pp. 139-144.   http://www.strojarska-tehnologija.hr/img/pdf/Conference_Proceedings_MTSM_2019.pdf#page=147

[38] M. Rogante, I.K. Domanskaya, E.S. Gerasimova, A. Len, L. Rosta, N.K. Székely, E. Vladimirova, Nanoscale investigation of Polymer Cement Concretes by Small Angle Neutron Scattering, Science and Engineering of Composite Materials, Vol. 24, Issue 1 (2017), pp. 67-72. https://doi.org/10.1515/secm-2015-0013

[39] M. Rogante, V. Havránek, P. Mikula, V. Ryukhtin, SANS and PIXE characterization of Polymer Cement Concretes, Proc. 6th Int. Conf. "Mechanical Technologies and Structural Materials" MTMS2016, Split, Croatia, 22-23/09/2016, S. Jozić, B. Lela, Eds., Croatian Society for Mechanical Technologies, Split, Croatia (2016), ISSN 1847-7917, pp. 119-125. http://www.strojarska-tehnologija.hr/img/pdf/ZBORNIK_RADOVA_MTSM_2016.pdf#page=127

[40] M. Rogante, I.K. Domanskaya, E.S. Gerasimova, E. Vladimirova, Feasibility Study for a Neutron-Based Investigation of Polymer Cement Concretes, Universal Journal of Applied Science, Vol. 1, Issue 1 (2013), pp. 11-17. https://doi.org/10.13189/ujas.2013.010103

[41] E. Retfalvi, Gy. Török, L. Rosta, Radiation damage study using small-angle neutron scattering, Physica B 276-278 (2000), pp. 843-844. https://doi.org/10.1016/S0921-4526(99)01307-1

[42] V.T. Lebedev, Gy. Torok, V.I. Didenko, A.N. Lapin, V.A. Petrov, B.Z. Margolin, Steel nanostructure under thermal treatment modeling irradiation induced embrittlement, Abstract book of 3rd European Conf. on Neutron Scattering, Sept. 3-6, 2003, Montpellier, France (2003), p. 136.

[43] V.T. Lebedev, Gy. Torok, V.I. Didenko, A.N. Lapin, V.A. Petrov, B.Z. Margolin, Investigation of nanostructure of reactor pressure vessel steel with differrent degree of embrittlement, Physica B: Condensed Matter, Vol. 350, Issues 1-3, Supplement (2004), pp. E471-E474. https://doi.org/10.1016/j.physb.2004.03.123

[44] V.M. Lebedev, V.T. Lebedev, I.N. Ivanova, S.P. Orlov, D.N. Orlova, Structure of aluminum alloys irradiated with reactor neutrons, Physics of the Solid State, Vol. 52 (2010), pp. 996-999. https://doi.org/10.1134/S1063783410050239

[45] M. Rogante, F.G. Cesari, G. Migliore, NPP decommissioning: a methodology to evaluate the gaseous emissions produced by thermal cutting processes, International Nuclear Safety Journal, Vol. 3, Issue 4 (2014), pp. 43-61. https://nuclearsafety.info/international-nuclear-safety-journal/index.php/INSJ/article/view/43

[46] F. Cesari, M. Rogante, A. Giostri, Results of the experimental campaign on contaminated metal components parameters and suggestions for safely NPP component dismantling, Nuclear Engineering and Design, Vol. 238, Issue 10, (2008), pp. 2801-2810. https://doi.org/10.1016/j.nucengdes.2008.05.009

[47] F.G. Cesari, M. Rogante, A. Giostri, Precautions arising from the experimental campaign on contaminated metal components parameters for safely nuclear power plant components dismantling, Transactions, 19th International Conference on Structural Mechanics in Reactor Technology SMiRT 19, Toronto, 12-17/08/2007, paper # W01/4 (2007), p. 7. https://repository.lib.ncsu.edu/bitstream/handle/1840.20/31406/W01_4.pdf

[48] F. G. Cesari, M. Rogante, A. Giostri, G. Conforti, Contaminated metal components in dismantling by hot cutting processes, Proc. ICONE14 Int. Conf. on Nuclear Engineering, July 2006, Miami, Florida, USA, ASME ICONE14-89451 (2006), p. 10. https://doi.org/10.1115/ICONE14-89451

[49] F. Cesari, A. Giostri, M. Rogante, E. Sirito, M. Sirito, Hot cutting processes and emissions characterization in metal components dismantling, Proc. of 11th Int. Scientific Conf. on the Contemporary Achievements in Mechanics, Manufacturing and Materials Science CAM3S`2005, Gliwice-Zakopane, Poland, 06-09/12/2005, L.A. Dobrzański, Ed., International Organising Committee of the Scientific Conferences AMME World Press, Gliwice, Poland (2005), ISBN/ISSN 83-89728-19-2, pp. 1111-1116. http://www.acmsse.org/content/plyty/CAMS2005/papers/1258.pdf

TETRAPODS BASED SMART MATERIALS FOR ADVANCED TECHNOLOGIES

Reza Abolhassani [1], Fateme Mirsafi [1], Horst-Günter Rubahn [1], Yogendra Kumar Mishra [1]

[1] Smart Materials, NanoSYD, Mads Clausen Institute,

[1]University of Southern Denmark, Alsion 2, 6400, Sønderborg, DENMARK

Abstract

Considering the size dependent utilization complexities of nanoscopic dimensions towards real applications, the focus of nanomaterials community is merging to three-dimensional (3D) form of materials which are built out interconnected nanostructures. This talk will briefly introduce the importance of complex shaped nanostructures towards smart 3D nanomaterials structuring. A simple flame based single step approach was developed for synthesizing zinc oxide tetrapods which demonstrated many applications in different technologies. These tetrapods have been used as building blocks to construct highly porous interconnected 3D nanonetworks in form of flexible ceramics which offer further new application avenues. Additionally, these 3D networks have been utilized as sacrificial templates to develop hollow tetrapodal 3D networks from almost any desired material, carbons, nitrides, oxides, polymers, hydrogels, etc. The sacrificial template-based strategy offers new and unique opportunities in the direction of 3D nanomaterials engineering and accordingly advanced technological applications. Some examples of 3D nanomaterials engineering will be demonstrated alongwith their applications [1-10]. The scopes of 3D nanostructuring based smart materials in sensing, electronics, optoelectronics, energy, and biomedical engineering will be briefly highlighted in the talk.

Keywords: Smart materials; Tetrapods, Hybrid Nanomaterials, Advanced Technologies

* Corresponding Author e-mail : mishra@mci.sdu.dk

GROWTH OF IRON DIBORIDE LAYER ON SAE 1020 STEEL BY FOUR APPROACHES

Mourad Keddam[1*]

[1] University of Science and Technology Houari Boumediene, Laboratoire de Technologie des Matériaux, Bab-Ezzouar, Algiers, Algeria

Abstract

The pack-boriding kinetics of SAE 1020 steel has been studied through utilizing four mathematical approaches in case of the formation of iron diboride layers. For each model, the values of boron diffusivity in Fe_2B in the range of 850 to 950°C with incubation times included. Finally, the models were put to the test by comparing the predicted results to the simulated values of Fe_2B layer thickness determined at 925°C for 6 hours.

Keywords : Boriding, Iron Diboride, Kinetics, Activation Energy, Diffusion Models.

* Corresponding Author e-mail :keddam@yahoo.fr

HYDROPHOBIC COATING WITH SOL-GEL TECHNIQUE ON TITANIUM METAL SUBSRATE

Najran Mohammed Nasser Hosrom[1*] , Atilla Evcin[2]

[1] 22 may street apt:1 No:5 Amran, Yemen

[2] Afyon Kocatepe University, Materials Science and Engineering Department, Afyonkarahisar, Turkey

najranmh@gmail.com

1. Introduction

Protecting the surfaces of metals is protecting the metal itself. Because corrosion, which starts at a tiny point on the surface, progresses towards the inner parts of the metal over time, and corrosion and decay occur. This shortens the economic life of the metal in use. Considering that 20% of the iron produced annually is disabled in this way, it can be understood how important properties are. The development of high-performance surface coating materials and the search for new coating techniques have always been important to the metal coating industry (Gabe 1978, Tanwer et al 2022, Jiang et al 2022, Zhou et al 2022). Wetting behavior of solid surfaces is a very important issue for materials science and basic research. Since it has many potential application areas, intensive studies have been carried out on this subject in recent years (Xin et al 2022). The hydrophobicity properties of material surfaces can be modified by the application of nano-coatings. A hydrophobic (water repellent) coating is prepared by lowering the surface energy of the material (Fig. 1). Low surface energy causes water droplets to roll off the surface, taking the form of beads. Metal, glass, ceramic, textile, plastic etc. The aim of this work is to increase the corrosion resistance of the Titanium surface by creating water-repellent (hydrophobic) surfaces.
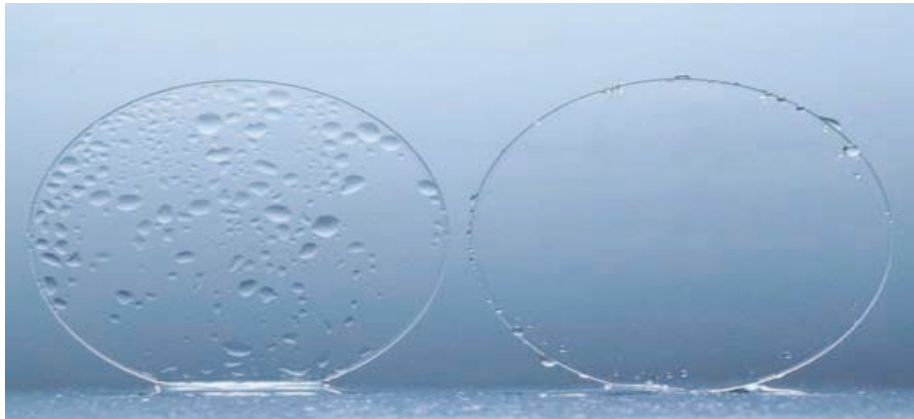

Fig. 1 Hydrophilic and hydrophobic surfaces (Int ref 1).

Contact angle is the quantitative measurement of the amount of a solid wetted by a liquid. If the contact angle is less than 90°, the liquid wets the surface; If it's greater than 90°, it means it's not getting wet (Öztürk 2019).

2. Sol-gel Processing

Sol-gel method is a coating technique applied to improve the surface properties of glass, ceramic, metal and plastic substrates and to gain new properties (such as optical, electronic, chemical and mechanical)(Klein 1988, Siti Sumaiyah et al 2014, Mindivan 2013).

Dip Coating

Spray Coating

Flow Coating

Spin Coating

Laminar Coating

Roll Coating

Printing (Augerter et al 2008).
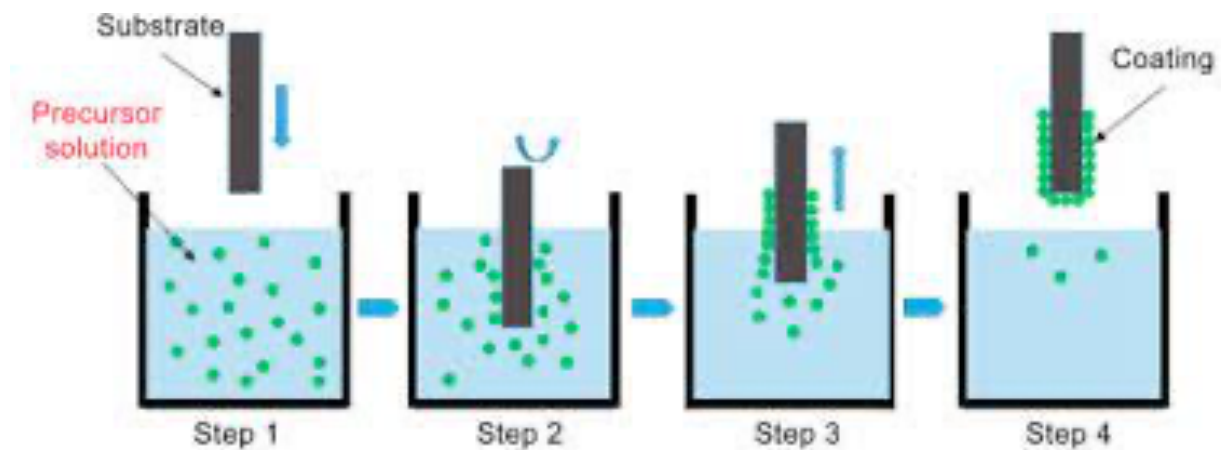
Figure 2 shows the stages of dip coating.

Fig. 2 Steps of dip coating process (El-Desoky et al 2020)

The thickness of film is usually calculated by the Landau-Levich equation (eq 1) (Faustini et al 2010).

$$h = 0.94 \frac{(\eta U)^{2/3}}{\gamma_{LV}^{1/6}(\rho g)^{1/2}}$$

(1)

Here;

h : film thickness η : viscosity of liquid

U : dipping rate γ_{LV} : liquid-vapour surface tensionr

ρ : density of solution   g   : gravity

3. Materials and Method

Precursors :

TEOS (C8 H20 O4 Si),

Etanol (C2 H6 0),

Heptadecafluoro-1-decanethiol HDFT (C10 H5 F17 S)
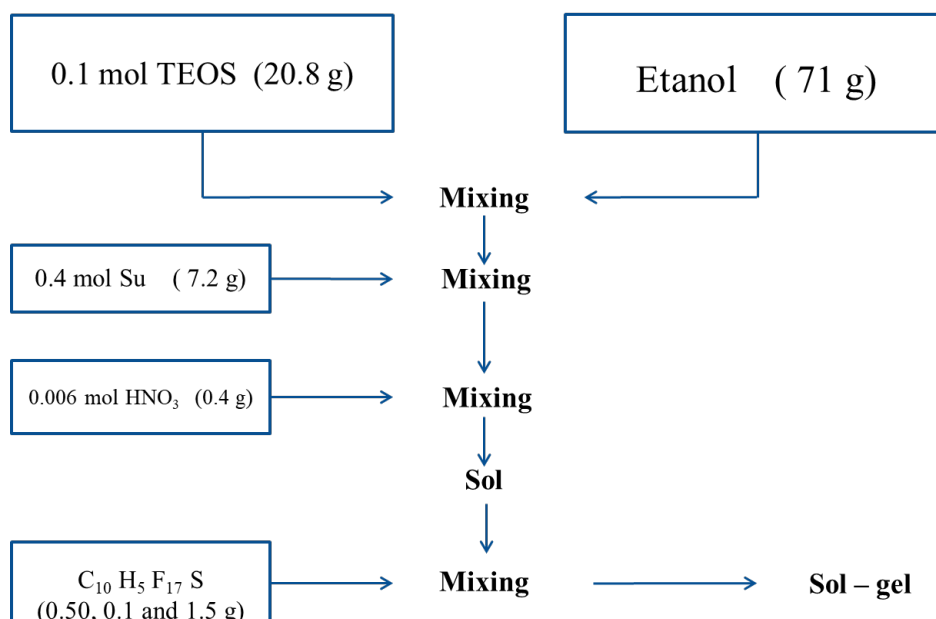
Nitric Acid (HNO3)

Fig. 3 Flow chart of experiment.

Table 1. Prepared compositions

Code	Solution	Amount by weight %
S1	Undoped solution	0
S2	Heptadecafluoro-1-decanethiol doped	0,5
S3	Heptadecafluoro-1-decanethiol doped	1,0
S4	Heptadecafluoro-1-decanethiol doped	1,5

As shown in Fig. 3, synthesis of silica sol by sol-gel process by using TEOS solution of, water and ethanol mixed in erlenmeyer. The mixture is stirred using a magnetic stirrer for 2 hours. The addition of 0.006 mol HNO3 (0,4 g) is carried out periodically dropwise. Then, by adding different amounts of additives (Heptadecafluoro-1-decanethiol), the compositions were prepared (Table 1). The prepared solution was coated on the metal substrate with a dip coating device. The coated thin film was dried at room temperature and then in an oven at 105°C. Then heat treatment was applied at 180 degrees in the oven. The contact angle measurement was determined with the KSV Attension Theta Lite TL 101 Optical Tensiometer (Fig. 4). Morphological examination of the formed thin films was made with the JEOL 6360 LV model scanning electron microscope (Figure 5).
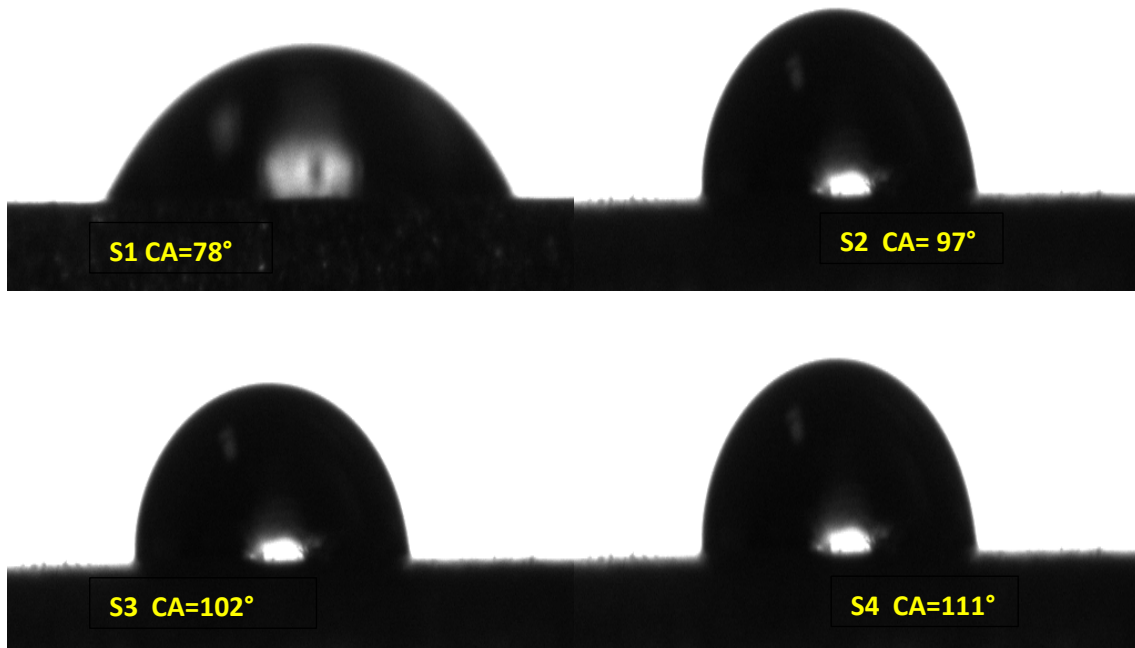
4. Results

Fig. 4 Contact angles of coated samples

The increase in HDFT contribution caused an increase in the contact angle. The maximum contact angle was obtained with 1.5% added composition. As a result, the hydrophilic metal surface was converted to the hydrophobic form. Corrosion resistance is increased with the water-resistant surface.

From the SEM images in Figure 5, it is seen that the coating thicknesses are between 10 and 12 μm. The coatings were obtained as homogeneous and smooth.
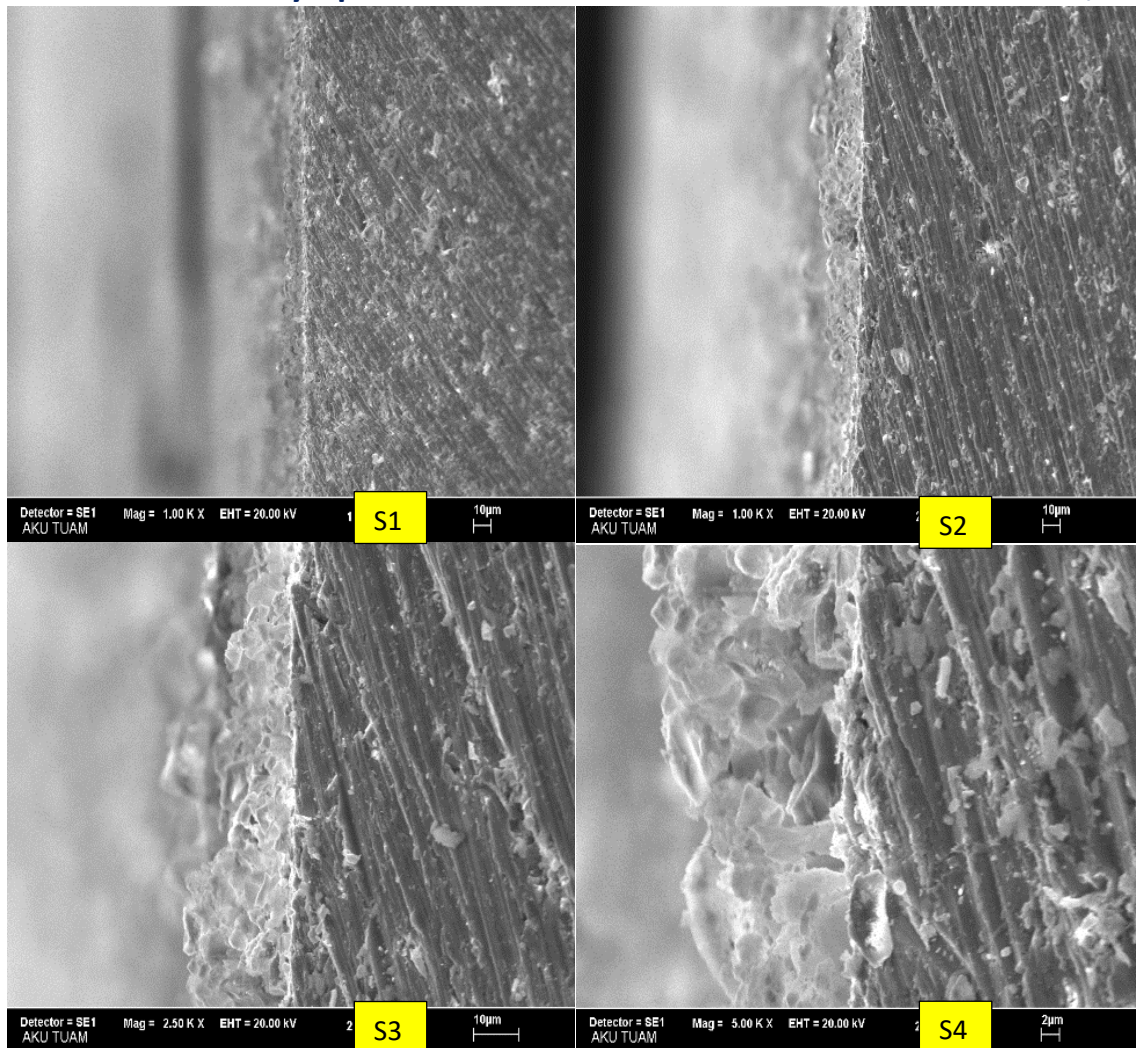
Fig. 5 SEM images of cross section of samples.

5. Conclusion

In the study, hydrophobic coating process was applied to the metal surfaces with the sol-gel technique using fluoro alkoxy silane compound.

In order to increase the superhydrophobic behavior of the surfaces, the contact angle was increased with amount of fluoro alkoxy silane. The maximum contact angle value was obtained with 111°.

The surfaces of the prepared samples were given a hydrophobic (water repellent) feature, and corrosion resistance was increased by preventing the formation of corrosion (oxide layer) caused by effects such as water and moisture.

References

Xin C, Yan J, Xin C, Wang Q, Feng W, Wang H, Effects of Ti content on the wetting behavior and chemical reaction in AgCuTi/SiO2 system, Vacuum, Volume 167, 2019, Pages 152-158, https://doi.org/10.1016/j.vacuum.2019.05.014.

Gabe D R, Series: International series on materials science, and technology ; v. 28 Publisher: Pergamon Press, Year: 1978

Jiang L, Dong Y, Yuan Y, Zhou X, Liu Y, Meng X, Recent advances of metal–organic frameworks in corrosion protection: From synthesis to applications, Chemical Engineering Journal, Volume 430, Part 3, 2022, 132823, https://doi.org/10.1016/j.cej.2021.132823.

Klein L C, Series: Materials science and process technology series Publisher: Noyes Publications, Year: 1988

Mindivan H, Effects of Combined Diffusion Treatments on the Wear Behaviour of Hardox 400 Steel, Procedia Engineering, Volume 68, 2013, Pages 710-715, https://doi.org/10.1016/j.proeng.2013.12.243.

Tanwer S, Kumar Shukla S, Recent advances in the applicability of drugs as corrosion inhibitor on metal surface: A review, Current Research in Green and Sustainable Chemistry, Volume 5, 2022, 100227, https://doi.org/10.1016/j.crgsc.2021.100227.

Zhou X, Xu D, Geng S, Fan Y, Yang C, Wang Q, Wang F, Microstructural evolution and corrosion behavior of Ti–6Al–4V alloy fabricated by laser metal deposition for dental applications, Journal of Materials Research and Technology, Volume 14, 2021, Pages 1459-1472, https://doi.org/10.1016/j.jmrt.2021.07.006.

Öztürk Y C, Production of photocatalytically active TiO2 - P2O5 glasses by the sol-gel process, METU Master Thesis, 2019

Siti Sumaiyah S.A.A, Nurhana Ilmira, H., Nunshaimah, S. and Syamsyir Akmal, S. and Azhan, H. and Siti Nor Hafiza, M.Y. and Yusoff, M.A. and Roslan, M.N. (2014) *Mechanochemical synthesis of CNT/ZnO hybrid materials.* In: 28th Regional Conference on Solid State Science and Technology 2014 (RCSSST 2014)., 25 - 27 November 2014, Cameron Highland, Pahang, Malaysia..

Aegerter, M.A., Almeida, R., Soutar, A. *et al.* Coatings made by sol–gel and chemical nanotechnology. *J Sol-Gel Sci Technol* **47,** 203–236 (2008). https://doi.org/10.1007/s10971-008-1761-9

El-Desoky, M. & Abdulrazek, M. & Sharaby, Y.. (2020). Characterization and optical properties of reduced graphene oxide doped nano-crystalline vanadium pentoxide. Optical and Quantum Electronics. 52. 10.1007/s11082-020-02430-5.

Faustini, Marco; Louis, Benjamin; Albouy, Pierre A.; Kuemmel, Monika; Grosso, David (2010). *Preparation of Sol−Gel Films by Dip-Coating in Extreme Conditions. , 114(17), 7637–7645.* doi:10.1021/jp9114755

Int ref 1 https://www.yaklasansaat.com/dunyamiz/bilim_ve_teknoloji/nanoteknoloji.asp

HAVA ARAÇLARINDA KULLANILAN HİBRİT TAKVİYELİ EPOKSİ KOMPOZİTLERİN ÜRETİMİ VEMEKANİK ÖZELLİKLERİ

Mürsel Ekrem[1][*]

[1] Necmettin Erbakan Üniversite, Makine Mühendisliği Bölüm, Konya, Türkiye

Özet

Bu çalışmada, ağırlıkça % 0.25 Çok Cidarlı Karbon Nanotüp (ÇCKNT) ile ağırlıkça farklı oranlarda (% 0.25, 0.5 ve 0.75) nanoSiO$_2$ parçacıklı epoksi esaslı nanokompozitlerin üretimi ve mekanik özellikleri incelenmiştir. ASTM D638-10 standardına göre üretimi yapılan epoksi esaslı hibrid nanokompozitlerin çekme numuneleri sabit çekme hızında çekme testine tabi tutulmuştur. Modifiye edilmiş epoksi hibrid nanokompozitlerin maksimum yükleri, çekme dayanımları, elastiklik modülleri, toklukları ve birim şekil değiştirme değerleri hesaplanmış olup, bu testin sonucunda bu özellikler epoksi numuneyle kıyaslanmıştır. Referans numune ile ağırlıkça % 0.25 oranındaki ÇCKNT ve ağırlıkça % 0.5 oranındaki nanoSiO$_2$ parçacık takviyeli nanokompozitin maksimum yükleri sırasıyla 1730 N ve 1875 N olup, 0.25CNT+0.5 nanoSiO$_2$ epoksi esaslı kompozit % 8 oranında artış gözlemlenmiştir.

Anahtar Kelimeler: Çekme Dayanımı, Epoksi Nanokompozitler, MWCNT, Nano SiO$_2$.

* İlgili yazar e-posta: mekrem25@hotmail.com

DOĞAL VE SENTETİK FİBER TAKVİYELİ POLİMER KOMPOZİTLERİN KURU KAYMA KOŞULLARINDA AŞINMA ORANI VE SÜRTÜNME KATSAYISI ARASINDAKİ İLİŞKİNİN BELİRLENMESİ

Lemiye Atabek Savaş[1]*

[1] Erciyes Üniversitesi, Malzeme Bilimi ve Mühendisliği Bölümü, Kayseri, Türkiye

Özet

Bu çalışmada yüksek-yoğunluklu polietilen (HDPE) matrisli karbon, bazalt ve kokonat fiber takviyeli (%10 ve %30) kompozitlerin kayma aşınma davranışları incelenmiş olup, aşınma oranları ile sürtünme katsayıları arasındaki ilişki araştırılmıştır. Kompozitler ergiyik harmanlama yöntemi ile üretilmiş, uyumlaştırıcı olarak maleik anhidrit-aşılı polietilen (PE-g-MA) kullanılmıştır. Ek olarak kokonat fiberlerin matris malzemesi ile karışabilirliğini bir adım daha artırmak için sodyum hidroksit (NaOH) çözeltisi içinde alkali yüzey işlemi uygulanmıştır. Aşınma testleri özel üretim bir ball-on-disk tribometresi kullanılarak kuru kayma şartlarında, 5 N normal yük ve 1100 dev/dak kayma hızında açık atmosfer koşullarında tamamlanmıştır. Yapılan tribo-testler sonucunda, kullanılan tüm bileşimlerdeki kompozitlerin sürtünme katsayılarının saf HDPE'den yüksek olduğu tespit edilmiştir. En düşük sürtünme katsayısına 0,121 ile saf HDPE'de ulaşılmıştır. %30 bazalt fiber içeren HD-BF30 numunesi 0,303 ile en yüksek sürtünme katsayısı değerini vermiştir. Aşınma oranı her bir fiber için konsantrasyon ile artış eğilimindedir. Karbon fiber takviyeli kompozitler saf polimerden yüksek sürtünme katsayısına sahip olsa da yüksek rijitliğinden dolayı daha yüksek aşınma direnci sergilemişlerdir. En düşük aşınma oranına $64×10^{-6}$ (mm3 N-1m-1) ile %10 karbon fiber içeren kompozitte ulaşılmıştır. Kokonat fiber takviyeli kompozitler karbondan sonra ikinci en yüksek aşınma direncine sahip kompozitler olup, aynı konsantrasyonda bazalt fiberden daha yüksek aşınma direnci göstermişlerdir. En yüksek aşınma oranı $177×10^{-6}$ (mm3 N-1m-1) ile %30 bazalt fiber içeren kompozitte görülmüştür. Sonuç olarak karşılaştırılan fiberler içerisinde karbon fiberin düşük sürtünme ve yüksek aşınma direnci anlamında diğer fiberlere göre üstün olduğu bulunmuştur. Fiber tipine göre sürtünme katsayısı ve aşınma oranı değerleri değişkenlik gösterebilmektedir.

Anahtar Kelimeler : Yüksek-Yoğunluklu Polietilen, Karbon Fiber, Bazalt Fiber, Kokonat Fiber, Aşınma Oranı, Sürtünme Katsayısı.

* İlgili yazar e-posta : atabekl@erciyes.edu.tr

SELF-CLEANING OF HYDROPHOBIC SURFACES

Abdullah Alawadhi[1*] , Atilla Evcin[2]

[1] Sana'a, Yemen

[2] Afyon Kocatepe University, Materials Science and Engineering Department, Afyonkarahisar, Turkey

al3wadhiabdullah@gmail.com

1. Introduction

The sol–gel process is a wet chemical method also defined as chemical solution deposition. This method is a simple, fast, and economical route in which nanomaterials can prepared functional coatings through dip-coating, spin-coating or spray-coating methods, The sol–gel process has several steps such as: hydrolysis, condensation, gelation, aging, drying (Lin et al 2022, Zhang et al 2022). A superhydrophobic surface refers to a type of surface where the WCA is greater than 150° . The surface of a lotus leaf is one example of superhydrophobicity (Jin et al 2022, Wang et al 2022). The superhydrophobic surfaces can be obtained by chemical vapor deposition, phase separation, hydrothermal, sol-gel, etching, one-step dip-coating, layer-by-layer deposition, and electrodeposition, etc (Wu et al 2022, Zhu et al 2022). The superhydrophobic surfaces exhibit some properties such as self-cleaning, anti-icing, anti-fouling, anti-fogging, oil-water separation, anti-corrosion, and membranes (Zhu et al 2022). The wetting type of surfaces can be classified into hydrophilicity and hydrophobicity, which is shown by Wenzel and Cassie–Baxter in Fig.1 and 2 (Zhang et al 2012).
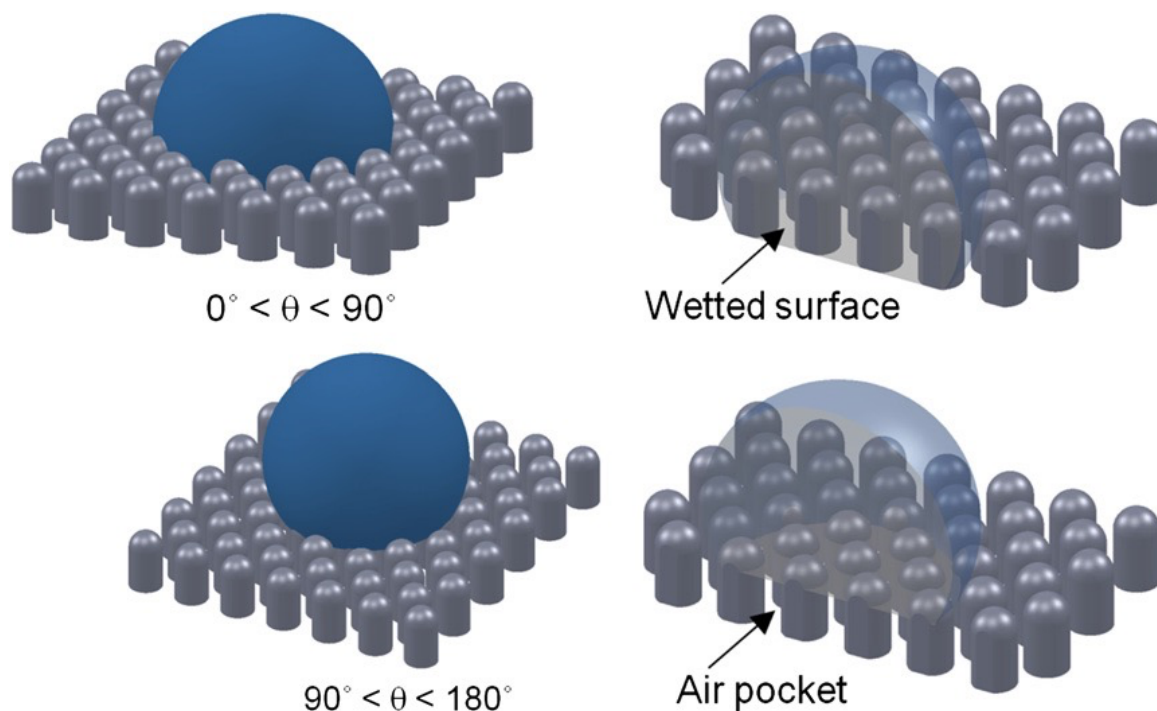

Fig. 1 (*a*) Wenzel (hydrophilic) surface. (*b*) Cassie–Baxter (hydrophobic) surface.

$\theta = 90°$ superhydrophilic

$0° < \theta < 90°$ hydrophilic

$90° < \theta < 150°$ hydrophobic
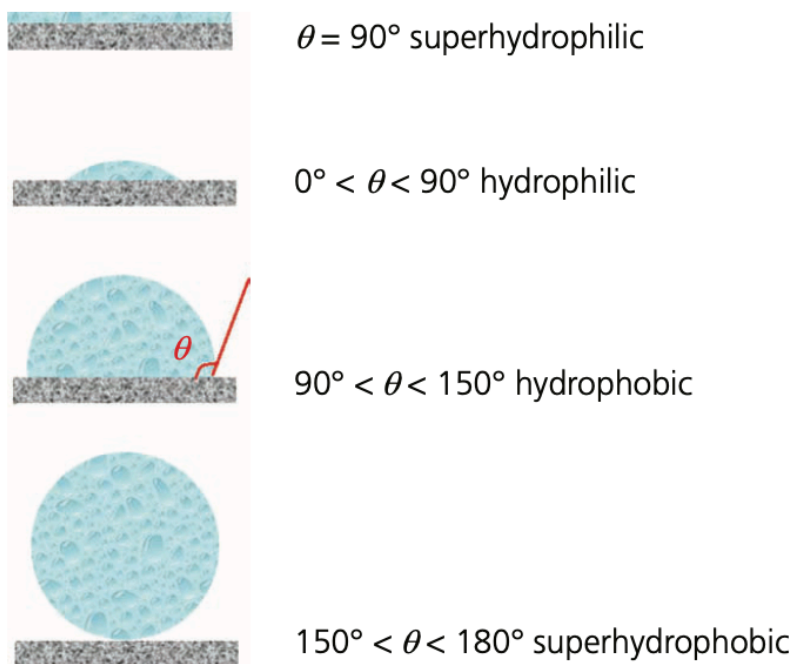
$150° < \theta < 180°$ superhydrophobic

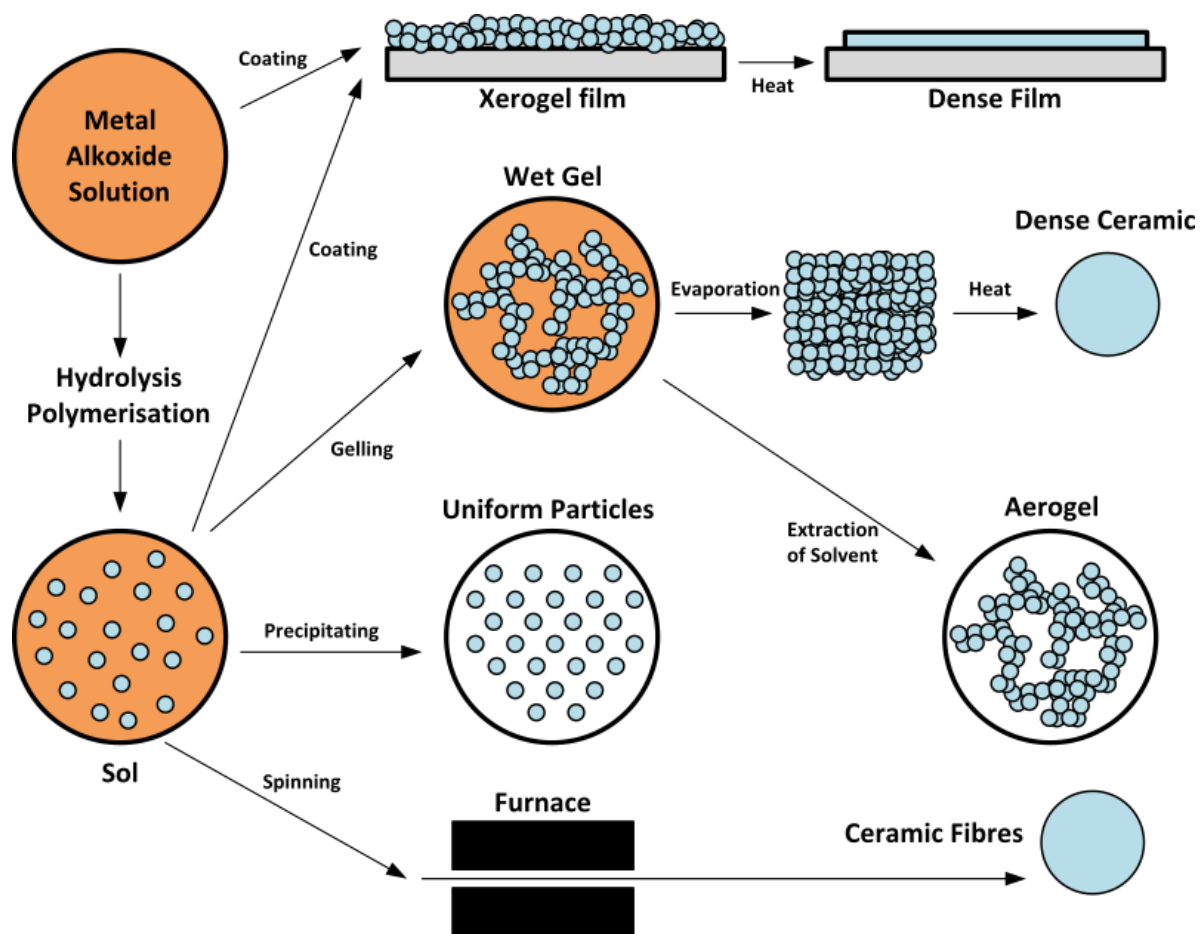**Fig. 2** Contact angles of surfaces (Evcin et al 2018)

Fig. 3 Schematic diagrtam of the different routes of the sol–gel process (Brinker and Sherer, 1990).

In this study, we reported a novel, cheap and simple route that combines the sol–gel process (Fig. 3) and dip-coating method to prepare superhydrophobic coatings.

2. Materials and Method

- RTV 664 A Silicone
- RTV 664 B Silicone
- Lam glass
- (3 Aminopropyl) triethoxysilane 3-APTES
- Calcium carbonate $CaCO_3$
- Zn Stearate $Zn(C_{18}H_{35}O_2)_2$
- Ca Stearate $Ca(C_{18}H_{35}O_2)_2$
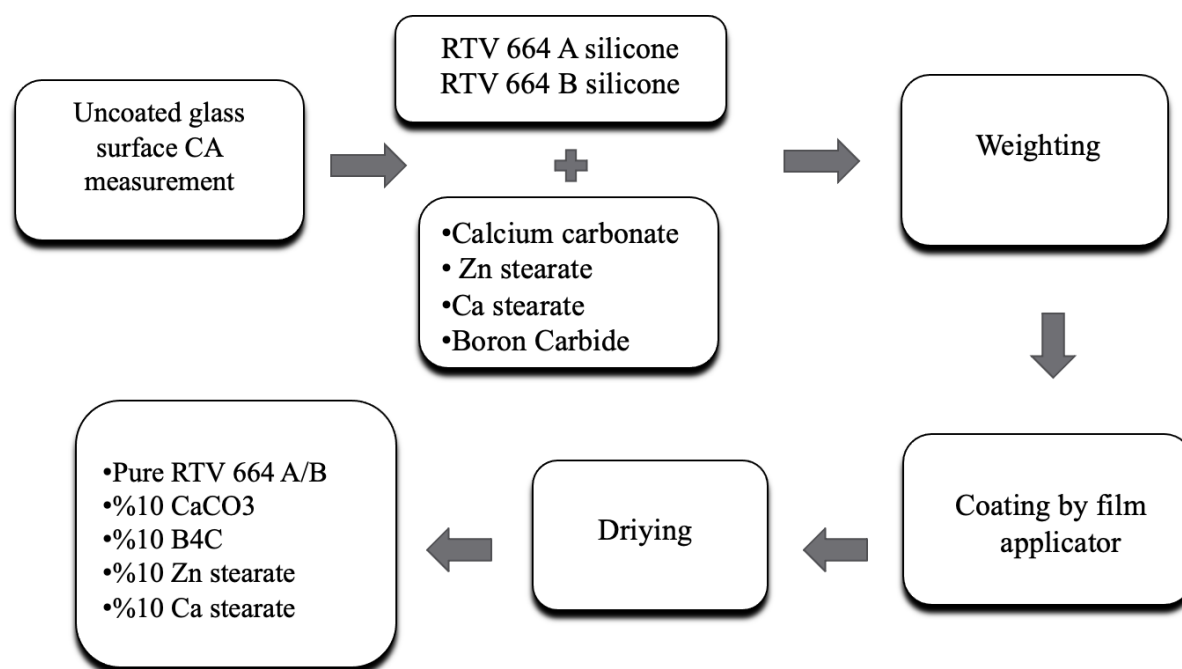- Boron Carbide B_4C

Fig. 4 Flow chart of experiment

After cleaning the glass substrates to be used, Silicon A/B and 3-APTES were put into the beaker and mixed. Different fillers were added to it and placed in a magnetic stirrer and allowed to mix for 10 minutes (Fig. 4). Film was taken on glass surfaces with a film applicator. Drying films were characterized. In the experiments, the contact angle measurement was made with the KSV Attension Theta Lite TL 101 Optical Tensiometer (Fig. 5). Morphological examination

of the formed thin films was made with the JEOL 6360 LV model scanning electron microscope (Figure 7).
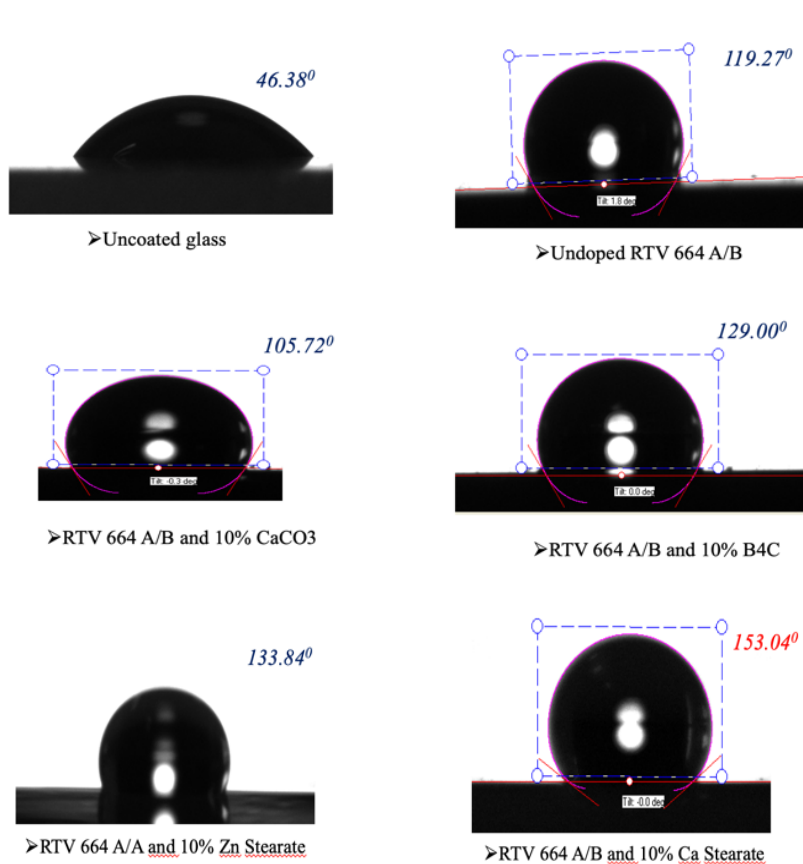
3. Results and Discussion

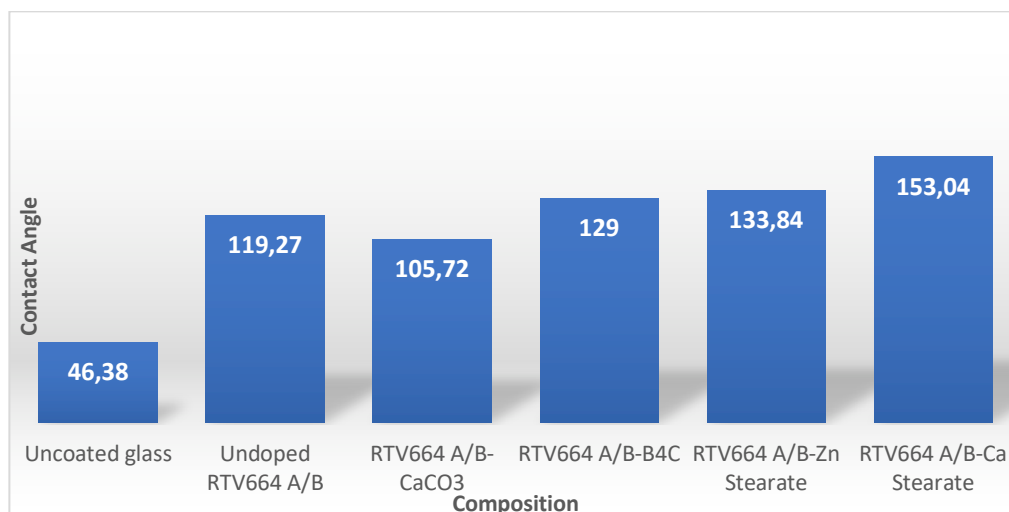**Fig. 5** Contact angle of different coatings

Fig. 6 Contact angle versus coating compositions.

As seen in Figures 5 and 6, all other coatings show hydrophobic properties compared to uncoated glass. In fact, the Ca-stearate filled silicon coating exhibited superhydrophobic properties. The maximum contact angle is 153 degrees for this coating.
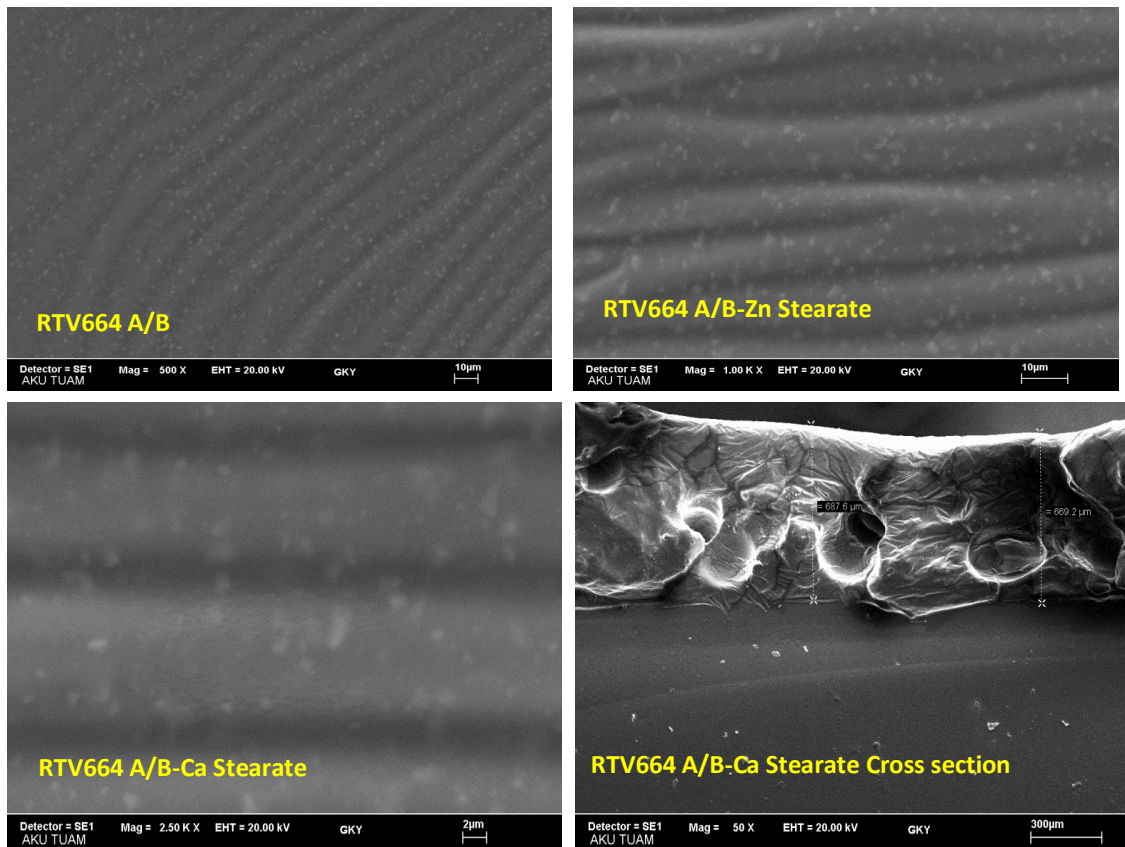
Fig. 7 SEM images of coatings.

As seen in Figures 5 and 6, superhydrophobic properties were obtained in Ca stearate filled silicon films.   As seen in Figure 7, the surface and cross-section are homogeneous.

4. Conclusion

In this study, it was planned and successful to create surfaces that do not like water, to obtain self-cleaning surfaces that are not affected by dirt and dust.

It has been observed that Calcium Carbonate reduce the contact angle compared to the contact angle of the silicon coated glass without additives, while Boron Carbide, Zn Stearate and Ca Stearate additives increase the contact angle.

As a result, hydrophobic glass surfaces were obtained.

References

Benfeng Zhu, Rujie Ou, Jiao Liu, Yumeng Yang, Si'an Chen, Guoying Wei, Zhao Zhang, Fabrication of superhydrophobic surfaces with hierarchical structure and their corrosion resistance and self-cleaning properties, Surfaces and Interfaces, Volume 28, 2022, 101608, https://doi.org/10.1016/j.surfin.2021.101608.

Brinker CJ and Sherer GW (1990) Sol-Gel Science. Academic Press, San Diego, CA, USA.

Chen Zhang, Huiyue Zhao, Yixuan Su, Hongqiang Wang, Jun Shen, Xiaodong Wang, Embedding constructed refractive index graded antireflective coating with high abrasion resistance and environmental stability for polycarbonate glass, Journal of Colloid and Interface Science, Volume 608, Part 1, 2022, Pages 13-21, https://doi.org/10.1016/j.jcis.2021.09.152.

Evcin A, Ersoy B, Uygunoğlu T and Güneş İ (2018) Farklı mineral katkıların epoksi Zemin kaplama malzemesinin ıslanmazlığına ve yüzey enerjisine etkisi. Gazi Üniversitesi Mühendislik Mimarlık Fakültesi Dergisi 33(2): 599–610, https://doi.org/10.17341/gazimmfd.416368.

Haofeng Lin, Zeyu Qiu, Peinian Huang, Longlong Zeng, Yunfeng Liang, Chunhong Zeng, Ruixi Lin, Mingyu Yuan, Ruijiang Hong, Preparation of antireflective coatings with moisture resistance and a widely tunable refractive index by combining the sol-gel method with evaporation concentration, Construction and Building Materials, Volume 318, 2022, 125810, https://doi.org/10.1016/j.conbuildmat.2021.125810.

Huichao Jin, Jianfu Wang, Limei Tian, Mingyao Gao, Jie Zhao, Luquan Ren, Recent advances in emerging integrated antifouling and anticorrosion coatings, Materials & Design, Volume 213, 2022, 110307, https://doi.org/10.1016/j.matdes.2021.110307.

Kang Wang, Sirong Yu, Xiaoli Yin, Lin Liu, Liyuan Wang, Guang Zhu, Jun Wang, Quan Li, Xizhen Yang, Preparation of ZnS superhydrophobic coating on 316L stainless steel with self-cleaning property and excellent stability, Colloids and Surfaces A: Physicochemical and Engineering Aspects, Volume 633, Part 1, 2022, 127871, https://doi.org/10.1016/j.colsurfa.2021.127871.

Yinglin Wu, Xinyu Tan, Yunkuan Wang, Fujun Tao, Meiling Yu, Xiaobo Chen, Nonfluorinated, transparent, and antireflective hydrophobic coating with self-cleaning function, Colloids and Surfaces A: Physicochemical and Engineering Aspects, Volume 634, 2022, 127919, https://doi.org/10.1016/j.colsurfa.2021.127919.

Zhang, Bong & Park, Jiyeon & Kim, Kwang & Yoon, Hyungkee. (2012). Biologically inspired tunable hydrophilic/hydrophobic surfaces: A copper oxide self-assembly multitier approach. Bioinspiration & biomimetics. 7. 036011. 10.1088/1748-3182/7/3/036011.

COATING OF TIO2 DOPED HYDROXYAPATITE ON TI6AL4V ALLOY WITH HVOF TECHNIQUE

Nada Alloush[1*], Atilla Evcin[2]

[1] Idlib, Suriye

[2] Afyon Kocatepe University, Materials Science and Engineering Department, Afyonkarahisar, Turkey

nada.alloush97@gmail.com

1. Introduction

Biomaterials are natural or synthetic materials used to strengthen tissues and cells that cannot fulfill their function in the body. Such as; treatment of skeletal fractures, heart vessels, hip prostheses, dental implants, biodegradable sutures etc (Chen and Liu 2016, Fergal 2011, Detsch et al 2018).

Hydroxyapatite is a calcium salt found in bone and teeth with the chemical formula $Ca10(PO4)6(OH)2$. It forms the inorganic part of the bone structure. Calcium phosphate based HA is used as a bioceramic material due to its biocompatibility. It can be used as the manufacture of various prostheses , repairing broken and cracked bones, coating metallic biomaterials (Al-Sanabani et al 2013, Pokhrel 2018, Fiume et al 2021).

Traditionally, the use of titanium has been concentrated in the aircraft, space and marine industries (Henriques 2009, Peters et al 2003). The metal's durability and rigid structure, low specific gravity and relative lightness, resistance to high temperatures and resistance to corrosion have led to its widespread use in these special areas. In recent years, there has been a significant increase in the medical and dental applications of titanium and titanium alloys (Mott 1951, Eshawish et al 2021, Hoppe et al 2020).

Advantages of titanium alloys;

Best compatibility in long-term implantation,

the probability of a chemical reaction is minimal.

Since it is non-magnetic, it is compatible for MR (Magnetic Resonance).

Due to its low density, it has a low weight.

It is hypoallergenic (less allergic) (Kurup et al 2021, Nicholson 2020)

2. High Velocity Oxy Fuel (HVOF) Coating

In the process, the combustion gases take place in a combustion chamber, the pressures of the combustion gases can be between 6 and 10 bar. After combustion, the velocity of the gases released can reach 2000 m/s. The sprayed particle velocity can vary between 500-700 m/sec depending on the particle size distribution and density (Fig. 1). The ideal spray distance varies between 220 mm and 380 mm (Cabral-Miramontes et al 2014, Sobolev et al 2004).
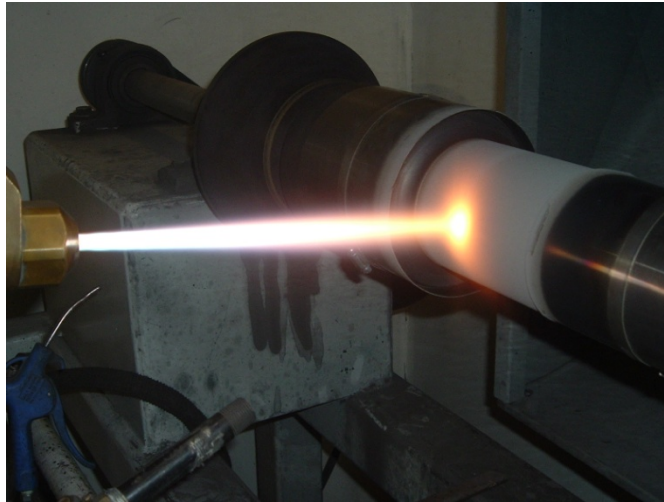
Fig. 1 HVOF gun

3. Materials and Method

In this study calcium nitrate [Ca(NO3)2 4H2O] was used as a calcium (Ca) source and phosphoric acid [H3(PO)4] was used as a phosphorus (P) source. The solutions in two separate containers were mixed for 30 minutes on a magnetic stirrer. After 30 minutes, phosphoric acid [H3(PO)4] solution was added to the mixture of calcium nitrate [Ca(NO3)2 4H2O] and water, which was stirred with a continuous stirrer, and mixed together for another 20 minutes.

In the meantime, ammonium was added until the pH of the solution (pH=9.2). After homogenity was achieved, the mixture poured into the tray. The dried mixture was sintered at 1100 degrees for 4 hours. It was then ground to 60 microns (Fig. 2).

Fig. 2 Prepared HA powder

20 samples of 1.5 cm length, 1 cm width and 0.2 cm thickness were prepared by cutting with water jet. 5 samples were coated with hydroxyapatite and 1-2-3% TiO2 doped hydroxyapatite (Fig. 3).
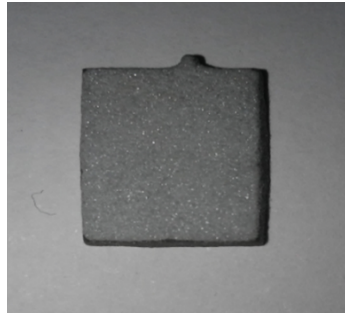
Fig. 3 Ti substrate

Powder mixtures were obtained by weighing the powder and placed in the gun chamber. Temperatures of 250∘ degrees to 300∘ degrees were reached by burning 1 bar propane gas and 2.3 bar oxygen together. The samples were placed on the panel. It was sprayed onto the sample at a speed of 1500m/s with 25 cm distance.

Fig. 4. Coating of Ti substrate by HVOF method

Table 1. Prepared compositions

Code	Solution
S1	Undoped solution
S2	1% TiO2/HA
S3	2% TiO2/HA
S4	3% TiO2/HA

4. Results

Fig. 5 Contact angles of coatings

Ra = average roughness value

Rz = the highest peak in the surface profile.

Rm = sum of maximum height and maximum depth for the entire measuring length

Rk = Average of 5 highest and 5 lowest points
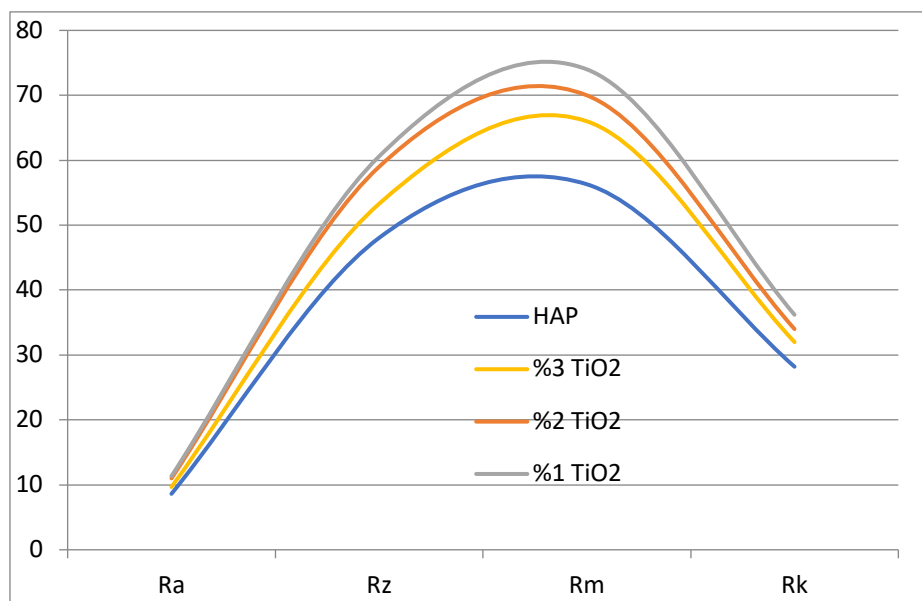
Fig. 6 Surface roughness of coatings
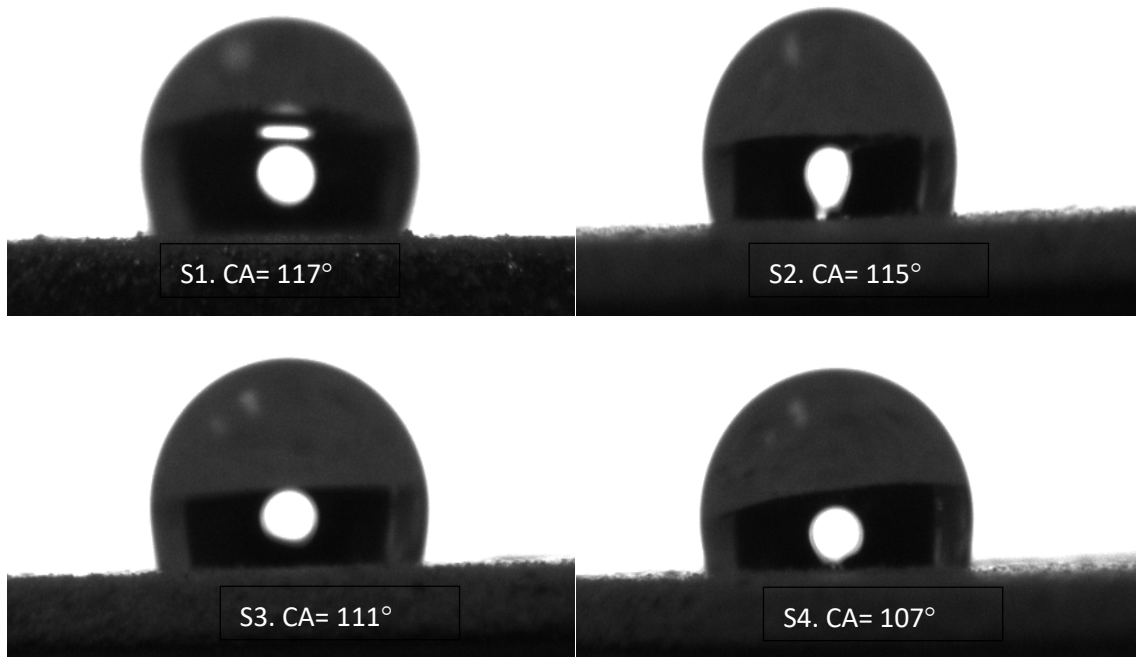
The samples were placed in the body fluid and their corrosive behavior in the body was examined. The changes in the amount of the substance were examined after the drying process by keeping it in the body for 4, 7, 14, 21 and 28 days. For 1, 2 and 3 percent TiO2, 4, 7, 14, 21 and 28-day tests were performed separately.
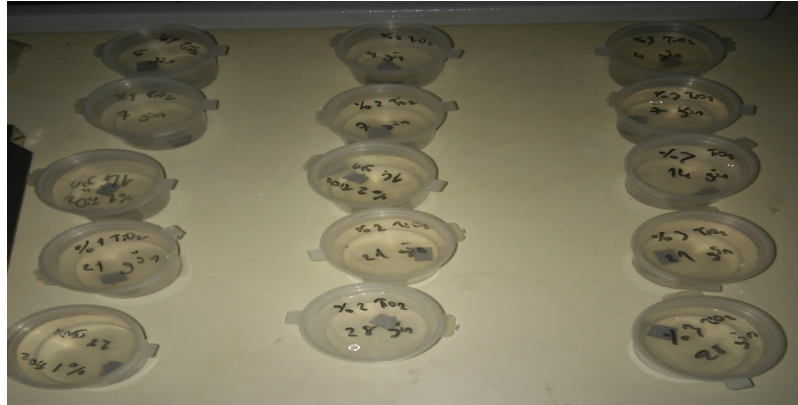
Fig. 7 Samples in SBF solutions.
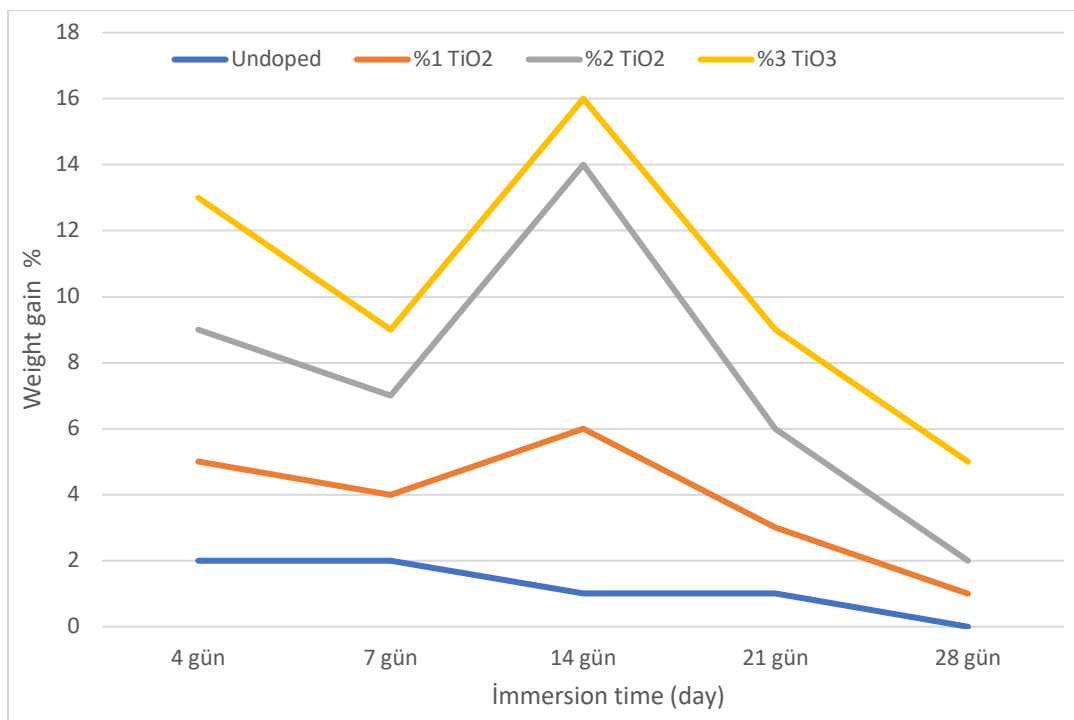
Fig. 8 Results of immersion tests

Weight gain rises with the increase of the immersion time of uncoated and coated samples in the SBF (Fig. 8). It can be said from the results that the doping of TiO2 directly affects nucleation and growth of apatite on the Titanium surface .
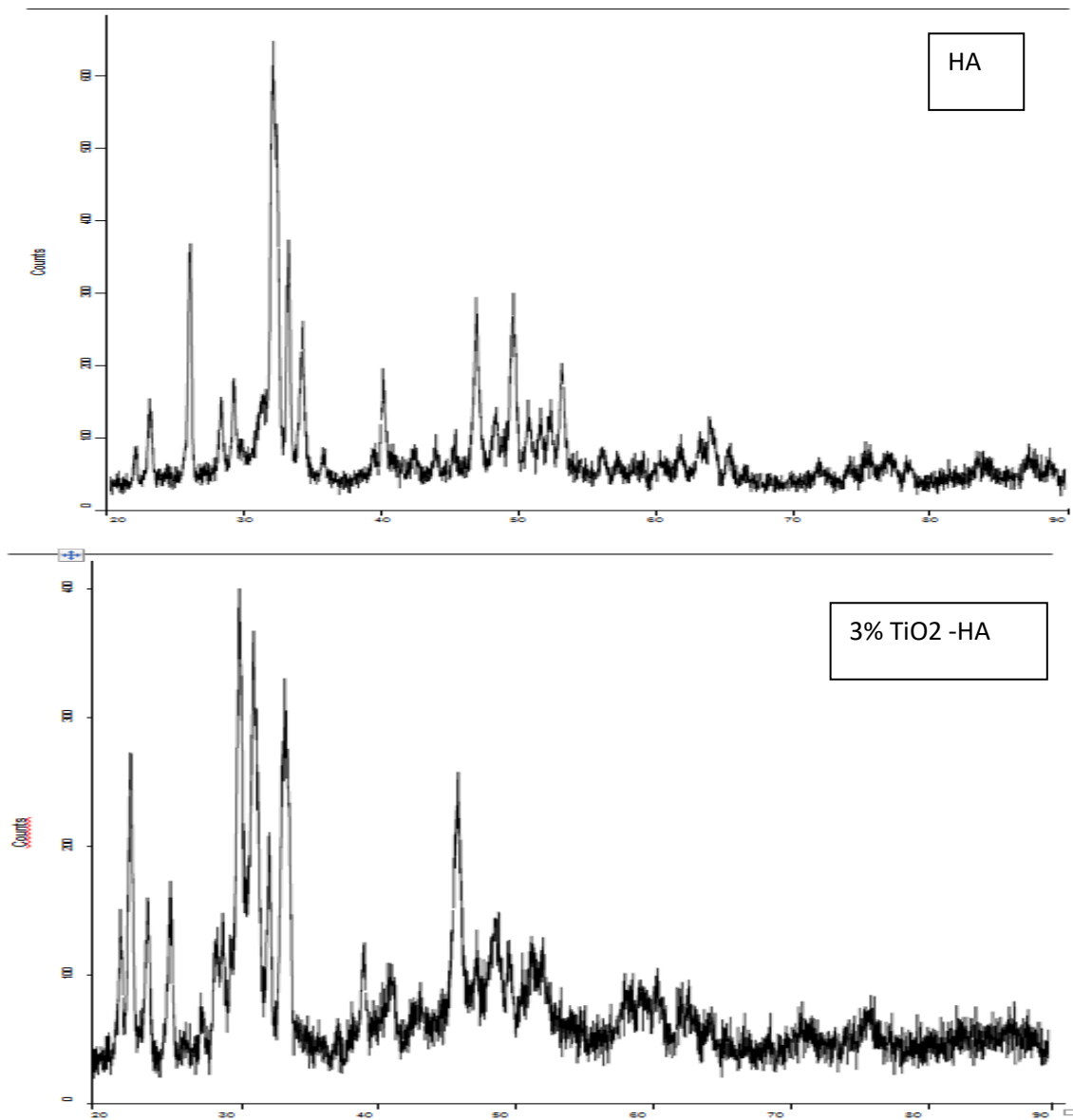
Fig. 9 XRD paterns of undoped and doped HA powders.

X-ray powder diffraction patterns for samples are shown in Fig. 9. All powder showed only diffraction peaks due to hydroxyapatite (ICDD ref: 01-074-0566. Fig. 9 shows the XRD pattern of the perovskite $CaTiO_3$. All of the diffraction peaks of $CaTiO_3$ can be indexed to the orthorhombic $CaTiO_3$ perovskite with the reported data of JCPDS No. 42-0423.

The samples were coated with bakelite. The sample surface was polished by passing through 120, 240, 320, 400, 600, 800, 1000, 1200 sandpapers, respectively, and then the images by the SEM were obtained.

HA   1% TiO2-HA

2% TiO2-HA   3% TiO2-HA
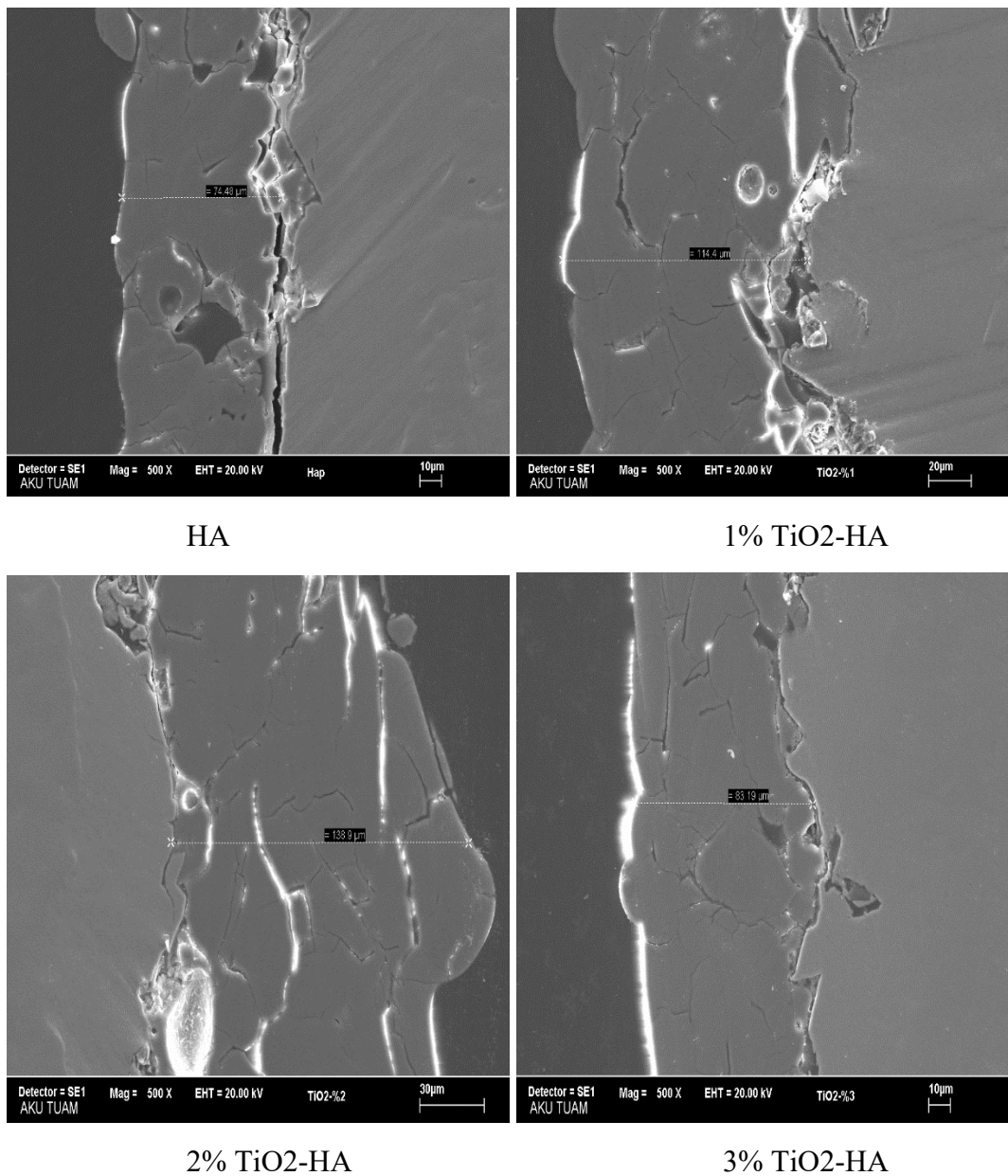
Fig. 10. SEM images of coatings.

5. Conclusion

TiO2 doped HA coating was successfully applied on the Ti implant. TiO2 additive reduced the surface contact angle. The increase in the amount of TiO2 in HA in the bioactivity test caused the Ti implant to gain weight positively. This weight increase indicates that HA nuclei are formed on the HA layer. In XRD analysis, phases formed in pure HA and TiO2 doped HA powders were determined. It was observed that CaTiO3 was formed with Calcium in HA in TiO2 contribution and it was attached to the structure by chemical bond.

References

Al-Sanabani, Jabr & Madfa, Ahmed & Al-Sanabani, Fadhel. (2013). Application of Calcium Phosphate Materials in Dentistry. International journal of biomaterials. 2013. 876132. 10.1155/2013/876132.

Cabral-Miramontes J. A., Gaona-Tiburcio C, Almeraya-Calderón F, Estupiñan-Lopez F H, Pedraza-Basulto G K, Poblano-Salas C A , "Parameter Studies on High-Velocity Oxy-Fuel Spraying of CoNiCrAlY Coatings Used in the Aeronautical Industry",*International Journal of Corrosion*, vol. 2014, Article ID 703806, 8 pages, 2014.https://doi.org/10.1155/2014/703806

Chen, F. M., & Liu, X. (2016). Advancing biomaterials of human origin for tissue engineering. *Progress in polymer science*, *53*, 86–168. https://doi.org/10.1016/j.progpolymsci.2015.02.004

Detsch R., Will J., Hum J., Roether J.A., Boccaccini A.R. (2018) Biomaterials. In: Kasper C., Charwat V., Lavrentieva A. (eds) Cell Culture Technology. Learning Materials in Biosciences. Springer, Cham. https://doi.org/10.1007/978-3-319-74854-2_6

Eshawish, N., Malinov, S., Sha, W. *et al.* Microstructure and Mechanical Properties of Ti-6Al-4V Manufactured by Selective Laser Melting after Stress Relieving, Hot Isostatic Pressing Treatment, and Post-Heat Treatment. *J. of Materi Eng and Perform* **30,** 5290–5296 (2021). https://doi.org/10.1007/s11665-021-05753-w

Fergal J. O'Brien, Biomaterials & scaffolds for tissue engineering, Materials Today, Volume 14, Issue 3, 2011, Pages 88-95, https://doi.org/10.1016/S1369-7021(11)70058-X.

Fiume,E., Magnaterra,G., Rahdar, A., Verné, E., Baino, F. Hydroxyapatite for Biomedical Applications: A Short Overview. *Ceramics* **2021**,*4*,542–563. https://doi.org/10.3390/ceramics4040039

Henriques, Vinicius. (2009). Titanium production for aerospace applications. Journal of Aerospace Technology and Management. 1. 10.5028/jatm.2009.01010717.

Hoppe, V., Szymczyk-Ziółkowska, P., Rusińska, M., Dybała, B., Poradowski, D., & Janeczek, M. (2020). Assessment of Mechanical, Chemical, and Biological Properties of Ti-Nb-Zr Alloy for Medical Applications. *Materials*, *14*(1), 126. doi:10.3390/ma14010126

Kurup A, Dhatrak P, Khasnis N, Surface modification techniques of titanium and titanium alloys for biomedical dental applications: A review, Materials Today: Proceedings, Volume 39, Part 1, 2021, Pages 84-90, https://doi.org/10.1016/j.matpr.2020.06.163.

Mott N F, 1951 Proceedings of the Physical Society. Section B, Volume 64, Number 9, 729

Nicholson, J.W (2020). Titanium Alloys for Dental Implants: A Review. *Prosthesis*, *2*(2), 100–116. doi:10.3390/prosthesis2020011

Peters, M., Kumpfert, J., Ward, C.H., Leyens, C.. (2003). Titanium Alloys for Aerospace Applications. Advanced Engineering Materials. 5. 419 - 427. 10.1002/adem.200310095.

Pokhrel S, Hydroxyapatite: Preparation, Properties and Its Biomedical Applications, Advances in Chemical Engineering and Science, Vol.8 No.4, 2018

Sobolev V, Guilemany, J M, Nutting J, (2004). High Velocity Oxy-Fuel Spraying. W.S.Maney & Sons Ltd. The Institute of Materials, Minerals and Mining. 397p. London.UK.

MANUFACTURING OF COCOON PLANTER USING INDEGENIOUS RECYCLABLE MATERIAL

Enjila Irfan [1], Areeba Alam [1], Hafsa Shafi [1], Afifa Baqai [1]

[1] Materials Engineering Department, NED Universitty of Engineering an Technology

Abstract

"Cocoon planter" is a water-efficient technology that helps trees to survive with little irrigation even in desert-like climates. It provides a safe shelter from the harsh surrounding environment and an adequate water for irrigation of first critical year of tree. Cocoon Planter is basically an Innovative technologies of planting and foresting to people living in arid and semi-arid climates.In our Cocoon Planter we aren't using the standard materials that are being used until now by Land Life and Groasis Companies. Instead we are using an indigenous material that are available in Pakistan to make the Cocoon Planter.

Keywords : Cocoon Planter, Water-Efficient Technology, Recycle

SYSTEMATIC REDUCTION OF CASTING DEFECTS WITH THE HELP OF MODELING AND SIMULATION

Muhammmad Abdul Hai [1], Shaheer Siddiqui [1], Kamran Khalid [1], Hammad Siddiqui[1]

[1] NED University Of Engineering and Technology, Materials Engineering Department

Abstract

Sand casting, also known as sand molded casting, is a metal casting process characterized by using sand as the mold material. Over 60% of all metal castings are produced via sand casting process. Modeling refers to creation of a 3d model using a CAD software. It is then exported to a CAE software for Simulation or to a CAM software for manufactur-ing. Simulation is the imitation of a situation or process on a CAE Soft-ware. It is used for the purpose of thermal analysis, removing defects, optimization etc. It includes designing a 3d model on a CAD software, exporting it to a CAE software for simulation, filling in the parameters, and observing the results.

Keywords : Sand Casting, Metal Casting, Cad

DESIGN AND DEVELOPMENT OF SUPERCRITICAL DRYING SYSTEM (SCD) FOR SILICA AEROGEL PRODUCTION

[1] M.Saad Khan, [1] Usama Khan, [1] Ahazam Ansari, [1] Tayyab Azad Khan

[1] Ned University of Engineering and Technology Karachi Department of Materials Engineering

Abstract

Aerogels belongs to an innovative class of advanced materials with applications ranging from heat transfer to fluid separation processes. This research study focuses on the development of a Super critical drying (SCD) systems which is an integral part to produce fine quality aerogels. A typical SCD system consists of a high pressure chamber (up to 100bar) with temperature range of 50°C. After research and the group has completed the procurement of the SCD parts, and assembly of the system[2]. This SCD system was designed and developed and the synthesis of Silica aerogel was performed by using different organic chemicals i.e TMOS, Methanol, Ammonium Hydroxide. The study aims at synthesis of silica-based aerogels using phase one SCD system and got the final product which is Silica Aerogel. [2] The silica aerogel is characterized by using Scanning Electron Microscopy, X-ray Diffraction and Fourier Transfrom Infrared Spectroscopy to conclude the final product which is Silica Aerogel.

Keywords: Silica Aerogel, Advanced Materials, Super Critical Drying

JOINING AND ANALYSING THE EFFECT OF TIG AND FS-WELDING ON NONFERROUS ALLOYS

M.Hassan Bin Shaukat[1], S.M AbuTalib Zaidi [1], M.Shariq Hasnain [1]

[1] Ned University of Engineering and Technology Karachi, Department of Materials Engineering

Abstract

Joining is a fundamental manufacturing process that is essential for making any assembly such that jet plane could never be possible to form in a single piece.In joining category, welding class has strongest and permanent joint moreover welding result in changing metallurgical, mechanical and physical properties in weld and near weld region. In the current research, TIG welding is applied to overcome welding problems in nonferrous alloys whereas FSW welding is adopted to replace fusion (TIG) welding because of various metallurgical, environmental and mechanical strength disadvantages occurred in fusion welding.

Keywords : TIG welding, FS-Welding, Nonferrous Alloys

SIMULATION OF BORIDING KINETICS OF AISI T 1 STEEL BY INTEGRAL MODEL

Brahim Boumaalı [1*]

[1] University of Science and Technology Houari Boumediene, Laboratoire de Technologie des Matériaux, Bab-Ezzouar, Algiers, Algeria

Abstract

AISI T1 steel was hardened by the solid boriding process in the temperature range 1123-1273K, for a period of 2 to 8 hours. A kinetic model, based on the integral method, was applied to the growth of a single boride (Fe2B) layer on the surface of AISI T1 steel.The activation energy for the diffusion of boron in AISI T1 steel was estimated at 213.03 kJ mol-1 and a comparison was made with other values available in the literature.A satisfactory concordance has been observed when comparing the experimental values of Fe2B layers' thicknesses with the predicted results. This diffusion model has been validated experimentally by considering two additional boriding conditions.

Keywords : Boriding, AISI T1 Steel, Integral Model

* Corresponding Author e-mail : brahimboumaali@yahoo.com

DESIGN AND DEVELOPMENT OF GREEN COMPOSITES USING NATURAL FIBERS

Hafiz Muhammed Bilal Hussain [1], Muhamed Sami Khan [1], Ebad Hassan Khan [1]

[1]Ned University of Engineering & Technology Department of Materials Engineering

Abstract

Green composites are basically sustainable composites materials that are combination of Natural Fibers and Natural resins. Importance of these materials is biodegradability, use of natural material and strength, due to these characteristics they have gained a lot of importance in the field of Materials engineering. The overview of the project is as follows; To Develop a fiber reinforced green composite having gelatin matrix reinforced with natural fibers (include coconut, banana and sugar cane). To Compare the mechanical properties of different fibers reinforcement in a similar matrix. To Compare the effect of fiber length (different Grades of Fibers) on mechanical properties of a similar material in same matrix. Fibers were collected from the warehouse and then shredded and boiled in hot water in order to remove contamination. Banana & Sugarcane fibers are rich in sugar so their boiling is mandatory to remove the juicy liquid from them. After boiling in hot water for half an hour they were filtered and then dried in air for five days. After complete drying they were subjected to grinding to obtain a workable size of them to proceed further for composite making. According to the given composition matrix was prepared and then fibers are embedded in mold and samples are prepared through hand layup process.

Keywords : Green Composites, Natural Fibers, Natural Resins, Biodegradability

DESIGN OF EXPERIMENTS (DOE) FOR THE DEVELOPMENT OF GREEN TYRE TREAD BY REDUCING CARBON WITH ECO-FRIENDLY FILLER

Hamna Siddiqui [1], Syed Usama Athar [1], Arsal Sohal [1], Asad Raza [1]

[1]Ned University of Engineering and Technology Materials Engineering Department

Abstract

Design of experiments(DOE) is defined as a branch of applied statistics that deals with planning, conducting, analyzing, and interpreting controlled tests to evaluate the factors that control the value of a parameter or group of parameters. DOE is a powerful data collection and analysis tool that can be used in a variety of experimental situations. DOE is suitable for a condition where more than one in put factors are suspected of influencing the output. For instance it maybe desirable to understand the effect of binder and pigment on the adhesion of paints. Or one want to analyze the effect of temperature, pressure and alloying elements on a steel alloy. Or the one is evaluating the tire performance on the basis of various factors in the recipe. So precisely it is applicable for all the industries dealing with recipes for the product development. Through DOE, you can deal with even up to 6 or 8 factors of that particular recipe. It is a one time effort approach resulting in the production to be tim effective, free of vaining raw materials, efficient, as results compiled on the basis of equations/designed models. From the obtained results it can be analyzed that the motive which is to minimize the rolling resistance yet with better traction has been achieved throgh DOE based investigation,Thus an healthy eco-system can be established with lowest amounts of fuel consumption.

Keywords : DOE (Desing of Experiments), Carbon Reducing, Eco-Friendly

DESIGN & DEVELOPMENT OF CERAMICS FOR THERMOPOWER APPLICATIONS

Syeda Sabika Fatima [1], Faaz Ahmed Khan [1], Muhammad Ahmed Raza [1], Muhammad Usman [1]

[1]Ned University Of Engineering And TechnologyDepartment Of Materials Engineering

Abstract

Strontium titanate(STO) ceramics were synthesized by solid state sintering using strontium carbonate and titanium dioxide. The samples were doped with bismuth oxide and iron oxide in different proportions. Compound to be formed as thermoelectric ceramic consist of SrBiTiFeO3. With the help of this project we learned that how thermoelectricmaterial ceramics can be of great importance other than their high temperature and corrosion resistance properties.

Keywords: Strontium Titanate, Thermoelectric Ceramic,

PHOTOCATALYTIC DEPOSITION OF HIERARCHICAL STRUCTURES

Salih Veziroglu[1*], Cenk Aktas [1], Franz Faupel[1]

[1] Chair for Multicomponent Materials, Institute of Materials Science, Kiel University, 24143 Kiel, Germany

Abstract

Noble metal (Au, Ag, and Pt, etc.) hierarchical structures have been received remarkable attention during the last decades, due to their special shape, high surface area, electronic, and catalytic properties. Especially, the incorporation of these hierarchical structures with wide-bandgap metal oxide semiconductors such as titanium oxide (TiO_2) and zinc oxide (ZnO) has been shown many times for various applications such as photocatalysis [1,2,] water splitting, self-cleaning[3], biomolecular detection, sensor applications, and so on. There are various studies about the synthesis of hierarchical structures with well-defined size and morphology in the literature. However, it is still a challenge to achieve good adhesion between hierarchical structures and metal oxide surfaces, especially with TiO_2 thin film. Therefore, some approaches (seed-mediated growth, etc.) have been published to enhance the adhesion of metallic hierarchical structures on TiO_2 thin film by using some binder molecules (thiols and silanes, etc.). Mostly organic molecules are used for binding metallic hierarchical structures with a solid substrate. However, these may decrease the surface conductivity and contaminate the surface which affects the performance of the hierarchical structures. Similarly, electrodeposition methods can also be used to prepare metallic hierarchical structures on solid substrates. But the electrodeposition process is only applied on the conductive substrate such as indium tin oxide (ITO). Therefore, there is a need to prepare stable Au or Ag hierarchical structures on TiO_2 thin films without using any organic molecules (binders) or a conductive electrode. Here, we demonstrated a novel photocatalytic deposition approach for preparing Au and Ag hierarchical structures on TiO_2 thin film surface by UV illumination with strong chemical adhesion for wide-range applications such as photocatalytic degradation of organic contaminants, self-cleaning and oil-water separation. This method allows the controlling the geometry, size, and distribution of such Au and Ag hierarchical structures on TiO_2 thin film by simply changing the deposition solution, photocatalytic activity of metal oxide, UV illumination intensity, and time.

Keywords: Hierarchical, Metallic and Bimetallic Structures, Photocatalytic Deposition, TiO_2Thin Film

* Corresponding Author e-mail:sve@tf.uni-kiel.de

WO₃ VE TEO₂ İLAVESİNİN BAZALT CAMLARININ RADYASYON ZIRHLAMA ÖZELLİKLERİ ÜZERİNDEKİ ETKİLERİ

Bilgehan Güven[1*], Ediz Ercenk[1], Şenol Yılmaz[1]

[1] Sakarya Üniversitesi, Mühendislik Fakültesi, Metalurji ve Malzeme Mühendisliği Bölümü, Sakarya, Türkiye.

Özet

Bu çalışmada doğal volkanik kayaç bazalttan elde edilen camın radyasyon zırhlama uygulamalarında kullanılabilirliği araştırılmıştır. Kırma öğütme sonrası toz hale getirilen bazalt kayacına ağırlıkça % 30 WO_3 ve TeO_2 katılarak elde edilen bileşimler homojenizasyon için bilyalı değirmende karıştırma işlemine tabi tutulmuştur. Katkısız, WO_3 ve TeO_2 katkılı olarak hazırlanan 3 bileşim 1500 °C'de ergitilerek bazalt camları elde edilmiştir. Katkı maddelerinin bazalt camının radyasyon zırh kabiliyeti üzerine etkilerini incelemek amacıyla camların 276, 302, 356 ve 383 keV enerji değerlerinde lineer zayıflatma katsayıları, yarı-değer kalınlık ve ortalama serbest yol değerleri elde edilmiştir. Elde edilen değerler ele alındığında katkı maddelerinin bazalt camının radyasyon zırhlama özelliğini arttırdıkları tespit edilmiştir. Ayrıca WO_3 ilavesinin bazalt camının zırhlama kabiliyetini arttırmada TeO_2 ilavesinden daha iyi etki ettiği görülmüştür.

Anahtar Kelimeler: Bazalt, Cam, Radyasyon Zırhlama.

* İlgili yazar e-posta: bilgehanguven07@gmail.com; bilgehan.guven2@ogr.sakarya.edu.tr

FONKSİYONEL DERECELENDİRİLMİŞ Si₃N₄ ESASLI SERAMİKLERİN ÜRETİMİNDE FARKLI SOĞUK İZOSTATİK PRES (CIP) BASINÇLARININ ETKİSİNİN İNCELENMESİ

Beyza Kasal[1,2]*, Ertancan Babaç[1,2], Yasemin Tabak[1], Bayise Kavaklı Vatansever[1], Ayşen Kılıç[1],   Metin Usta[1,2]

[1]TÜBİTAK Marmara Araştırma Merkezi, Malzeme Enstitüsü, Gebze, Kocaeli, Türkiye

[2]Gebze Teknik Üniversitesi, Malzeme Bilimi ve Mühendisliği Bölümü, Gebze, Kocaeli, Türkiye

Özet

Silisyum nitrür seramikler sitotoksik olmaması, yüksek kırılma tokluğu, uzun ömürlü olması, aşınma direnci ve düşük sürünme katsayısı gibi üstün özellikleri nedeniyle biyo uygulamalarda gün geçtikçe daha fazla kullanım alanı bulmaktadır. Bu çalışmada, şerit döküm yöntemi ile biyomalzeme uygulamalarında kullanılmak üzere fonksiyonel derecelendirilmiş Si₃N₄ malzemesinin, organik bazlı süspansiyonlarının hazırlanması ve hazırlanan şeritlerin farklı soğuk izostatik pres basıncında (1000-1500-2000-2500 bar) preslenmesi hedeflenmiştir. Kullanılan hammaddelere XRD, SEM, tane boyut analizi yapılıp hazırlanan süspansiyonun zeta potansiyeli ve reolojik ölçümleri yapılmış, optimum koşullarda döküm işlemi gerçekleştirilmiştir. Yapılan deneysel çalışmada ana hammadde olan Si₃N₄'ün dışında solvent, bağlayıcı, plastikleştirici, sinterleme katkısı ve por yapıcı (grafit tozu) gibi ilaveler kullanılmıştır. Hazırlanan süspansiyonlar 18 saat karıştırılmış ve şerit döküm cihazı ile döküm yapılarak ham şeritler elde edilmiştir. Ham şeritler kurutulduktan sonra belirlenen boyutlarda kesilip 4 farklı porozite oranında (her katman 5 şerit olacak şekilde) lamine edilmiştir. Ardından üretilen silisyum nitrür şeritlerin şekillendirmesi için ise soğuk izostatik presleme (CIP) yöntemi kullanılmıştır. Şekillendirilen parçalara bağlayıcı giderme işlemi uygulanmış olup ardından hava ortamında 1500 °C'de sinterleme işlemi yapılmıştır. Sinterlenmiş olan poroz numunelerin taramalı elektron mikroskobu (SEM) ile yapılan mikroyapı analizlerinde şeritler arasındaki bağlanma, grafitin por oluşumuna etkisi, por yapısı ve dağılımı, sinterlenmenin gelişimi incelenmiştir. Sinter sonrası XRD analizi yapılarak fazlar incelenmiş olup sonuçların değerlendirmeleri yapılarak beklenen özellikleri sağlayan CIP basıncı seçilerek proses optimize edilmiştir.

Anahtar Kelimeler: Silisyum Nitrür, Fonksiyonel Derecelendirilmiş Malzeme, Şerit Döküm, Soğuk İzostatik Presleme.

* İlgili yazar e-posta: b.kasal2020@gtu.edu.tr

KUBBE-İ HADRA RESTORASYON ÇİNİLERİNİN KARAKTERİZASYONU

Çetin Öztürk[1*]

[1] Necmettin Erbakan Üniversitesi, Geleneksel Türk Sanatları Bölümü, Konya, Türkiye

cozturk@erbakan.edu.tr

1. Giriş

En son 1965 yılındaki [Bakırcı 2020] restorasyonda yenilenen Mevlana Türbesinin çini kaplı dış cephe duvar yüzeylerinde enine ve dikine derin çatlaklar, yer yer kabarmalar, kubbenin uç kısmına doğru kavlama, kopma ve dökülmeler tespit edilmesi sonucu kubbe restorasyona alınmıştır.

Yaklaşık 55 yıl dayanan kubbe çinilerinde meydana gelen tahribatın nedenleri araştırıldığında çini plakalar arasındaki derz dolgularında çözünme ve boşalmaların olduğu görülerek yapının su aldığı anlaşılmıştır. Konya gibi özellikle kışın meydana gelen donma ve çözülme olayları duvar kaplama malzemelerinin su emme, basınç ve aşınma dayanımlarını olumsuz etkilemektedir. Bununla birlikte kubbeden kopan çini parçalarındaki harç kalıntılarından çinilerin kubbeye çimento ile tutturulduğu belirlenmiştir. Dönemin şartlarına göre kullanıldığı düşünülen çimento çini restorasyonlarında tercih edilmeyen bir malzemedir. Çünkü çimento zamanla tuz oluşumuna neden olmakta ve oluşan tuz nem ve ısı etkisiyle kristalleşerek çinilerde çatlamalar ve kopmalara yol açmaktadır [Işıkhan 2012]. Bu yüzden Kubbe-i Hadra gibi tarihi yapıtların dış cephe kaplama malzemeleri yenilenirken, sadece üretilecek olan çininin teknik kalitesi değil aynı zamanda çinilerin yapıştırılmasında kullanılacak olan harç ve derz seçimi de çini ömrü açısından oldukça önemlidir.

Türk İslam Mimarisinde sert ve dayanıklı yapılarından dolayı duvar kaplama malzemesi olarak sıklıkla yüksek silisli (en az % 85 silis) çiniler kullanılmaktadır [Mason 1994]. Yüksek orandaki silisin pişme sonrası nihai ürün ebatlarında ölçü birliğinin korunmasında ve deforme olmaksızın büyük ebatlarda üretimi üzerinde olumlu etkileri vardır [Arcasoy 1983]. Osmanlıdan günümüze yüksek oranda silis içerikli çinilerin şekillendirilmesi "tap tap" yöntemi olarak adlandırılan kalıba elle sıkıştırma tekniği ile gerçekleştirilmiştir [Kızıl 2010]. Tap tap şekillendirme yöntemi bünyede su tahliyesini kolaylaştıracak bir gözenek dağılımı sağlamaktadır [Öztürk 2020].

Günümüzde kaplama malzemesinin teknik özelliklerin belirlenmesinde o bölgenin iklim şartlarına göre hazırlanmış 'Ayrışma İndeksi' olarak adlandırılan verilerden faydalanılmaktadır. İskender Işık ve arkadaşları tarafından hazırlanan Türkiye'nin ayrışma indeksi haritasında Konya donma/çözülme olaylarının sert görüldüğü bölgede yer almaktadır [Işık ve ark. 2017]. Bu yüzden restorasyonda kullanılacak çinilerin seçiminde mukavemet, dona ve termal şoka dayanım belirleyici faktör olmaktadır.

Restorasyon sürecinde aslına uygun olarak yenilenecek olan kubbe çinilerinin yüksek oranda silis içerikli (en az % 85 SiO_2), örtücü turkuaz sırlı, yüksek mukavemetli ve dona dayanıklı olması gibi bazı kriterlere sahip olması gerektiği Müze Müdürlüğü tarafından oluşturulan bilim kurulunca belirlenmiştir.

2. Deneysel Çalışma

Konya Müze Müdürlüğünce farklı firmalara 12cm x 24cm x 2cm ebatlarında ürettirilen çini örneklerine Eskişehir Seramik Araştırma Merkezinde (SAM) su emme testi, mukavemet testi, termal şok dayanım testi, dona dayanım testi, kimyasal analiz, renk değişimi tayini, kimyasallara dayanım testleri yaptırılmıştır. Restorasyonda kullanılacak çinilerin belirlenmesinde yol gösterici olması için çini örneklerine SAM'da yaptırılan test ve analiz sonuçları teknik açıdan değerlendirilmiştir.

2.1. Su Emme Analizi ve Mukavemet Test Sonuçları:

Su emme testi TS EN ISO 10545-3 standartlarına, mukavemet testi ise TS EN ISO 10545-4 standartlarına göre yapılmıştır. Her iki test için 10 adet numune kullanılmış ve test sonucunda elde edilen ortalama değerler Grafik 1'de verilmiştir.
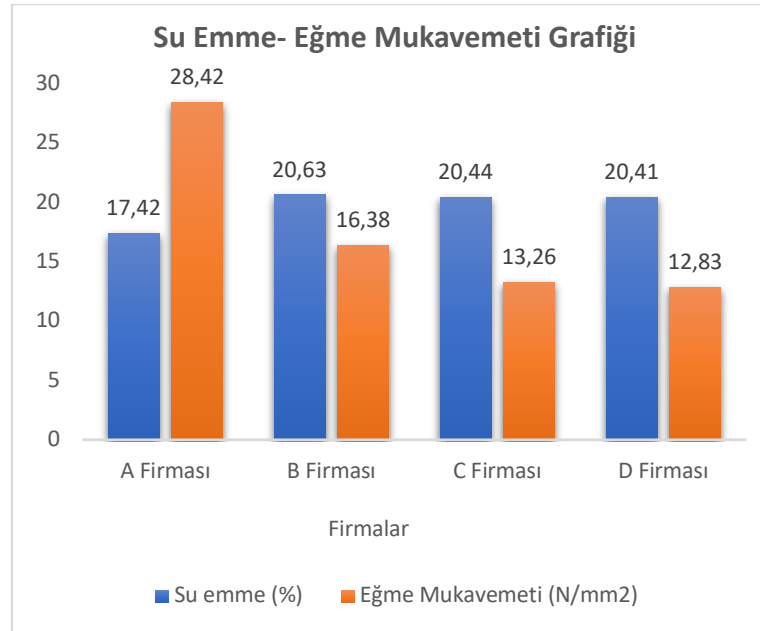
Grafik 1. Su emme deney sonuçları

Grafik 1'de verilen su emme ve mukavemet testi sonuçları incelendiğinde A firmasına ait çini örneklerinin su emme değerlerinin diğer test numunelerine göre düşük (% 17,42) mukavemetinin ise oldukça yüksek (28,42 N/mm^2) olduğu görülmektedir.

2.2. Kimyasal Analiz (XRF) Sonuçları:

Çinilerin bünye kimyasal analizi Tablo 1'de verilmiştir. Tabloda alkali (Na_2O ve K_2O), toprak alkali (MgO ve CaO) ve PbO oranı toplam değer olarak sunulmuştur. Yüksek silisli bünye (en az % 85) çini seçiminde belirleyici etmenlerden biridir.

Tablo 1. Firma çinilerinin bünyelerindeki silis oranı

Oksitler (%) Firmalar	SiO_2	Al_2O_3	Fe_2O_3	TiO_2	P_2O_5	Σ(Alkali+ Toprak Alkali+ PbO)	A.Z.*
A Firması	90,45	4,30	0,44	0,12	-	4,43	0,26
B Firması	88,32	1,72	0,26	0,33	0,02	9,25	0,10
C Firması	77,51	9,19	0,27	0,10	0,05	12,34	0,54
D Firması	77,35	9,24	0,49	0,15	0,06	12,49	0,22

*A.Z. Ateş Zayiatı

2.3. Termal Şok Dayanım Test Sonuçları:

Termal şok dayanım testi TS EN ISO 10545-9 standartlarına uygun olarak yapılmıştır. 5 adet çini örneği üzerinde gerçekleştirilen test sonucunda elde edilen değerlendirme sonucu Tablo 2'de verilmiştir.

Tablo 2. Termal şok dayanım test sonuçları

Firmalar	A Firması	B Firması	C Firması	D Firması
Termal Şok Dayanımı	5/5 Hasarsız	5/5 Hasarsız	5/5 Hasarsız	5/5 Hasarsız

Tablo 2'de verilen Termal şok dayanım test sonuçlarından tüm çini örneklerinin termal şoka karşı dayanıklı olduğu anlaşılmaktadır.

2.4. Dona Dayanım Test Sonuçları:

Dona dayanım testi TS EN ISO 10545-12 standartlarına uygun olarak yapılmıştır. 10 adet çini örneği üzerinde gerçekleştirilen test sonucunda elde edilen sonuçlar Tablo 3'de verilmiştir.

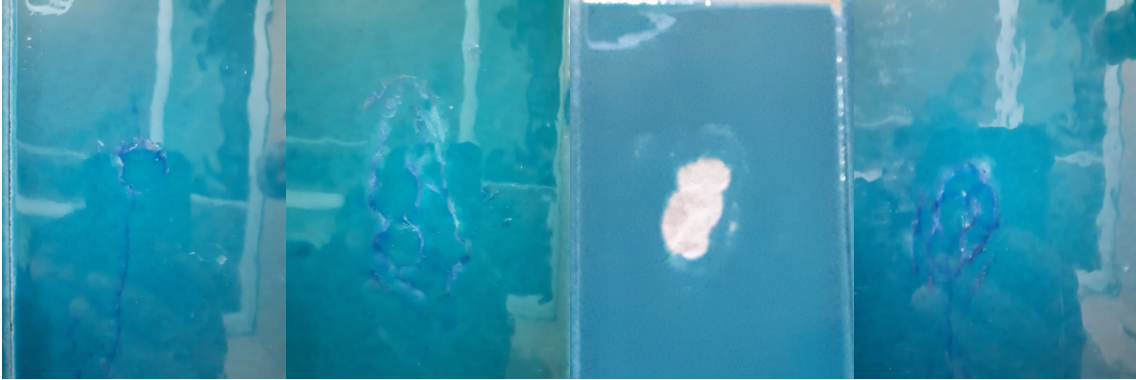**Tablo 3.** Dona Dayanım Testi Sonuçları

Firmalar	A Firması	B Firması	C Firması	D Firması
Dona Dayanım	**100** Çevrimde Hasarlı: 5 **Sağlam:5** Su Emme: **13,83- 14,46**	**24** Çevrimde Hasarlı: 10 **Sağlam:0** Su Emme:-	25 Çevrimde Hasarlı: 10 Sağlam:0 Su Emme:-	100 Çevrimde Hasarlı: 6 Sağlam:4 Su Emme: 17,51-18,68

Tablo 3' de sunulan dona dayanım testi sonuçlarına göre A firmasına ait çini örneklerinin tamamı 100 çevrimden geçmiş ve 10 numuneden 5 tanesinde hasar tespit edilmiştir. Test numunelerinde tespit edilen tahribatlar Fotoğraf 1'de verilmiştir. Buna göre hasarlar çini sırlı yüzeyin tek noktasında oluşmuş olup ilerleme göstermeden sönümlenmiştir.
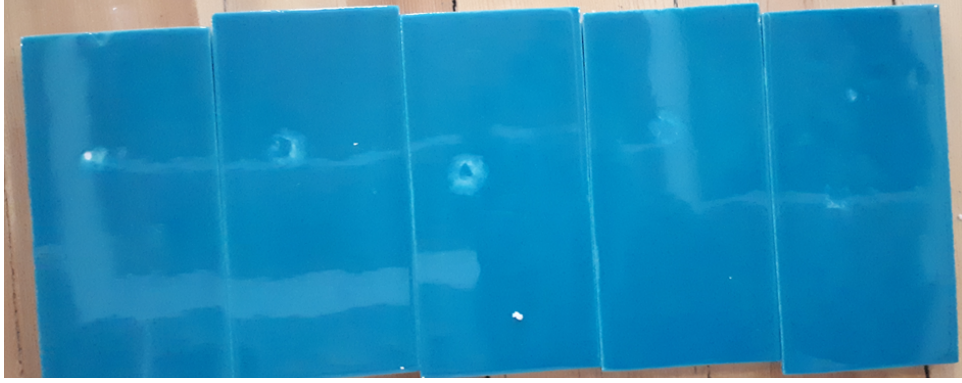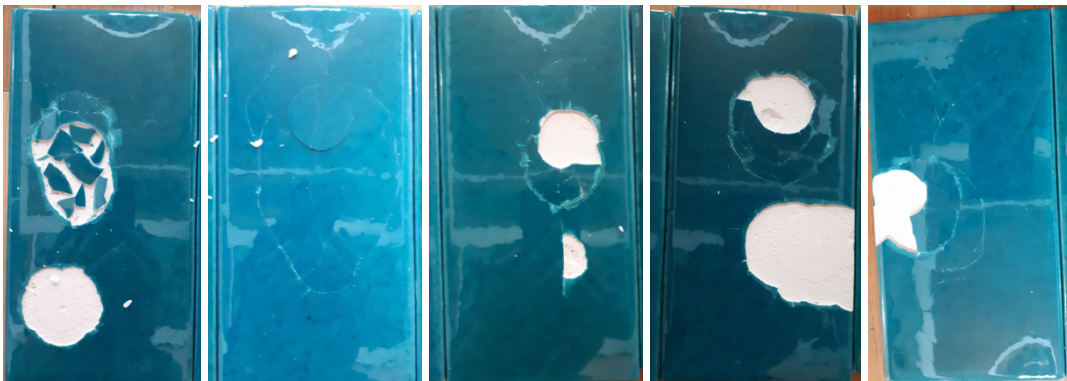
Fotoğraf 1. A firmasına ait çini örneklerinin dona dayanım testi sonrası görünümü.

B firmasına ait çini örneklerinin dona dayanım testinde ise 25. çevrimde numunelerin tamamında tahribat meydana gelmiştir (Tablo 3). Tahribat meydana gelen test numuneleri Fotoğraf 2'de görülmektedir. Test sonucunda numunelerinin sırlı yüzeylerinde bölgesel kavlama, dikine uzun çatlama ve ağ şeklinde çatlamalar oluşmuştur.

Fotoğraf 2. B firmasına ait çini örneklerinin dona dayanım testi sonrası görünümü.

C firmasına ait çini örneklerinin dona dayanım testinde 24. çevrim sonucunda test numunelerinde tahribat meydana geldiği görülmektedir (Fotoğraf 3). Fotoğraf 3'e göre deney numunelerinin sır tabakaları bünyeden ayrılmıştır. Tahribat oluşum şeklinden çini bünyesi ile çini sırı arasındaki uyumsuzluk olduğu anlaşılmaktadır. Bunula birlikte sır bütünlüğü açısından da yer yer farklılıklar bulunmaktadır.

Fotoğraf 3. C firmasına ait çini örneklerinin dona dayanım testi sonrası görünümü.

D firmasına ait çini örneklerinde dona dayanım testi sonrasında test numunelerinin 4'ü 100 çevrim sonucunda dona dayanım sağladığı belirlenmiştir. Fotoğraf 4' te dona dayanım testi sonucunda test numunelerde görülen tahribatlardan örnekler görülmektedir. Tahribatlar sırlı yüzeylerde kavlamalar, sır çatlakları, sırda kabarmalar ve uzayan çizgisel çatlaklar şeklindedir. Bunula birlikte sırda güçlü bir örtücülük elde edilememiştir.

Fotoğraf 4. D firmasına ait çini örneklerinin dona dayanım testi sonrası görünümü.

Dona dayanım test sonuçlarına göre A firmasına ait çini örneklerinde dona dayanımının diğerlerinden daha yüksek olduğu anlaşılmaktadır.

2.5.Kimyasallara Dayanım Testi:

Kimyasallara dayanım testi TS EN ISO 10545-13 standartlarına göre gerçekleştirilmiş olup deney için her bir çini üreticine ait 3 adet çini örneği kullanılmıştır.

Tablo 4. Kimyasallara dayanım testi sonuçları

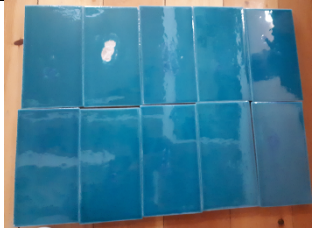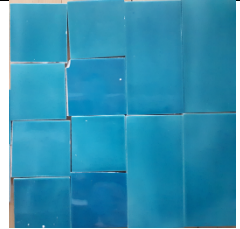| Firmalar	Ev Kimyasalları	Yüzme Havuzu	Düşük Konsantrasyonlar			Yüksek Konsantrasyonlar		
			HCl	Sitrik Asit	Alkali	HCl	Laktik Asit	Alkali
A Firması	A	A	LB	LB	LA	HC	HB	HA
B Firması	A	A	LB	LA	LA	HB	HA	HA
C Firması	A	A	LB	LB	LA	HB	HB	HA
D Firması	A	A	LA	LA	LA	HA	HA	HA

L: Düşük, H: Yüksek, A: Görülebilir değişiklik yok, B: Görünüşte belirgin değişiklik yok, C: Orijinal yüzeyde kısmen veya tamamen bozulma

Kimyasallara dayanım test sonucunda tüm çini örneklerinin kimyasallara karşı istenen düzeyde dayanıklı olduğu görülmüştür.

2.6.Renk Bütünlüğü:

Firmalara ait test numuneleri fiziksel muayene ile incelenmiş ve ulaşılan bulgular Tablo 5'te sunulmuştur

Tablo 5. Test numunelerinin renk bütünlüğü muayenesi

Firmalar	A Firması	B Firması	C Firması	D Firması
Renk Bütünlüğü	Renk bütünlüğü tam sağlanmış	Renk bütünlüğü tam olarak sağlanamamış ve renkte dalgalanmalar mevcut	Farklı tonda görünümler mevcut, renk bütünlüğü sağlanmamış	Farklı tonda görünümler mevcut, renk bütünlüğü sağlanmamış
Fotoğraf				

Test numuneleri görsel olarak karşılaştırıldığında renk bütünlüğünün A firmasına ait çini örneklerinde sağlandığı görülmektedir.

3. Sonuç

Karakterizasyon çalışmaları sonucunda Müze Müdürlüğü tarafından oluşturulan bilim kurulunca belirlenen kriterlerde çinilerin üretildiği görülmüş ve genel olarak yüksek silis içerikli (>%90) çinilerin daha düşük su emmeli, yüksek mukavemetli olduğu ve ayrıca örtücü sırla iyi pekiştiği ve sırlı yüzeyde herhangi bir sır hatası içermediği anlaşılmıştır.

Kaynakça

Arcasoy A., ''Seramik Teknolojisi'', M.Ü. G.S.F. Seramik ASD Yay., No:2, İstanbul, (1983), 119-120.

Bakırcı N., 2020,. Kubbe-i Hadrâ'nın Karamanoğlu Döneminden Günümüze Değişen Çinileri. İSTEM / 36: 541-557. https://doi.org/10.31591/istem.833936

Işık İ., Uzunoğlu Aydoğan D. ve Karaca M., 2017, Tarihi yapıların korunması ve güçlendirilmesinde ayrışma indeksi haritasının kullanımı, Uluslararası Katılımlı 6. Tarihi Yapıların Korunması ve Güçlendirilmesi Sempozyumu, 659 – 668. Trabzon: Karadeniz Teknik Üniversitesi.

Işıkhan, S. S., 2012, Tarihi Çinilerde Yapısal Özellikler Ve Karşılaşılan Bozulmalar, *Yedi, Dokuz Eylül Üniversitesi Güzel Sanatlar Fakültesi Dergisi*, **7**, 15 – 22.

Kızıl, M., ''Cumhuriyet Dönemi Kütahya Çinisinde Görülen Uygulama Teknikleri Ve Yenilikler'', Yüksek Lisans Tezi Afyon Kocatepe Üniversitesi, Sosyal Bilimler Enstitüsü, Seramik Anasanat Dalı, 2010, s.72.

Mason, R.B., Tite, M.S., 1994. ''The beginnings of Islamic stonepaste technology'' Archaeometry 36, 77-91.

Öztürk, Ç. 2020, Mevlana Kubbe-i Hadra (Konya) Dış Duvarının 1912 ve 1965 Yıllarındaki Onarımlarında Kullanılan Çinilerin Karakterizasyonu. Afyon Kocatepe Üniversitesi Fen Ve Mühendislik Bilimleri Dergisi, 20 (5) , 900-907. DOI: 10.35414/akufemubid.703885

CHARACTERIZATION OF CREAM AND CREAM OILS' OBTAINED FROM COW MILK

Sabire Duman[1], Erman Duman[2]*

1 Afyonkarahisar Sağlık Bilimleri Üniversity, Health Sciences Faculty, Nutrition and Dietetic Department, Afyonkarahisar, Turkey

2 Afyon Kocatepe Üniversitesi, Engineering Faculty, Food Engineering Department, Afyonkarahisar, Turkey

Abstract

The aim of this study was to investigate the physico-chemical properties of cream and cream oil obtained from cow's milk, such as dry matter, non-fat dry matter, protein, acidity, pH, fatty acid composition, saponification number, unsaponifiable matter and sterol composition. ; As physical and chemical analysis, the amount of dry matter in cow cream was 61.72%, the amount of non-fat dry matter was 6.72%, pH values were 7.28, protein content was 4.45%, fat content was 55.0%, acidity was 1.05%. In cream oil, the free fatty acidity is 0.078% and the peroxide number is 0.55 meq-O_2 / kg, respectively. The total saturated fat content of the fatty acid content obtained from cow's milk was determined as 66.706%, and the total unsaturated fatty acid ratio was determined as 33.699%. When the fatty acid composition values of the oil obtained from cow cream were examined, it was determined that the highest value in terms of saturated fatty acids was palmitic acid and 35,547%, and when it was examined in terms of unsaturated fatty acids, the highest value was oleic acid and 26,509%. In addition, the saponification number, the number of unsaponifiable matter and the sterol composition of the fat obtained from cow cream were determined. Studies have generally focused on cow and buffalo cream, and it will fill an important gap in the literature on the characterization of cream obtained from cow's milk as a result of our research.

Keywords: Cow milks' Cream, Cream Fat, Characterization, Sterol composition.

* Corresponding Author e-mail : eduman@aku.edu.tr

INVESTIGATION OF CORROSION BEHAVIOR OF CONSTRUCTION STEELS IN HYDROCHLORIC ACID

İbrahim Güneş [1]

[1] Giresun University, Department of Civil Engineering, Giresun, Turkey

ibrahim.gunes@giresun.edu.tr

1. Introduction

Concrete is a material that is highly resistant to external influences. In order to increase the tensile strength of concrete, mild steels known as rebar are used today. Concrete is the most commonly used material in our constructions where steel is used less, that is, it contains steel in various amounts and thicknesses (prior or unstressed). Construction rebar is used in the construction industry construction, which is one of the most important construction works. The steel used in reinforced concrete is non-mechanical and hydrated iron. However, the concrete corrosion rate of this steel is very slow. This is due to the basic property of the concrete surrounding the steel. At the same time, the atmosphere is difficult for concrete in cloudy steel, which again helps in acceleration. Steel donated concrete is one of the most used construction materials in the world. A quality concrete in the structures to be formed with iron frost in concrete; Proper curing, properly placed, appropriate water/usable,appropriate aggregate use etc. achieved under the conditions. Corrosion of the reinforced concrete also affects the strength of reinforced concrete structures [1-3]. In this study, some mechanical properties of construction steel in HCl acid was investigated. In the literature, properties of construction steel such as section losses and weight losses after acidic effect have not been investigated much. In order to fill this gap, the corrosion behavior of rebar exposed to acidic effects at different times was investigated

2. Material and Method

In this study, 24 samples of 16 cm length were cut from ribbed construction steels of Ø14 diameter with the help of cutting device (Figure 1a). An acid solution of 1.5M concentration was prepared (Fig. 1b). Ribbed construction steels in Ø14 diameters were divided into 6, 4 pieces in each jar and immersed in acid solutions with a concentration of 0.5M, 1M, 1.5M (Figure 1c.) In our experimental studies, 0.5 M every seven days for four weeks. The weight losses were measured by washing, alcoholing and drying one by one, ribbed construction steels with Ø14 diameters immersed in acid solution with a concentration of 1 M, 1.5 M. (Figure 1d.)

Figure 1. Tools used in the experimental study

3. Results and Discussion

Construction steels (Ø14 mm) were prepared metallographically and the microstructure of the corroded edges was examined (Figure 2). The surface edge section microstructures of the reinforcement were examined, it was observed pitting corrosion that it was corroded in the form of small cavities from the outside to the inside.
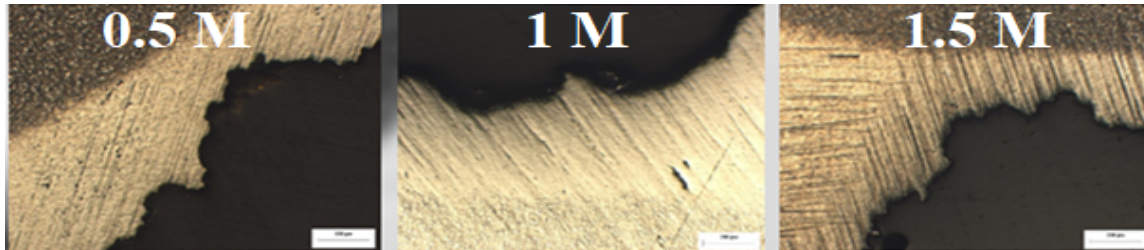

Figure 2. Optical microstructures of rebars soaked in HCl acid

Large decreases were observed in yield strength, tensile strength and percent elongation values after construction corrosion. In addition, reductions in steel diameters due to corrosion occurred. While the least decrease in the mechanical properties of the steels was observed in the samples in 0.5 M acid, the highest decrease was observed in the samples that were corroded at 1.5 M (Table 1).

Table 1. Changes in reinforcement after corrosion

Acidity rate	Week	Molarity (M)	Diameter change after acid			Weight loss			Mechanical properties		
			First	End	Differ-ence	Before	After	Total	Yield	Tensile	Elonga-tion
			mm	mm	mm	mg	mg	mg	N/mm²	N/mm²	%
Reference sample		0	-	-	-	-	-	-	452	570.7	29.8
HCl	1.	0.5 M	14.00	11.83	2.17	188.20	183.37	4.39	445	564	28.5
		1 M	14.00	11.68	2.37	182.36	174.43	7.35	440	560	25.9
		1.5 M	14.00	11.59	2.41	187.75	179.59	12.16	434	553	22.4
	4.	0.5 M	14.00	11.73	2.27	183.20	177.25	5.16	436	554	25
		1 M	14.00	11.42	2.58	182.91	172.37	8.41	427	544	22.7
		1.5 M	14.00	10.88	3.12	186.50	169.93	13.55	417	535	18.9

4. Conclusions

In this study, the corrosion behavior of all kinds of construction steels in Ø14 diameters was investigated by corroding in HCI solutions with 0.5M, 1M, 1.5M concentrations.

- The surface edge section microstructures of the reinforcement were examined, it was observed that it was corroded in the form of small cavities from the outside to the inside.
- The cross-sectional diameters of the samples also decreased due to corrosion.
- The samples showed decreases in yield strength, tensile strength and percent elongation values after corrosion.
- Passivity was observed in the solution after the 4th week, as the solution was not mixed during the experiment.

- While the least decrease in the mechanical properties of the steels was observed in the samples in 0.5 M acid, the highest decrease was observed in the samples that were corroded at 1.5 M.

5. References

[1] https://www.uslularhadde.com/betonun-celik-korozyonuna-etkisi

[2] http://web.hitit.edu.tr/dosyalar/duyurular/abdurrahmanasan@hititedutr041120159U6G8P9S.pdf

[3] Bayol E., Gürten A.A., Sürme Y., (2014), "Inhibitive performance of glycolicacidethoxylate4-nonylphenyl ether in acid solution for corrosion of mild steel", El-Cezerî Journal of Science and Engineering, Vol. 1, No. 3,30-39.

Ti-6Al-4V ALAŞIMININ PLAZMA PASTA BORLANMASI

İbrahim Güneş[1*]

[1] Giresun University, Department of Civil Engineering, Giresun, Turkey

ibrahim.gunes@giresun.edu.tr

1. Giriş

Yeni bir borlama yöntemi olan plazma pasta borlama işlemi pasta borlama işleminin plazma ortamında 700-1000°C arasında Ar ve H_2 gibi gazlarla belirli bir vakum basıncı altında yapılmaktadır. İşlem vakum altında gerçekleştiği için herhangi bir koruyucu atmosfere gerek yoktur. Bor içerikli tozları pasta olarak kullanarak plazma pasta borlama yöntemiyle çeliklerin daha düşük sıcaklık ve sürelerde borlanması ve çelikler üzerinde kompleks borür tabakalarının oluşturulması sağlanabilmektedir. Plazmanın en önemli avantajlarından biri sıcaklığın etkisiyle termo-kimyasal biriktirmenin yanında, hızlandırılmış atom ve iyon hareketleri sayesinde fiziksel bir biriktirme mekanizması oluşturmasıdır. Plazma ortamı ve bor esaslı bir pastanın birleştirilmesiyle çeliklerin üzerinde son derece fonksiyonel tabakaların oluşturulabilmesi muhtemeldir. Ayrıca plazma borlamada bor kaynağı olarak kullanılan gazların (B_2H_6, BCl_3) pahalı, zehirli ve patlayıcı nitelikte olması bazı dezavantajlara da sahiptir. Plazma pasta borlama ile bu zararlı etkilerden kurtulmak mümkündür. Plazma destekli pasta borlama yüzey işlemi ile plazma borlama işlemindeki dezavantajlar yok edilebilmektedir. Kullanılan pastanın çevreye zararsız bor hammaddeleri olması, gazların ise genelde inert karakterde olan hidrojen, argon ve azot olması bu işlemi avantajlı kılmaktadır [1,2].

Bu çalışmada B_2O_3 pastası ile Ti-6Al-4V alaşımı plazma ortamında borlanmıştır. Plazma pasta borlama işlemi sonrasında oluşan borür tabaka kalınlığı, mikro sertlik değerleri, yüzey morfolojileri ve faz analizleri, taramalı elektron mikroskobu ve X-ışınları difraksiyon analizi yardımıyla gerçekleştirilmiştir.

2. Materyal ve Yöntem

Bu çalışmada Ti-6Al-4V alaşımı15x8 mm boyutlarında kesilerek elde edilen numuneler ön hazırlık metalografik işlemlerden geçirilmiştir.Nunumeler B_2O_3 pastası ile 800°C'de 6 saat süresince %80 Ar-%20 H_2 gaz karışımında, 800°C'de 6 saat süresince 5 mbar basınç altında plazma pasta borlanmıştır (Şekil 1). Borlama işleminden sonra numuneler kesitten kesilerek gerekli metalografik işlemlerden geçirilmiştir. Plazma pasta borlanama işlemi sonrasında oluşan borür tabakalarının yüzey morfolojileri ve faz analizleri, taramalı elektron mikroskobu ve X-ışınları difraksiyon analizi yardımıyla yapılmıştır. Oluşan borür tabakalarının sertlikleri Knoop sertlik ölçme yöntemiyle borür tabakalarının sertlikleri ölçülmüştür.
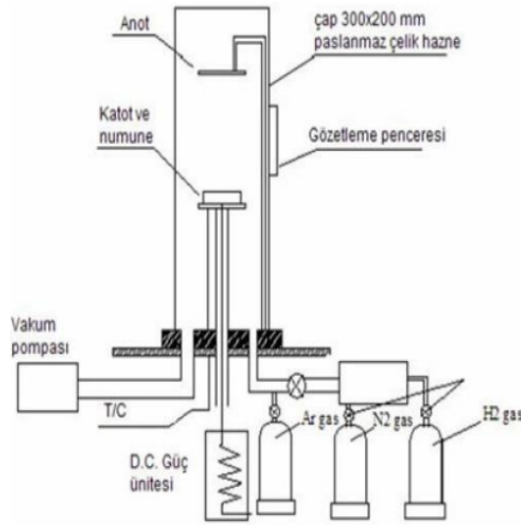
Şekil 1. Plazma pastası borlama cihazı

3. Sonuçlar ve Tartışma

Şekil 1' de 800°C'de 6 saat süreyle, % 100 B_2O_3 pastası ile plazma pastaborlanmış Ti-6Al-4V alaşımının SEM kesit mikro yapısı görülmektedir. Plazma pasta borlama sonucunda numune yüzeyinin üst kısmında borca zengin titanyum diborür (TiB2), alt tarafında ise iğnesel yapılı TiB tabakasının oluştuğu tespit edilmiştir. Ti-6Al-4V alaşımının B_2O_3 pastası ile plazma pastaborlanması sonucunda 8,72 µm borür tabakası elde edilmiştir. X-ışını analizi sonucunda Ti6Al4V alaşımında TiB ve TiB_2 fazları elde edilmiştir (Şekil 3).
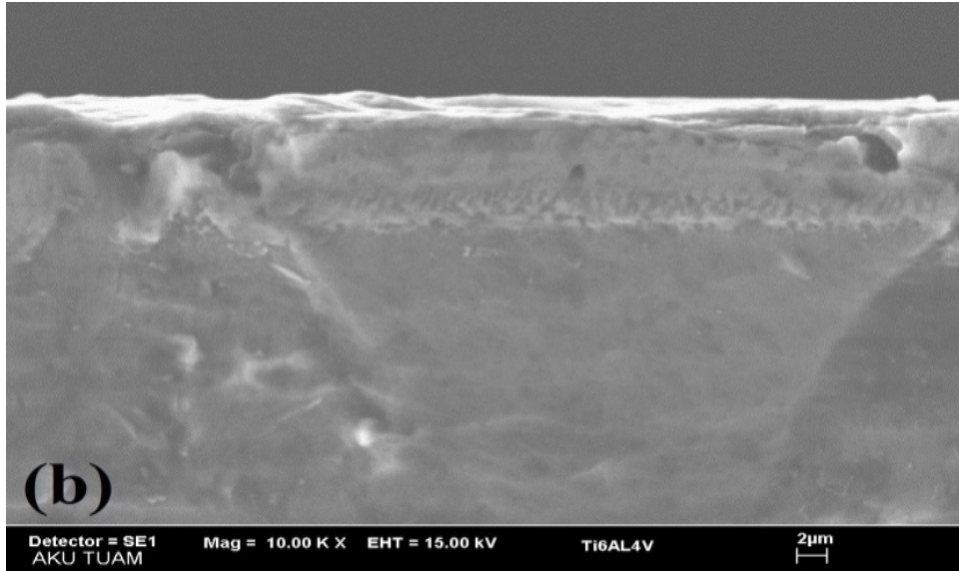
Şekil 2. B_2O_3 pastası ile plazma pastaborlanmış Ti-6Al-4V alaşımının SEM görüntüsü
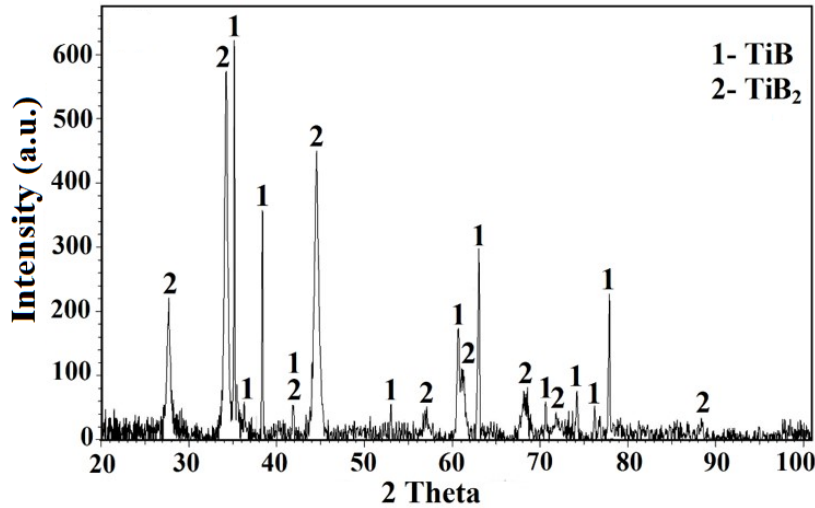
Şekil 3. B_2O_3 pastası ile plazma pasta borlanan Ti6Al4V alaşımının XRD paterni.

Mikrosertlik ölçümler sonucunda plazma pasta borlanmış Ti6Al4V alaşımının yüzey sertliği ortalama 2472 $HK_{0.025}$ olarak tespit edilmiştir.

4. Conclusions

- Borlama işlemi sonucunda Ti6Al4V alaşımında yaklaşık 8,72 μm borür tabakası elde edilmiştir.
- Metalografik incelemeler sonucunda, kaplama/matris ara yüzeyi ve matrisin belirgin olarak birbirinden ayrıldığı ve borür tabakasının kolonsal bir yapıya sahip olduğugözlenmiştir.
- X-ışınları difraksiyon analizi sonuçlarında, plazma pasta borlama sonucunda TiB ve TiB_2 borür fazları elde edilmiştir.
- 800 °C'de 6 saat süresince işlemi plazma pasta borlanmış Ti6Al4V alaşımında 2472 $HK_{0.025}$ yüzey sertlik değeri elde edilmiştir.

5 REFERENCES

[1]Gunes, I., 2010. Çeliğinin Değişik Pasta Karışımlarında Plazma Pasta Borlanması ve Yüzey Özelliklerinin İncelenmesi, Doktora Tezi. Afyon Kocatepe Üniversitesi, Afyon.

[2] Gunes, I., Wear Behavior of Plasma Paste Boronized of AISI 8620 Steel with Borax and B_2O_3 Paste Mixtures, J. Mater. Sci. Technol., 2013, vol. 29, 662–668

PLASMA PASTE BORIDING OF PURE TITANIUM

Redouane Chegroune[1*], Mourad Keddam[1], İbrahim Güneş[2], Atila Gürhan Çelik[2]

[1] University of Science and Technology Houari Boumediene, Laboratoire de Technologie des Matériaux, Bab-Ezzouar, Algiers, Algeria

[2] Giresun University, Department of Civil Engineering, Giresun, Turkey

chegroune_redouane@yahoo.fr

1. Introduction

Boriding is a thermochemical surface treatment, in which boron atoms diffuse into the surface of a workpiece to form borides with the base material [1-3]. Boriding can be carried out in many ways, such as can, liquid, gas, plasma boriding and plasma paste boronizing [4-6]. Plasma paste boronizing is an alternative method to boriding media mentioned above. This method (PPB) is very important in terms of the abundance, cheapness and evaluation of B_2O_3 boron paste used in plasma paste boronizing in our country. Yoon et al. [7] applied the paste consisting of borax ($Na_2B_4O_7$) and amorphous boron mixture on 304 stainless steel and boronized it in Ar/H_2 plasma at different temperatures and investigated the diffusion kinetics and morphology of the layer. Also, a paste containing different borax and amorphous boron compounds was used for optimum boride layer thickness. As a result of the studies, they stated that the cake containing 70% borax and 30% amorphous boron gave the highest thickness, and the cake containing 100% borax formed a boride layer on stainless steel. As a result of the diffusion kinetic studies, they emphasized that the boride layer realized with plasma paste boronizing is thicker and the activation energy is lower than other boronizing media [8]. Gunes et al. [3,5,6] deposited 100% borax paste on the surface of some steels containing various alloying elements and made paste boronizing in the plasma environment. However, there is no information about the surface properties boronized of pure titanium with boric acid paste. The main objective of this study was to investigate the surface properties boronized titanium with boric acid paste and structural properties were investigated using XRD, SEM and microhardness tests.

2. Material and Method

In the experimental study, cylindrical pure titanium dimensions of 15x8 mm was used. Boriding process of titanium was carried out in a vacuum environment with 80% Ar - 20% H2 gas mixture at 800ºC for 6 hours under 5 mbar pressure using plasma paste boriding method (Fig. 1).

Figure 1. Plasma paste boriding device

Plasma paste boronized samples were molded by cutting with a SiC cutting disc from the section and polished in 0.1 μm alumina suspension by passing through 240-1000 grit SiC sandpaper. Metallographic samples were prepared. Analysis of the phases formed on the titanium surface was investigated using X-ray diffraction. The layer thicknesses of plasma paste boronized titaniumwas obtained from 10 different regions with the help of an apparatus connected to an Olmypus BX-60 optical microscope, and it was observed that the boride layer thicknesses increased with the arithmetic average.

3. Results and Discussion

3.1 Characterization of Boride Coatings

The cross-sections of the optical micrographs of the borided titanium at the temperature of 850 for 6 h is shown in Figure 2. It was found that the coating/matrix interface and matrix could be significantly distinguished and the boride layer had a columnar structure. As a result of the boriding process, a boron-rich titanium diboride (TiB$_2$) layer was observed on the upper part of the sample surface and a needle-like TiB layer on the lower part. As a result of boriding, a boride layer thickness of 11.46 μm was obtained.
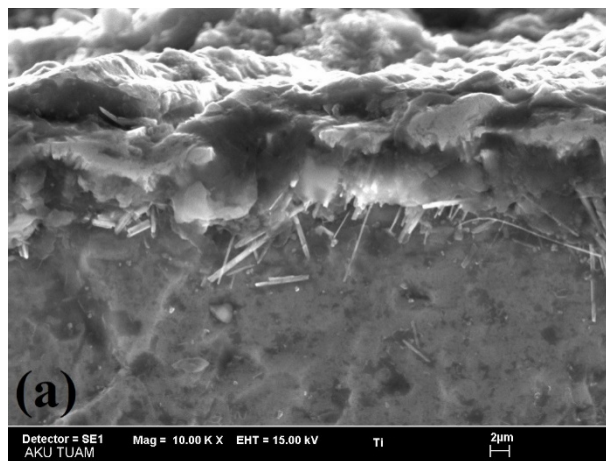

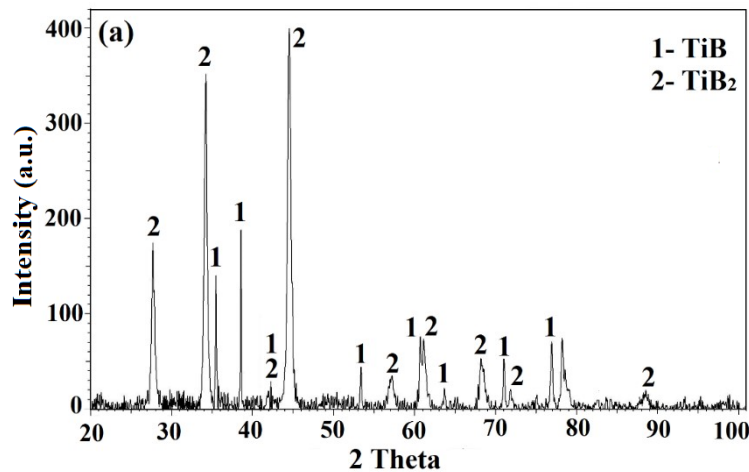**Figure 2.** The SEM image of the boronized pure Titanium

Figure 3. X-ray diffraction patterns of boridedpure Titanium

In this study, the presence of borides was identified using XRD analysis; see Fig. 3.XRD patterns show that the boride layer consists of borides such as AB and AB_2 (A=Metal; Ti). XRD results showed that boride layers formed on the steel contained the TiB andTiB_2compounds, see Fig. 3.

The micro-hardness of the boride layers was measured at 10 different locations at the same distance from the surface and the average value was taken as the hardness. The surface hardness of boronized pure titanium was determined as 2472 $HK_{0.025}$ as a result of microhardness measurements.When the hardness of the boride layer is compared with the matrix, boride layer hardness is approximately seven times greater than that of the matrix.

4. Conclusions

In this study, surface properties of boridedpure titanium was investigated. Some of the conclusions can be drawn as follows.

- As a result of plasma paste boronizing of pure titanium at 800 °C for 6 hours, TiB and Ti_2B boride layers were obtained.
- As a result of boridingprocess, 11.46 µm boridelayerwasobtained in puretitanium.
- As a result of plasmapasteboronizingprocess at 800C for 6 hours, a surfacehardnessvalue of 2472 $HK_{0.025}$ wasobtained.

5. References

[1]Sinha AK (1991) Boronizing. ASM Handbook, Ohio.

[2]Bindal C, Ucisik AH (1999) Characterization of borides formed on impurity-controlled chromium-based low alloy steels. Surf Coat Technol 122:208-213.

[3]Gunes, I., WearBehavior of PlasmaPasteBoronized of AISI 8620 Steel withBorax and B2O3 PasteMixtures, J. Mater. Sci. Technol., 2013, vol. 29, 662–668

[4]Gunes, I., Yıldız I., Rate of growth of boride layers on steels, Oxidation Communications, 2015, vol. 38(4A), 2189-2198

[5]Gunes,I., Ş.Ülker, Ş., Taktak, S.,Kinetics of Plasma Paste Boronized AISI 8620 Steel in Borax Paste Mixtures, Protection of Metals and PhysicalChemistry of Surfaces, 49 (5), 567-573, 2013.

[6]Gunes,I., Ş.Ülker, Ş., Taktak, S, InvestigationTribologicalBehaviour of PlasmaPasteBoronized of AISI 8620, 52100 and 440C steels, IndianJournal of Engineering&MaterialsSciences, 18, 370-376, 2011

[7] Yoon, J. H., Jee Y. K., Lee S. Y., "Plasma Paste Boronizing Treatment of the Stainless Steel AISI 304", Surface and Coatings Technology, 112, 71-75, 1999.

[8] Gunes,I., Ş.Ülker, Ş., Taktak, S, SurfaceCharacterization of Pack And PlasmaPasteBoronized of 21NiCrMo2 Steel, JournalFac. Eng. Arch. Gazi Univ. 27, 99-108, 2012

INVESTIGATION OF CORROSION BEHAVIOR OF S500 STEEL

Ibrahim GUNES[1*]

[1]Giresun University, Department of CivilEngineering, Giresun, Turkey

ibrahim.gunes@giresun.edu.tr

1. Introduction

In some soils or wastewater, there are bacteria and microbes that affect metals chemically or electrochemically. This is one of the main causes of rapid corrosion, which is noticedin iron and is generally explained by the graphitization phenomenon.Among the bacteria, the most dangerous are sulfate-reducing bacteria.These bacteria reduce sulphates in soil, underground or waste water and release H_2S, which affects iron alloys very quickly.The liberated H_2S combines with the O2 in the air to form the $H2_SO_4$ acid known as sulfuric acid. H_2SO_4 acid, which is a strong acid, settles on the concrete surface and causes a decrease in the pH level there, and dissolves the cement hydration products and easily reaches the steel reinforcement bearing the tensile stresses. The mechanical strength of the corroded concrete material decreases. The rate and severity of the acid reaction; depending on the exposure time and acid density. Hydrochloric acid, popularly known as the spirit of salt, is a chemical compound formed from the elements hydrogen and chlorine. hydrochloric acid actually has a toxic content. Causes damage to many surfaces, including the human body. Care must be taken when handling this acid and necessary precautions must be taken. It has both toxic and irritating effects [1-5].In this study, some mechanical properties of construction steel in H2SO4 acid was investigated.

2. Material and Method

In this study, 24 samples of 16 cm length were cut from ribbed construction steels of Ø14 diameter with the help of cutting device (Figure 1a). An acid solution of 1.5M concentration was prepared (Fig. 1b). Ribbed construction steels in Ø14 diameters were divided into 6, 4 pieces in each jar and immersed in acid solutions with a concentration of 0.5M, 1M, 1.5M (Figure 1c.) In our experimental studies, 0.5 M every seven days for four weeks. The weight losses were measured by washing, alcoholing and drying one by one, ribbed construction steels with Ø14 diameters immersed in acid solution with a concentration of 1 M, 1.5 M. (Figure 1d.)
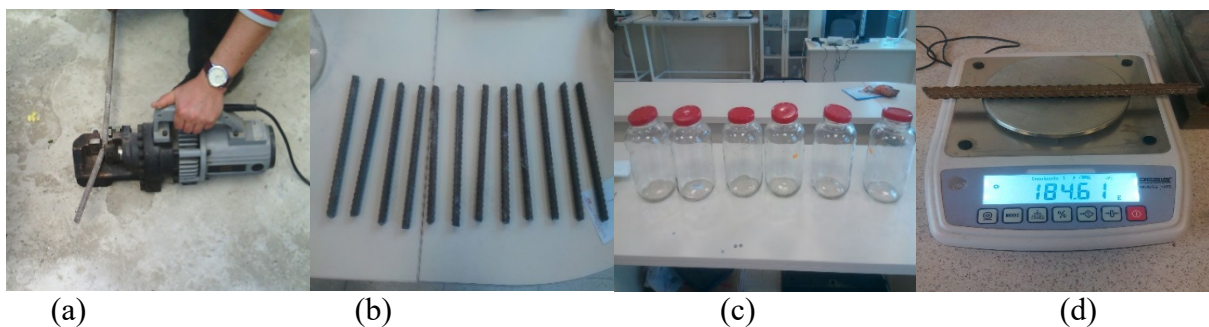

| (a) | (b) | (c) | (d) |

Figure 1. Tools used in theexperimentalstudy

3. Results and Discussion

Ø14 diameter steels were prepared metallographically and the microstructure of the corroded edges was examined (Figure 2).
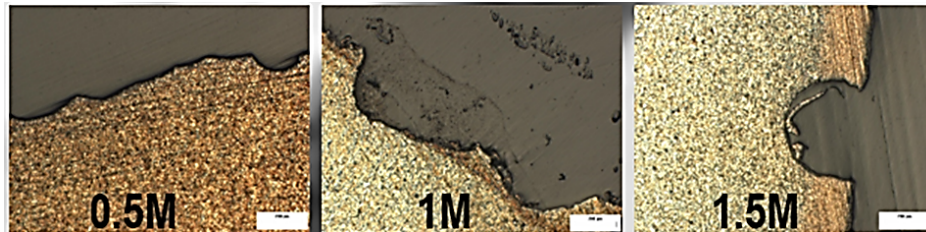

Figure 2. Optical microstructures of rebars soaked in H2SO4 acid

When the surface edge section microstructures of the reinforcement were examined, it was observed that it was corroded in the form of small cavities (pits / pitting) from the outside to the inside. In the samples, decreases were observed in the yield strength, tensile strength and percent elongation values after corrosion. In addition, reductions in steel diameters due to corrosion occurred. While the least decrease in the mechanical properties of the steels was observed in the samples in 0.5 M acid, the highest decrease was observed in the samples that were corroded at 1.5 M. The decrease in the mechanical properties of the steels is due to the reduction in the cross section diameter. Therefore, the surfaces of these steels must be coated to increase their resistance to corrosion or to take precautions against oxidation and rusting such as water and moisture. In the samples, decreases were observed in the yield strength, tensile strength and percent elongation values after corrosion. In addition, reductions in steel diameters due to corrosion occurred. While the least decrease in the mechanical properties of the steels was observed in the samples in 0.5 M acid, the highest decrease was observed in the samples that were corroded at 1.5 M. The decrease in the mechanical properties of the steels is due to the reduction in the cross section diameter. Therefore, the surfaces of these steels must be coated to increase their resistance to corrosion or to take precautions against oxidation and rusting such as water and moisture.

Table 1. Changes in reinforcement after corrosion

Acidity rate	Week	Molarity (M)	Diameter change after acid			Weight loss			Mechanical properties		
			First	End	Difference	Before	After	Total	Yield	Tensile	Elongation
			mm	mm	mm	mg	mg	mg	N/mm²	N/mm²	%
Reference sample		0	-	-	-	-	-	-	452	570.7	29.8
H₂SO₄	1.	0.5	14.00	11.20	2.8	183.69	158.44	25.25	435	550	27.8
		1	14.00	10.31	3.69	186.07	136.59	49.48	428	539	24.3
		1.5	14.00	9.99	4.01	185.77	123.29	62.48	415	512	21.5
	4.	0.5	14.00	10.90	3.10	186.15	159.95	26.20	418	527	20.6
		1	14.00	9.77	4.23	179.25	128.53	50.72	404	494	16.3
		1.5	14.00	9.18	4.82	183.12	118.22	63.90	389	482	11.67

4. Conclusions

In this study, the corrosion behavior of all kinds of construction steels was investigated by corroding in H_2SO_4 solutions with 0.5M, 1M, 1.5M concentrations

- It was observed that the construction steels were more corroded and lost weight in the H_2SO_4 solution. Since the solution was not mixed during the experiment, passivity was observed in the solution after the 4th week. Passivity; It is the loss of chemical activity of some metals and alloys under certain environmental conditions.
- When the surface edge section microstructures of the reinforcement were examined, it was observed that it was corroded in the form of small cavities (pits / pitting) from the outside to the inside.
- While the yield strength of the reference sample was 452 N/mm2, the yield strength decreased to 389 N/mm2 after 4 weeks of corrosion. The tensile strength has decreased from 570.7 N/mm2 to 482 N/mm2.
- The percent elongation of rebar decreased from 29.8% to 11.6%.

5 References

[1] Mathur, P.B., Vasudevan, T (1982), "Reaction rate studies for the corrosion of metals in acids. I. Iron in mineral acids." Corrosion (NACE), 38(3), 171-178.

[2] Baradan, B., Yazıcı, H., Ün, H., Beton ve Betonarme Yapılarda Kalıcılık (Durabilite), Türkiye Hazır Beton Birliği Yayınları, İstanbul,2010.

[3]Oguzie, E.E (2008), "Evaluation of theinhibitiveeffect of someplantextracts on theacidcorrosion of mildsteel." CorrosionScience, 50, (11),2993-2998.

[4]Sayed ARS., HazzaziOmar A., Amin Mohammed A., (2008), "Thecorrosioninhibition of lowcarbonsteel in concentratedsulphuricacidsolutions", CorrosionScience, Vol. 50, 2258-2271.

[5] Uygunoğlu, T., Güneş, İ., Topçu, İ. B., İnşaat Çeliğinde Biyolojik Korozyon, Yapı Dünyası Dergisi, Kasım-Aralık 2014, 26-30, ISSN: 1300-977x

FLY ASH BASED FOAM GEOPOLYMERS WITH IMPROVED DRYING SHRINKAGE PROPERTIES

Cansu Kurtuluş[1*], Mustafa Serhat Başpınar[2]

[1] Afyon Kocatepe University, Materials Science and Engineering Department, Afyonkarahisar, TURKEY

[2] Afyon Kocatepe University, Metallurgy and Materials Engineering Department, Afyonkarahisar, TURKEY

cansudemir@aku.edu.tr

1. Introduction

The rapid growth of different industrial areas has unfortunately significantly increased the consumption of cement and other natural resources. The concrete and cement sector is frequently criticized because it consumes many natural resources and energy, causes high emissions of emissions such as CO_2, especially NO_x, originating from cement production, and causes the formation of particulate matter that seriously affects the respiratory tract when inhaled[1]. From another point of view, many river beds are destroyed to provide the cement and aggregates needed to construct buildings and pavements in the construction sector, but it also causes the natural balance to deteriorate. Criticisms on both emission and environmental destruction force the construction industry to seek alternative raw materials. In cement-based systems (such as plaster, mortar, concrete), industrial wastes with pozzolanic properties such as fly ash, blast furnace slag, and silica fume can minimize carbon dioxide emissions, and the need for natural resources and energy is reduced[2], [3]. The potential of using wastes such as fly ash as building materials thanks to geopolymer technology geopolymer materials comes to the fore. On the other hand, among the targets set by the European community regarding the protection of the environment and the improvement of its quality, the targets of reducing emissions by 40% until 2030, 80% by 2050, and increasing energy efficiency by at least 32.5% [4]. Dissemination of geopolymer technology and solving the problems encountered in this technology becomes the driving force.

Three-dimensional network geopolymers prepared with alumino-silicate-containing raw materials have become a hot research topic as they have the potential to recycle industrial solid wastes such as fly ash and blast furnace slag [5]–[7]. Geopolymer materials have attracted great attention with their excellent mechanical, physical and thermal properties[8]. Geopolymer chemistry generally involves the dissolution of aluminosilicate minerals in a strongly alkaline medium (alkali metal carbonate, alkali metal fluoride, alkali metal hydroxide, alkali metal aluminate, and alkali metal silicate) followed by the polymerization of the surface-active groups and dissolved groups of the particles to form the geopolymer structure [9]. The alkaline medium is generally prepared with the help of Na and K-based raw materials (NaOH, KOH, sodium silicate, potassium silicate). When evaluated in terms of price performance, solutions containing Na are preferred more often than those containing K. One can say that because Na-based geopolymers encourage dissolution reactions, they gain almost twice the strength compared to K-based geopolymers, and they are pretty cheap [10].

There are many problems encountered in every newly developed technology. Drying shrinkage seen in geopolymer materials is one of the most important problems limiting the

spread of these materials. The volumetric shrinkage that occurs during drying causes cracks on the material and therefore decreases the mechanical properties. With the studies on drying shrinkage, which is also observed in cementitious systems, the situations that cause the problem have been revealed, and more or less strategies have been developed for the solution. However, no clear strategy has been developed to prevent drying shrinkage for geopolymer materials. Olalekan [11], Chindaprasirt [12], Kheradmand [13], Kuenzel [14], Zhu [15] have done studies to reduce the pore sizes in the geopolymer mixture and thus to reduce the drying shrinkage.

The present study aims to analyze the effect of different geopolymer formulations on drying shrinkage. For this purpose, the effects of molarity, fly ash-metakaolin ratio, calcium stearate amount, and the curing temperature were investigated. The most influential parameters on drying shrinkage were analyzed.

2.   Material and Method

Low calcium content fly ash from Seyitömer Thermal Power Plant, and MEFISTO L05 metakaolin (conversion temperature 750°C) from Czechia was used as aluminosilicate raw material. The chemical compositions of the raw materials used are shown in Table 1, and specific powder properties are given in Table 2. Also XRD patterns of raw materials are given in Figure 1. The raw materials used as aluminosilicate sources are amorphous. Fly ash and metakaolin contain residual quartz, and peaks are observed depending on the quartz content.

Foam geopolymer specimens were prepared using sodium-based promoters. Sodium hydroxide and sodium silicate were mixed to prepare an alkaline environment. Chopped polypropylene fibers (1cm long) and perlite particulates (1mm diameter) were added into the liquid alkaline mixture to get strong bonding between additives. Liquid mixture was poured on the dry aluminosilicate powder mixture and geopolymer paste was prepared for 5 minutes. Afterward, hyrdogen peroxide was added into the mixture with surface active agent and mixed for additional 30 seconds. Surface active agent was used to keep stabile porosities inside slurry, and to get homogeneous pore distribution. Compositional informeaions are given in Table 3 in detail. The geopolymer mixture is then poured into 40x40x160mm molds used to measure the drying shrinkage properties of samples (Figure 2). Prismatic beams were cured, than ASTM C157 procedure was conducted to measure deformation and total length change followed by reading a daily length and mass difference. Microstructures of geopolymer foams were investigated by SEM.

Table 1. Chemical compositions of raw materials.

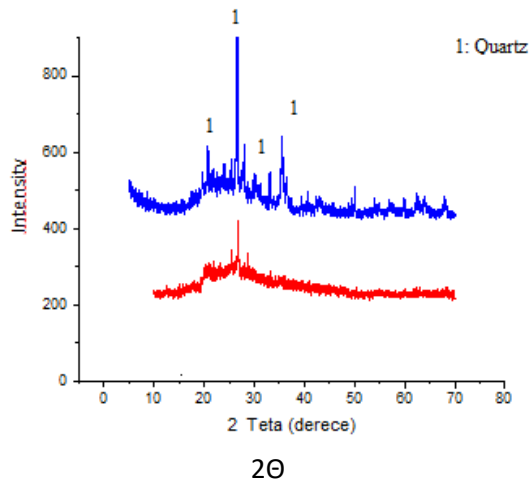| Raw Materials (%)		
Content	**Metakaolin**	**Fly Ash**
MgO	0.15	4.67
Al_2O_3	41.32	19.10
SiO_2	51.49	50.30
P_2O_5	0.04	0.13
SO_3	0.13	1.80
K_2O	0.53	2.16
CaO	0.16	4.55
TiO_2	1.65	0.81
V_2O_5	0.07	0.05
Fe_2O_3	1.16	12.40

Figure 1. XRD patterns of aluminosilicate raw materials. (Blue Line: Fly Ash, Red Line: Metakaolin).

Table 2. Properties of powder raw mateials.

Raw materials	Particle Size (µm)	Specific Surface Area (m²/g)	Specific Density (g/cm³)
Fly Ash	29.97	7.91	2.58
Metakaolin	3.0	17.08	2.5

Table 3. Compositional informations of foam geopolymers.

Sample Codes	Molarity	Fly Ash (%)	Calcium Stearate (%)	Perlite (%)	Curing Temperature (°C)	H_2O_2 (%)
85F-60C-1	8	85	0,45	2,75	60	1
95F-60C-1	8	95	0,45	2,75	60	1
85F-80C-1	8	85	0,45	2,75	80	1
95F-80C-1	8	95	0,45	2,75	80	1
85F-60C-2	8	85	0,45	2,75	60	2
95F-60C-2	8	95	0,45	2,75	60	2
85F-80C-2	8	85	0,45	2,75	80	2
95F-80C-2	8	95	0,45	2,75	80	2

Figure 2.a) Drying shrinkage samples, and b) analysis equipment.

3. Results and Discussion

From Figure 3 it appears that decreasing the amount of fly ash in compositions is very effective on drying shrinkage. According to the study of Kuenzel et al., the amount of structural water in the compositions is directly related to drying shrinkage. The increase in the amount of fly ash provides a decrease in the amount of structural water and provides a more stable geopolymer structure [14]. The drying shrinkage increased with the increase in the amount of hydrogen peroxide. It has been proven that foam geopolymers also show more shrinkage than dense structures like foam concretes. The drying shrinkage of foam concrete, measured after one year, ranges from 0.1% to 0.36%; this is 5-10 times higher than the typical shrinkage of dense mortar and concrete samples [16].The increase in curing temperature also caused an increase in drying shrinkage. Environmental conditions such as temperature, humidity, wind speed are essential factors affecting drying shrinkage. Especially low humidity, hot and windy conditions cause drying shrinkage to accelerate and high drying shrinkage to ocur [17]. The samples showed a rapid drying shrinkage in the first 11 days after almost curing, reaching almost stable dimensions in the following days. The sample sizes did not decrease completely but increased at some times. Since the relative humidity values can vary, it is thought that the samples show shrinkage or expansion behavior.
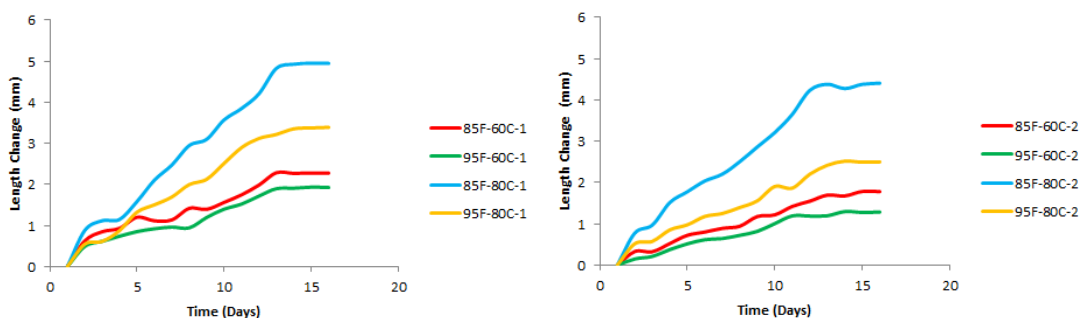
Figure 3.15-day drying shrinkage measurements of foam geopolymer samples.

Drying shrinkage and mass changes in the samples were compared. Figure 4 shows the change in mass of the samples during the 15-day curing period. Samples containing 2% hydrogen peroxide lost mass more rapidly than samples containing 1% peroxide. Therefore, samples containing 2% peroxide reached a fixed weight in a short time, like six days, while foam

samples containing 1% peroxide took ten days to reach a constant weight. There is no correlation between mass loss concerning curing temperatures and fly ash content.When the mass losses and drying shrinkage of the samples are evaluated comprehensively, a direct link cannot be established. It is not possible to interpret as the one with the most mass loss contracted the most[18]. Many factors affect drying shrinkage, such as pore sizes, additives, the structural water content of samples, reaction rates of raw materials, and the resulting reaction products.
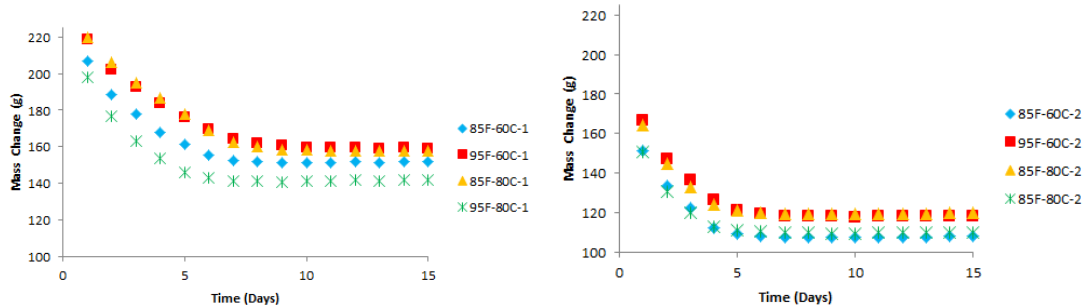
Figure 4. Mass change of foam geopolymer samples during drying.

Samples were also investigated by means of the scanning electron microscope. The most striking detail in the images obtained by scanning electron microscope is that H_2O_2 increases the pore size of the foam geopolymer (Figure 5a, 5b). The amount of dissociated O_2 increased with the increase of H_2O_2 caused the pores to enlarge and the formation of more porosity.

The increase in the curing temperature also caused the pore size to decrease. The main reason behind the shrinkage is that the geopolymer network begins to form, and the system quickly solidifies without sufficient time for the pores to mature. Although the increased curing temperature also accelerates the degradation of H_2O_2, accelerated geopolymer reactions do not allow the pores to grow (Figure 5c, 5d).

With the increase in the amount of fly ash, some increase in pore size is observed. Increasing pore size is due to the larger grain size of fly ash than metakaolin (Table 2). Therefore, the increase in fly ash negatively affects the particle packing in the geopolymer mixture surrounding the pore and reduces the pressure on the pores. For this reason, the pores tend to grow. As the amount of metakaolin used in the geopolymer foam mixture increases, the pore sizes become thinner (Figure 5e, 5f).
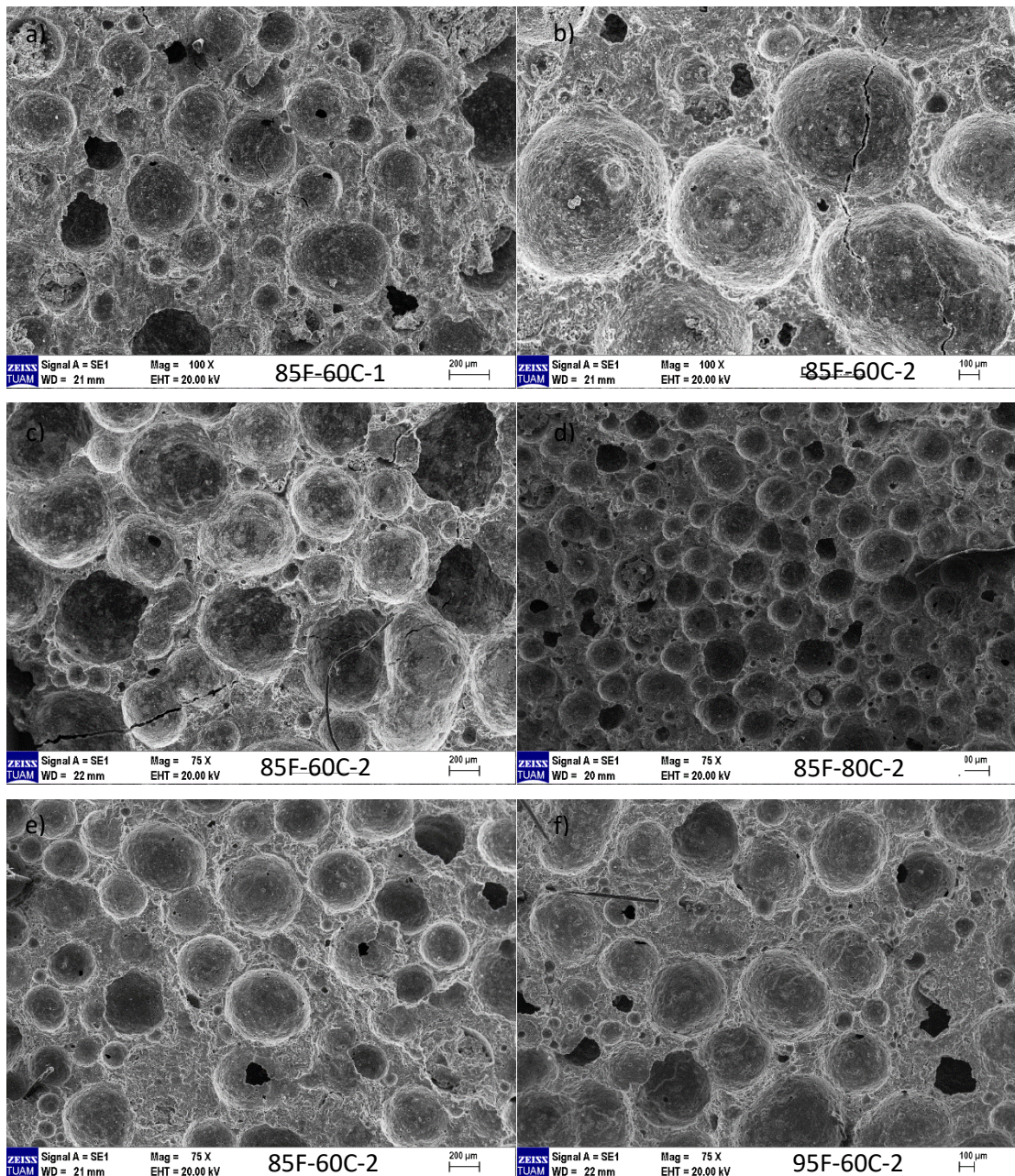
Figure 5. Scanning electron microscope images of samples.a)85F-60C-1 b) c)85F-60C-2 d)85F-80C-2 e)85F-60C-2 f)95F-60C-285F-60C-2.

4. Conclusions and Recommendations

This article investigated the effects of fly ash content, H_2O_2 amount, and curing temperature on drying shrinkage in fly ash-based geopolymers.According to the drying shrinkage measurements, one can report thatfly ash amount effective on decreased drying shrinkage. This situation is thought to be related to structural water.The increase in the amount of H_2O_2 and the increase in the curing temperature increase the drying shrinkage.The authors also investigated mass losses in the samples during the drying shrinkage measurements. There is no correlation between mass loss and the amount of drying shrinkage.

5. Acknowledge

References

[1]   J. Thaarrini and S. Dhivya, "Comparative Study on the Production Cost of Geopolymer and Conventional Concretes," *Int. J. Civ. Eng. Res.*, vol. 7, no. 2, pp. 2278–3652, 2016.

[2]   Y. H. M. Amran, R. Alyousef, H. Alabduljabbar, and M. El-Zeadani, "Clean production and properties of geopolymer concrete; A review," *J. Clean. Prod.*, vol. 251, p. 119679, 2020, doi: 10.1016/j.jclepro.2019.119679.

[3]   WBCSD, "Cement technology roadmap plots path to cutting CO2 emissions 24% by 2050," *Int. Energy Agency*, no. April, pp. 1–3, 2018.

[4]   C. European, "Climate strategies & targets." [Online]. Available: https://ec.europa.eu/clima/policies/strategies_en. [Accessed: 24-Aug-2021].

[5]   L. Dembovska, D. Bajare, V. Ducman, L. Korat, and G. Bumanis, "The use of different by-products in the production of lightweight alkali activated building materials," *Constr. Build. Mater.*, vol. 135, pp. 315–322, 2017, doi: 10.1016/j.conbuildmat.2017.01.005.

[6]   N. Toniolo and A. R. Boccaccini, "Fly ash-based geopolymers containing added silicate waste. A review," *Ceram. Int.*, vol. 43, no. 17, pp. 14545–14551, Dec. 2017, doi: 10.1016/j.ceramint.2017.07.221.

[7]   Z. Abdollahnejad, M. Mastali, and T. Luukkonen, "Construction and Demolition Waste as Recycled Aggregates in Alkali- Construction and Demolition Waste as Recycled Aggregates in Alkali-Activated Concretes," no. December, 2019, doi: 10.3390/ma12234016.

[8]   J. Davidovits, *Geopolymer Chemistry and Applications*. Saint-Quentin: Institut Géopolymère, 2008.

[9]   B. Walther, B. Feichtenschlager, and S. Zhou, "Self foaming geopolymer composition containing Al dross," 2015.

[10]   M. Taxiarchou, A. Karalis, D. Panias, C. Panagiotopoulou, J. K. Hicks, and C. Dedeloudis, "Study on the Suitability of Volcanic Amorphous Aluminosilicate Rocks (Perlite) for the Synthesis of Geopolymer-Based Concrete," *Geopolymer Bind. Syst.*, no. 636876, pp. 34–53, 2013, doi: 10.1520/stp156620120077.

[11]   M. O. Yusuf, M. A. Megat Johari, Z. A. Ahmad, and M. Maslehuddin, "Shrinkage and strength of alkaline activated ground steel slag/ultrafine palm oil fuel ash pastes and mortars," *Mater. Des.*, vol. 63, pp. 710–718, 2014, doi: 10.1016/j.matdes.2014.06.062.

[12] P. Chindaprasirt, S. Homwuttiwong, and V. Sirivivatnanon, "Influence of fly ash fineness on strength, drying shrinkage and sulfate resistance of blended cement mortar," *Cem. Concr. Res.*, vol. 34, no. 7, pp. 1087–1092, 2004, doi: 10.1016/j.cemconres.2003.11.021.

[13] M. Kheradmand, Z. Abdollahnejad, and F. Pacheco-Torgal, "Drying shrinkage of fly ash geopolymeric mortars reinforced with polymer hybrid fibres," *Proc. Inst. Civ. Eng. Constr. Mater.*, vol. 173, no. 1, pp. 28–40, 2020, doi: 10.1680/jcoma.16.00077.

[14] C. Kuenzel, L. J. Vandeperre, S. Donatello, A. R. Boccaccini, and C. Cheeseman, "Ambient temperature drying shrinkage and cracking in metakaolin-based geopolymers," *J. Am. Ceram. Soc.*, vol. 95, no. 10, pp. 3270–3277, 2012, doi: 10.1111/j.1551-2916.2012.05380.x.

[15] W. Zhu *et al.*, "Understanding restraint effect of coarse aggregate on the drying shrinkage of self-compacting concrete," *Constr. Build. Mater.*, vol. 114, pp. 458–463, 2016, doi: 10.1016/j.conbuildmat.2016.03.160.

[16] Z. Zhang, J. L. Provis, A. Reid, and H. Wang, "Fly ash-based geopolymers: The relationship between composition, pore structure and efflorescence," *Cem. Concr. Res.*, vol. 64, pp. 30–41, Oct. 2014, doi: 10.1016/J.CEMCONRES.2014.06.004.

[17] B. K. Ward, M. T. Mohammad, S. L. Whitney, G. F. Marchetti, and J. M. Furman, "Chapter 3 DRYING SHRINKAGE AND CREEP IN CONCRETE : A SUMMARY," *J. Vestib. Res. Equilib. Orientat.*, vol. 20, no. 5, pp. 43–84, 2006.

[18] F. Collins and J. G. Sanjayan, "Effect of pore size distribution on drying shrinkage of alkali-activated slag concrete," *Cem. Concr. Res.*, vol. 30, no. 9, pp. 1401–1406, 2000, doi: 10.1016/S0008-8846(00)00327-6.

THE IMPACT OF PARTICLE SIZE ON PHYSICAL AND MECHANICAL PROPERTIES IN WASTE-DERIVED GLASS FOAMS

Recep Kurtuluş[1*] , Cansu Kurtuluş[1], Hakan Çiftçi[2], Taner Kavas[1]

[1] Afyon Kocatepe University, Department of Materials Science and Engineering, Afyonkarahisar, Turkey

[2] Afyon Kocatepe University, Department of Mining Engineering, Afyonkarahisar, Turkey

Abstract

Glass foams (*GF*) possess great potential for waste valorization purposes. The foaming characteristics can be manipulated by variations in particle size (*PS*) distributions. In this study, we selected waste cathode-ray tubes (*CRTs*), glycerine (*G*), water glass (*WG*), and water (*W*) constituents with the roles of main waste, foaming agent, particle enveloping substance, and moisturizing content, respectively. Initially, the *GF* system was designed as follows: *90CRTs+2W+6WG+2W*. After that, four different particle size ranges in waste *CRTs* were chosen as (-500/+212 µm, *PS1*-coded), (-212/+125 µm, *PS2*-coded), (-125 µm, *PS3*-coded), and (-75 µm, *PS4*-coded). The *GF* pellets were prepared by weighing, mixing, and pressing stages, accordingly. The prepared pellets were then heated via a conventional electric resistance furnace under the conditions of a 5⁰C. min^{-1} heating rate up to 850⁰C, which were subsequently dwelled for 30 min at the peak temperature. The impact of *PS* on physical and mechanical properties was analyzed by measuring bulk density (ρ_{bulk}), predicted porosity (*PP*), and testing compressive strength (*CS*). According to the findings, the ρ_{bulk} values were equal to 599, 460, 303, and 264 kg. cm^{-3} for PS1 to PS4 samples in the respective order. Based upon the measured ρ_{bulk}, the *EP* values were found to be 78.3, 83.3, 89.1, and 90.4 percentages for PS1 to PS4 specimens, respectively. Lastly, the *CS* values revealed that decreasing *PS* caused the obtainment of diminishing resistance to mechanical failure. In conclusion, the authors deduced that waste CRTs can be valorized in an effective way with the aid of manipulating particle size.

Anahtar Kelimeler : glass foam, CRTs, waste valorization, particle size, sustainability

* Corresponding author : rkurtulus@aku.edu.tr

1. INTRODUCTION

Glass foams (GF) offer unique properties for different application areas. Their main benefits can be regarded as being waterproof and non-flammable, resistant to acids, providing precise dimension and easy cutting, and ensuring various waste valorizations [1], [2], [3]. With these superiorities, GF materials are extensively preferred by construction, building, underground plumbing, and metal filtration fields. Conceptually, GF systems are produced with the use of foaming mechanisms such as carbonaceous (*eg.* glycerine), neutralization (*eg.* $CaCO_3$), and oxidation/reduction (*eg.* Mn^{+2} to Mn^{+3}) [4], [5]. The fundamental goal is to expand the glass body by forming pores inside the material. The formation of opened-or-closed porous

determines GF material's application area. For instance, thermal insulation applications require closed pores for separating inside and outside atmospheres whereas metal filtration applications necessitate opened-porous for preventing undesired particles movement [6]. Therefore, the formation of pores and their size and distribution are the key factors for fabricating high-performance GF materials.

In addition to the excellent properties of GF materials, they present a great opportunity for valorizing waste substances in mass production. That is to say, solid waste substances such as glass, blast furnace slag, fly ash, and so on can be effectively utilized with the insertion of foaming agents under suitable process conditions to fabricate GF materials [7]. Such valorization is vital within the scope of environmental sustainability and a greener future. This is because a large number of waste substances or by-products have been landfilled every year without any benefit, indeed, they pollute the environment [8]. Based on these strong motivations, the scientific community has intensively concentrated on valorizing waste substances to produce value-added products. Among these, waste cathode-ray tubes (CRTs) glass take great importance and require urgent action for valorization intentions. The reason behind this urgency can be explained that light-emitting diodes (LEDs) have expeditiously replaced CRTs glass technology in the last quarter, which means that computers, TVs, or monitors, that use CRTs glass technology, have become useless [9]. The unusable has been doomed to accumulate in landfills, which in turn has begun to pollute the environment. Therefore, any attempt for valorizing waste CRTs substances is of importance for a more viable environment.

In the present study, the authors have two certain purposes: (1) to valorize unused CRTs panel glass in glass foam applications, (2) to understand the impact of particle size on physical and mechanical properties in glass foams. For achieving these, we designed an experimental study based upon the following composition: *90CRTs+2G+6WG+2W* (G: glycerine, WG: water glass, and W: water). The main waste substance, CRTs, were sieved to four different particle size range as (-500/+212), (-212/+125), (-180), and (-80). Providing that each sample was prepared by using the corresponding particle size range, four specimens as PS1 to PS4 were fabricated at 850 ºC (heating rate of 5 ºC.min^{-1}), which were subsequently dwelled for 30 min at the peak temperature. The synthesized GF series were analyzed by using Archimedes' principle and mechanical testing. The findings were evaluated for calculating bulk density, estimated porosity, and compressive strength. Eventually, we discussed and reported the impact of particle size on physical and mechanical properties in waste-derived glass foams.

2. MATERIALS & METHODS

For producing the GF series, we initially supplied waste CRTs glass from the electronic disposal area at Afyon Kocatepe University. The supplied CRTs monitor was then disassembled to obtain panel glass as revealed in **Figure 1**. In **Table 1** the chemical composition of CRTs panel glass is also listed.
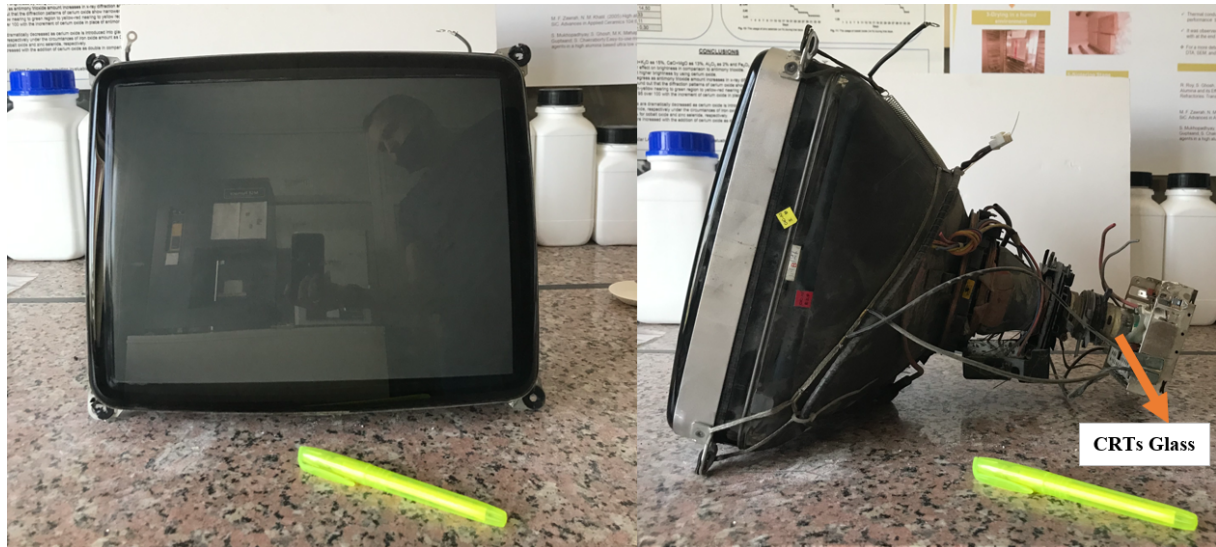
Figure 1. The photographs of the supplied CRTs monitor.

Table 1. The chemical composition of waste CRTs panel glass in wt%.

	Na₂O	K₂O	Al₂O₃	TiO₂	SiO₂	CaO	BaO	SrO	PbO	Fe₂O₃
CRTs Panel	5.19	9.29	4.64	0.39	60.56	2.09	7.49	9.98	0.17	0.20

The panel glass was washed and dried followed by a grinding process via alumina ball milling. The ground particles were then sieved to different particle size ranges, and their particle size distributions were plotted in **Figure 2**, as well as their d_{10}, d_{50}, and d_{90} values are given in **Table 2**. At this point, PS1 to PS4 sample codes signify -500+212, -212+125, -180, and -80 microns in the respective order.
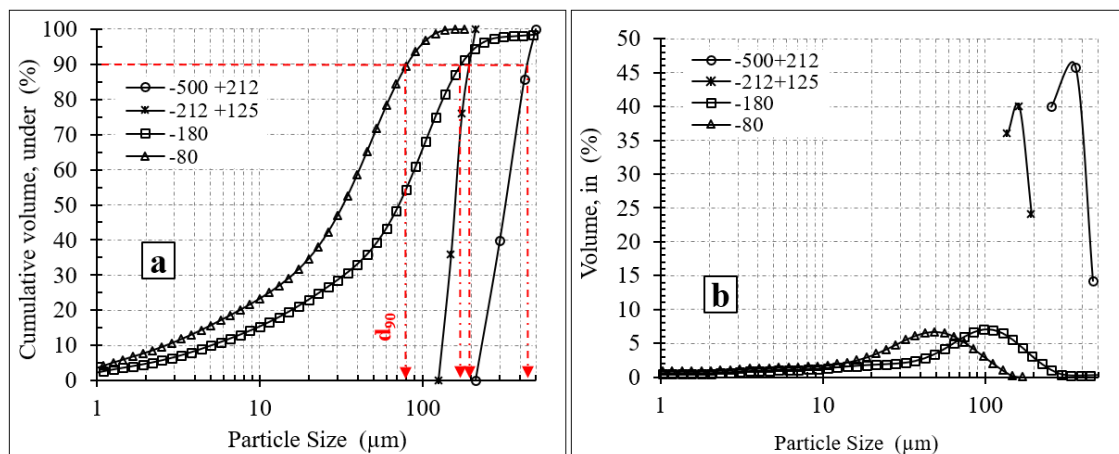
Figure 2. Different particle size distributions for the ground powders.

Table 2. d_{10}, d_{50}, and d_{90} values for the PS1 to PS4 samples.

Sample	d_{10} (µm)	d_{50} (µm)	d_{90} (µm)
-500+212 µm	~235.0	~320.0	~470.0
-212+125 µm	~135.0	~160.0	~195.0
-180 µm	5.1	72.0	173.5
-80 µm	2.7	32.7	80.6

Once four different particle size ranges, PS1 to PS4, were made ready we carried out pellet preparation step. Here, the batch composition, *90CRTs+2G+6WG+2G*, was followed for experimental procedure, and the corresponding particle sizes, as well as other constituents, were precisely weighed via analytical scale (Precisa XB200, ± 0.0001 g), were effectively homogenized via agate mortar, and were thoroughly pressed via uniaxial hydrolic pressing (at 0.6 MPa). The four prepared pellets were placed into a conventional electric resistance furnace to reach up to 850 ⁰C by applying 5 ⁰C.min^{-1} heating rate, which was then dwelled for 30 min at the peak temperature. Finally, glass foam series were obtained as demonstrated in **Figure 3**.
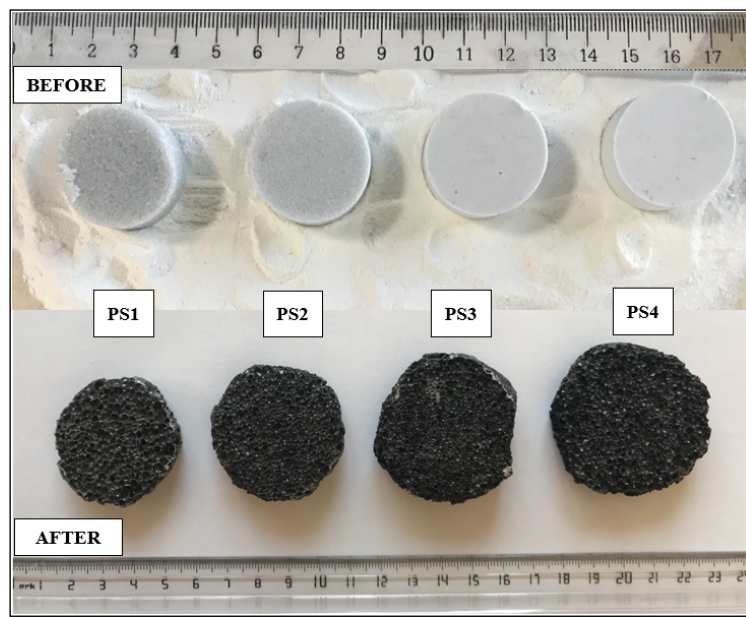
Figure 3. The photographs of unheated (upside) and heated (downside) glass foam series.

Some physical and mechanical analyses were conducted to understand the impact of particle size in waste-derived CRTs glass foams. At the beginning, Archimedes's principle was used to measure the bulk density (ρ_{bulk}) via Equation 1.

$$\rho_{bulk} = \frac{X_{air}}{X_{air} - X_{liquid}} \rho_{liquid} \tag{1}$$

where X_{air}, X_{liquid}, and ρ_{liquid} signify weight in air, weight in water, and density of water (0.997 g.cm^{-3}), respectively.

Based upon ρ_{bulk} value, the predicted porosity (*PP*) was calculated by using Equation 2. In this regard, theoretical density ($\rho_{theoretical}$, 2.759 g.cm⁻³) was figured out with the use of constituents' weight percentages and their density values.

$$PP\ (\%) = [\ (1) - \left(\frac{\rho_{bulk}}{\rho_{theoretical}}\right)\ ]\ x\ 100 \tag{2}$$

Finally, universal mechanical testing (Shimadzu AG IS 100 kN) was utilized to measure the compressive strength of the prepared glass foam series. Before testing, the specimens were ground to obtain flat and parallel surfaces.

3. RESULTS & DISCUSSIONS

As it is clear from **Figure 3** that we successfully fabricated the foam glass series. One can also see that all samples achieve nearly, at least, two times higher expansion characteristics when compared to their initial pellet size. This phenomenon tells us that foaming seems to be accomplishable with different waste CRTs particle size ranges. On the other hand, we can certainly say that the decreasing particle size range is highly beneficial for obtaining a more foamed structure, as well. Visually, the sample-PS1 containing coarser particles shows less foaming rather than sample-PS4 having finer particles.

When it comes to evaluating the fabricated samples in terms of numerical values based upon bulk density, predicted porosity, and compressive strength it becomes quite possible for better comprehension in relation to the impact of different particle size range on foaming characteristics. **Figure 4** plots the values for bulk densities for the intended foam glass samples. We can observe that the decreasing particle size range provides lower bulk density values. That is, samples-PS1-toPS4 have 0.600, 0.460, 0.303, and 0.264 g/cm³ in the respective order. In contrary to this, the predicted porosity, reveals an increasing trend with the decreasing particle size ranges, as expected based on bulk density variations, in **Figure 5**. The values for PS1 to PS4 samples are calculated as 78.25, 83.32, 89.03, and 90.43 percentages, respectively. Such findings are very desirable for foaming materials, especially lightweight building materials applications. In other respects, the variations in both parameters may be attributed to the total surface area ensured by different particle size ranges. In other words, when the contact area increases in a foam glass system, its dissolution increases which lead to a decrease in viscosity [10]. With this obtained, a more foamed structure can be achievable. As a result, the authors concluded that lower particle sizes aid to obtain lower bulk density and higher porosity aspects.
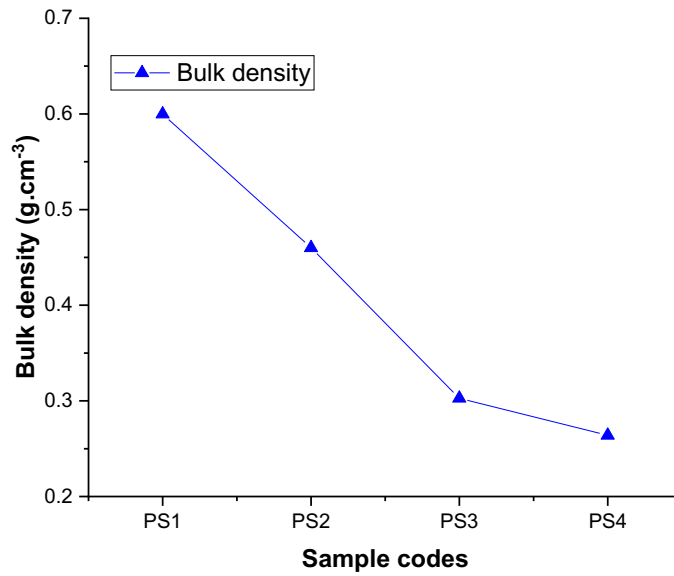
Figure 4. The alterations in bulk density values for the fabricated foam glass series.
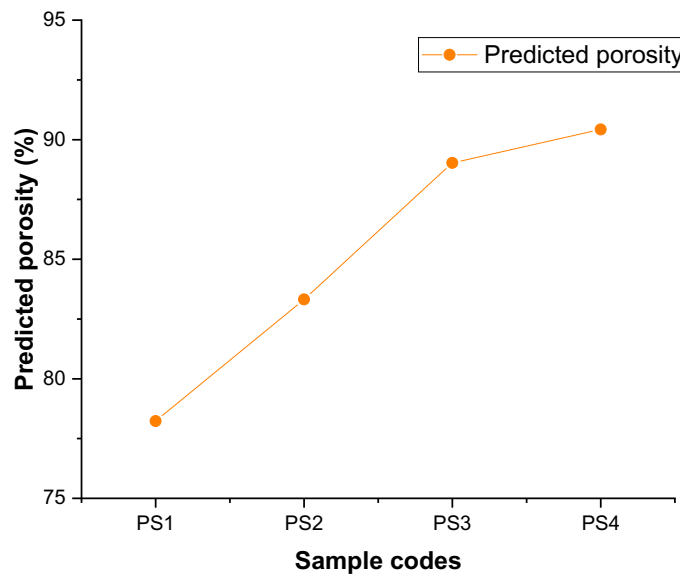

Figure 5. The change in the predicted porosity percentages for the foam glass samples.

Finally, we investigated the behavior of the prepared samples in subjection to the compression. **Figure 6** illustrates the compressive strength trend for the samples. Apparently, the values are found to be in decreasing way as the particle size lowers. Namely, PS1 to PS4 samples have 1.32, 1.13, 1.01, and 0.94 MPa in the respective order. These values seem to be quite acceptable, for example, lightweight building materials, however, if one requires higher values against mechanical failure should follow coarser particle size, though.
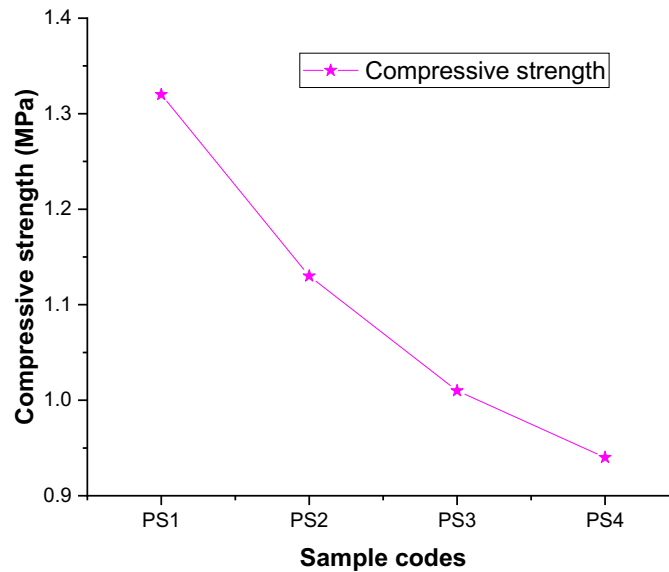
Figure 6. The compressive strength trend for the produced samples.

4. CONCLUSIONS

The present study addresses the preparing foam glass that is composed of fully waste CRTs glass. Another goal was targeted to understand the impact of changing particle size range on foaming characteristics. The prepared foam glass series with varying particle size ranges (PS1 to PS4) were subjected to some characterization analysis to figure out the alterations in bulk density, predicted porosity, and compressive strength. According to the bulk density measurements, the increasing particle size caused a decrease in density values from 0.600 to 0.264 g/cm^3. Therefore, we can say that the PS4 sample (-80 microns) can be regarded as the best one. In contrary to this, the predicted porosity values were equal to 78.25, 83.32, 89.03, and 90.43 percentages for PS1 to PS4 series, respectively, as expected. That means an increasing trend in the porosities as the particle size lowers. Furthermore, the compressive strength test obviously revealed that the decreasing particle size leads to the decreasing resistance to mechanical failure, namely 1.32, 1.13, 1.01, and 0.94 Mpa for PS1 to PS4, respectively. After these findings, we can report that a fully-waste-derived foam glass can effectively be fabricated with acceptable technical properties for building materials applications, particularly lightweight purposes. Additionally, this study proved that lowering particle size aids to obtain high porosity values in waste CRTs-derived foam glass systems.

5. REFERENCES

[1]   S. Smiljanić, U. Hribar, M. Spreitzer, and J. König, "Influence of additives on the crystallization and thermal conductivity of container glass cullet for foamed glass preparation," *Ceram. Int.*, vol. 47, no. 23, pp. 32867–32873, Dec. 2021, doi: 10.1016/J.CERAMINT.2021.08.183.

[2]   N. Stiti, A. Ayadi, Y. Lerabi, F. Benhaoua, R. Benzerga, and L. Legendre, "Preparation and characterization of foam glass based waste," *Asian J. Chem.*, vol. 23, no. 8, pp. 3384–3386, 2011.

[3]   J. Bai, X. Yang, S. Xu, W. Jing, and J. Yang, "Preparation of foam glass from waste glass and fly ash," *Mater. Lett.*, vol. 136, pp. 52–54, Dec. 2014, doi: 10.1016/j.matlet.2014.07.028.

[4]   Y. Liu, J. Xie, P. Hao, Y. Shi, Y. Xu, and X. Ding, "Study on factors affecting properties of foam glass made from waste glass," *J. Renew. Mater.*, vol. 9, no. 2, pp. 237–253, 2020, doi: 10.32604/jrm.2021.012228.

[5]   M. Flood *et al.*, "Glass Fines: A review of cleaning and up-cycling possibilities," *Journal of Cleaner Production*, vol. 267. Elsevier Ltd, p. 121875, 10-Sep-2020, doi: 10.1016/j.jclepro.2020.121875.

[6]   L. Li, T. Jiang, M. Zhou, B. Chen, and C. Chen, "The influence of temperature and SiC content on the recycling of iron ore tailings for the preparation of value-added foam ceramics," *J. Mater. Cycles Waste Manag.*, pp. 1–11, Nov. 2020, doi: 10.1007/s10163-020-01135-x.

[7]   C. Kurtulus, R. Kurtulus, and T. Kavas, "Foam glass derived from ferrochrome slag and waste container glass: Synthesis and extensive characterizations," *Ceram. Int.*, vol. 47, no. 17, pp. 24997–25008, 2021, doi: 10.1016/j.ceramint.2021.05.228.

[8]   J. Spooren *et al.*, "Near-zero-waste processing of low-grade, complex primary ores and secondary raw materials in Europe: technology development trends," *Resour. Conserv. Recycl.*, vol. 160, no. January, p. 104919, 2020, doi: 10.1016/j.resconrec.2020.104919.

[9]   M. B. Østergaard, R. R. Petersen, J. König, H. Johra, and Y. Yue, "Influence of foaming agents on solid thermal conductivity of foam glasses prepared from CRT panel glass," *J. Non. Cryst. Solids*, vol. 465, pp. 59–64, Jun. 2017, doi: 10.1016/j.jnoncrysol.2017.03.035.

[10]   J. König, R. R. Petersen, and Y. Yue, "Influence of the glass particle size on the foaming process and physical characteristics of foam glasses," *J. Non. Cryst. Solids*, vol. 447, pp. 190–197, Sep. 2016, doi: 10.1016/j.jnoncrysol.2016.05.021.

INDEX

İsmail Yıldız · 13

K

Kadir Akgöl · 13
Kamran Khalid · 71
Karima Akool Al-Salihi · 12
Kaveh Ostad-Ali-Askarı · 12
Kaveh Ostad-Ali-Askari · 14

L

Lemiye Atabek Savaş · 55

M

M.Hassan Bin Shaukat · 73
M.Saad Khan · 72
M.Shariq Hasnain · 73
Manjunath Patel · 12, 16
Massimo Rogante · 12, 32
Metin Usta · 80
Michal Kulka · 12, 14
Mourad Keddam · 12, 14, 47, 95
Muhamed Sami Khan · 75
Muhammad Ahmed Raza · 77
Muhammad Usman · 77
Muhammmad Abdul Hai · 71
Muhsin Alçı · 23
Mustafa Kocabaş · 13
Mustafa Serhat Başpınar · 101
Mustafa Ulutan · 13
Mürsel Ekrem · 54

N

Nada Alloush · 62
Najran Mohammed Nasser Hosrom · 48
Nalan Çiçek Bezir · 13
Nodar Lekishvili · 12, 14
Nuriye Kalkmaz · 14

O

Oğuzhan Evcin · 14
Osman Gençel · 12

Ö

Ömer Saltuk Bölükbaşı · 13
Özgür Yazıcı · 13, 14

P

Prasad Chandran N · 16

R

Rabia Almamlook · 12, 14
Recep Güneş · 23
Recep Kurtuluş · 109
Redouane Chegroune · 95
Reza Abolhassani · 46

S

S.M AbuTalib Zaidi · 73
Sabire Duman · 88
Shaheer Siddiqui · 71
Soner Savaş · 13, 14
Süleyman Akpınar · 13
Svetlana Lilkova · 12, 14
Svetlana Lilkova-Markova · 17
Syed Usama Athar · 76

Ş

Şenol Yılmaz · 79

T

Taner Kavas · 109
Tayfun Uygunoğlu · 12
Tayyab Azad Khan · 72

U

Usama Khan · 72

V

Vijay Kumar · 12, 14

Y

Yasemin Tabak · 14, 80
Yogendra Kumar Mishra · 7, 46

Z

Zahide Bayer Öztürk · 13
Zeki Ünal Yümün · 13
Zeynep Taşlıçukur Öztürk · 14

SPONSORS